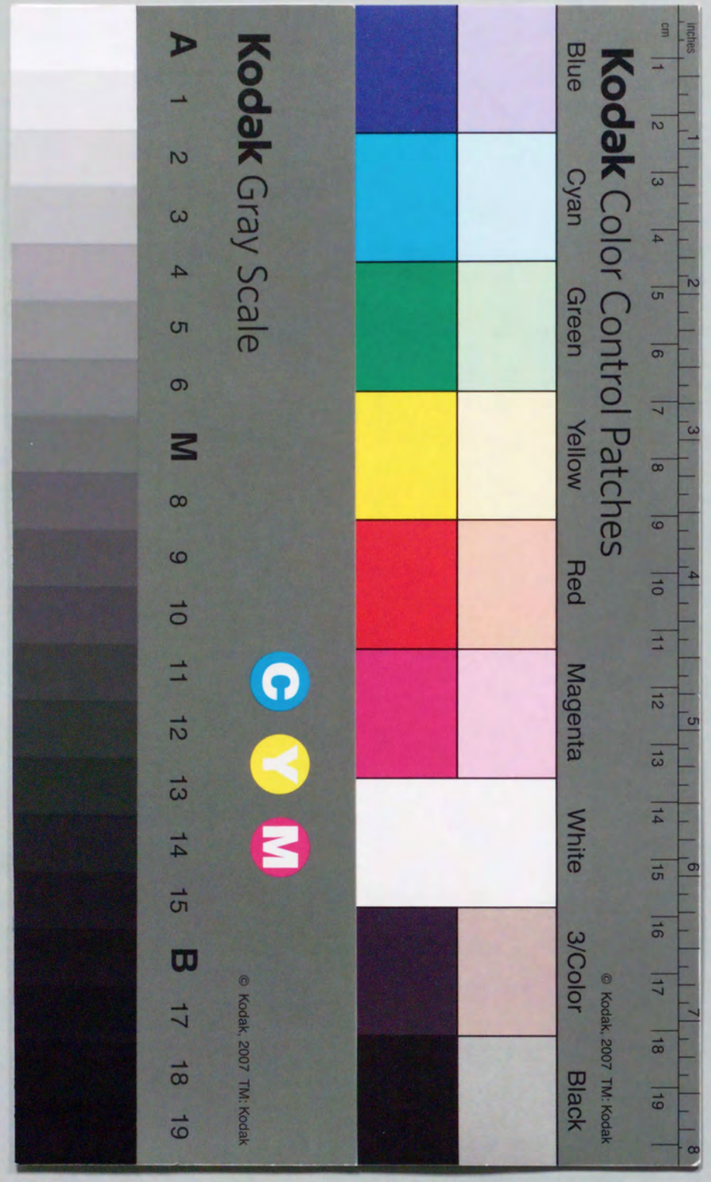

Theoretical Studies of Exchange-Coupled Network Systems and Development of Genetic Algorithms for Ising Model

Akifumi Oda

Osaka University
March 2000

Theoretical Studies of Exchange-Coupled Network Systems and Development of Genetic Algorithms for Ising Model

Akifumi Oda

Osaka University
March 2000

Acknowledgment

This thesis has been conducted under the guidance of Professor Kizashi Yamaguchi. The author would like to express sincere gratitude for his many valuable discussions, some useful advice and encouragement throughout the course of the present work.

The author would like to acknowledge Professor Wasuke Mori (Kanagawa University, at present), Associate Professor Yasunori Yoshioka, Associate Professor Sadamu Takeda (Gunma University, at present), Associate Professor Hidemi Nagao (Kanazawa University, at present) and Dr. Masayoshi Nakano for continuous encouragement and valuable suggestions.

The author gratefully acknowledges Professor Tadashi Sugawara, Dr. Akira Izuoka, and Dr. Michio M. Matsushita (Tokyo Metropolitan University, at present) of the University of Tokyo for their sincere collaboration about intermolecular interactions of dihydroxyphenyl nitronyl nitroxides.

The author is very grateful to Professor Minoru Kinoshita (Science University of Tokyo in Yamaguchi, at present), Dr. Masafumi Tamura (Toho University, at present) and Dr. Yuko Hosokoshi (Institute for Molecular Science, at present) for offers of their experimental measurements for *p*-CNPNN and HNN.

The author is indebted to Dr. Takashi Kawakami (The Institute of Physical and Chemical Research) and Dr. Goro Maruta (High Energy Accelerator Research Organization) for their helpful comments and advice on nitroxide derivatives.

Many thanks are given to all the members of the laboratory of Professor Kizashi Yamaguchi, especially to Dr. Daisuke Yamaki, Dr. Yasuteru Shigeta, Mr. Shinji Kiribayashi, Mr. Yu Takano and Mr. Yasutaka Kitagawa for the valuable discussions about molecular magnetism and for indispensable helps in development of genetic algorithms.

The author would like to thank his family and his friends for understanding of the author's study and their affections.

Contents

PART I

Intermolecular Interactions of Nitronyl Nitroxide derivatives

Chapter 1

General Introduction

1. 1 Introduction

The studies of spin networks, which contain organic radicals, are interesting targets of research from the aspect of developing novel magnetic materials. Organic radicals are suitable for investigating the magnetism of nearly ideal Heisenberg spin systems and they almost have intermolecular antiferromagnetic interactions. Genuine organic ferromagnets consisting only of the light elements of C, H, N, O were researched for a long time, experimental and theoretical studies have been reported by many researchers. In 1991, Kinoshita and co-worker reported that the β phase crystal of *p*-nitrophenyl nitronyl nitroxide (*p*-NPNN) undergoes a ferromagnetic transition at 0.6 K [1-3]. This finding has activated the study of the molecular magnetism. Follow this, several organic bulk ferromagnets have been reported within a few years. Not only many experimental but also theoretical studies have been carried out to elucidate the mechanism of the magnetic interaction [4, 5]. In β-*p*-NPNN crystal, theoretical studies suggest that close contact between nitronyl nitroxide groups and nitrophenyl moieties of nearest neighbor play important roles for ferromagnetic phase. γ phase of *p*-NPNN are also investigated, crystal structure has a great influence on magnetic properties [6].

These theoretical treatment based on molecular orbital calculations have been performed in not only *p*-NPNN but also several groups for various molecular systems in cooperation with experimental studies. It was shown that the magnetic interaction between organic radicals can be characterized quantitatively by the effective exchange interactions (J_{ab}). Theoretical studies were shown that the sign and magnitude of the calculated J_{ab} values

depend sensitively on the stacking mode of the radical molecules. The spin alignment rules were derived on the basis of the calculated results for nitronyl nitroxide derivatives.

On the other hand, magnetic networks are related with optimization methods. Neural network calculations, which are one of the most important optimization method, are inspired by Ising model [7]. They are able to treat several optimization problems, and the detailed studies of magnetic networks are expected to develop the optimization methods.

The ground states of spin glasses are also one of the most important optimization problem. The search for them is NP-hard problem [8]. Because 2^N spin states are considerable for a N-spin cluster, calculational times exponentially increase with a growth of the number of spin sites. Several optimization methods have been used for this problem, and genetic algorithms are one of them. They are carried out for Edwards-Anderson $\pm J$ Ising spin glass with short-range interactions [9-12].

The purpose of the thesis is to investigate the magnetic behavior of crystals and clusters, and propose the calculational methods which can treat spin clusters. In this study, semiempirical and *ab initio* MO methods are used for organic radical crystals which were found by many researchers. Experimental results have been reproduced by calculations. On the other hand, genetic algorithms (GA's) are developed for the calculations of magnetic properties of spin clusters. The author could search the global minima of Ising spin glass, and investigate the dependence of magnetizations and susceptibilities on temperature.

1. 2 Nitronyl nitroxide derivatives

The search for a bulk ferromagnet consisting only of the light elements of C, H, N and O has been one of the most interesting target of research in the field of material science. There are some difficulties to study organic ferromagnetic materials. Organic materials are diamagnets in general, because the electronic structure of organic molecules is of a closed-shell. Although free radicals have an open-shell structure, an antiparallel electron spin alignment is favorable between the unpaired electrons on the basis of the chemical bonding. Therefore, preparations of persistent radicals and the control of the spin alignment are indispensable to developments of organomagnetic materials.

The crystal structure and the existence of the intermolecular ferromagnetic interactions of the β-*p*-NPNN, which consists only of the light elements of C, H, N and O, were reported in 1989 [13]. The ferromagnetic transition of it was reported in 1991, and it is the first organic bulk ferromagnet. For the γ phase of p-NPNN, intra-plane ferromagnetic interactions and the inter-plane antiferromagnetic interaction are found. A theoretical explanation for β- and γ-phase crystals of *p*-NPNN was already carried out.

p-NPNN is one of nitronyl nitroxide derivatives. Because nitronyl nitroxide derivatives have been expected to be ferromagnets, several compounds are synthesized and measured.

Ferromagnetic and antiferromagnetic interactions were found in these crystals, and the ferromagnetic phase transition is reported for some of these compounds. Nitronyl nitroxide derivatives are illustrated in **Fig. 1. 1**.

One of the nitronyl nitroxide derivatives which does not have phenyl rings is MeNN (**2**). Hosokoshi and co-worker reported the magnetic measurements of it [14]. The MeNN crystals involves the close spacing between the NO group and the methyl group at 2-position. There are both of the ferromagnetic and antiferromagnetic coupling in this crystal. This molecular packing is an example of the close spacing between the ONCNO moieties to give ferromagnetic coupling.

Phenyl nitronyl nitroxide (PNNO) derivatives are one of the most significant compounds for organic ferromagnets. Various compounds were synthesized and measured in experimental studies. Inoue and co-worker reported synthesis and magnetic measurements of $NNBA^-$ (**4**) salts [15]. They performed the magnetic measurements and manifested that dimers have a short intermolecular contact between the oxygen atom in NN group and the alpha carbon atom in the nearest-neighbor NN group with T-shape conformation. These salts provided the first example of ferromagnetic dimers of radical anions. Hosokoshi and co-worker reported the p-FPNN (**5**) crystal and it was said that the magnetic properties are explained by the formation of a triplet state within the dimer and additional inter-dimer ferromagnetic interactions [16].

Theoretical studies have been also carried out for these derivatives. In theoretical studies, molecular orbital calculations have been carried out for pair models of PNNO derivatives to elucidate J_{ab} values in their crystals. It was shown that the sign and magnitude of the calculated J_{ab} values depend sensitively on the stacking mode of the radical molecules [4]. The spin alignment rules were derived on the basis of the calculated results for PNNO derivatives [17-21].

1. 3 Intermolecular magnetic interaction (J_{ab})

1. 3. 1 Calculation for J_{ab}

The spin Hamiltonian models can reproduce the experimental results for molecular magnetic materials. The intermolecular interactions of nitronyl nitroxide derivatives are able to be explained by Heisenberg Hamiltonian which has only one term for magnetic interaction:

$$\hat{H} = -2\sum J_{ab}\hat{S}_a \cdot \hat{S}_b \qquad (1.\ 1)$$

J_{ab} is the parameter of the magnetic interaction, as illustrated in **Fig. 1. 2**.

In this thesis, two sites models are considered. J_{ab} are able to be calculated by $\langle \hat{S}^2 \rangle$

and Heisenberg Hamiltonian.

For two sites model, Heisenberg Hamiltonian are expressed by

$$\hat{H} = -2J_{ab}\hat{S}_a \cdot \hat{S}_b \tag{1. 2}$$

The operator $\hat{S}^2$ is mentioned as

$$\hat{S}^2 = \hat{S}_a^2 + \hat{S}_b^2 + 2 \cdot \hat{S}_a \cdot \hat{S}_b \tag{1. 3}$$

where,

$$\hat{S} = \hat{S}_a + \hat{S}_b \tag{1. 4}$$

From the eq. (1. 3), the expectation value of energy is calculated as

$$\begin{aligned} E &= \left\langle \Psi \middle| -2J_{ab}\hat{S}_a \cdot \hat{S}_b \middle| \Psi \right\rangle \\ &= -J_{ab}\left(\left\langle \hat{S}^2 \right\rangle - \left\langle \hat{S}_a^2 + \hat{S}_b^2 \right\rangle \right) \end{aligned} \tag{1. 5}$$

therefore,

$$J_{ab} = \frac{E(LS) - E(HS)}{\left\langle \hat{S}^2 \right\rangle_{HS} - \left\langle \hat{S}^2 \right\rangle_{LS}} \tag{1. 6}$$

where $E(LS)$ and $E(HS)$ are the energies of the low spin and high spin states, respectively.

In this thesis, positive J_{ab} means ferromagnetic interaction, and negative J_{ab} leads the antiferromagnetic coupling, as shown in **Fig. 1. 2**.

1. 3. 2 Three terms of J_{ab}

The effective exchange integral J_{ab} for a radical pair is generally expressed by three different terms under the approximately spin-projected unrestricted Hartree-Fock (APUHF) approximation, *i. e.* [21],

$$J_{ab}(\text{APUHF}) = J_{ab}(\text{KE}) + J_{ab}(\text{PE}) + J_{ab}(\text{SP}). \tag{1. 7}$$

The kinetic (KE) and potential (PE) exchange terms are, respectively, determined by SOMO-SOMO overlap S_{ab} and intermolecular exchange integral K_{ab}. The spin polarization (SP) term is given by the product of spin densities ($\rho_{a(b)}$) induced by the spin polarization effect [17].

The ferromagnetic interaction in molecular crystals can be explained by these terms. A simple classification of the magnetic interaction was derived [19, 20].

Case I	(J_{ab}(KE)<0, J_{ab}(PE)>0; J_{ab}<0)	(1. 8a)
Case II	(J_{ab}(KE)≈0, J_{ab}(PE)>0; J_{ab}>0)	(1. 8b)
Case III	(J_{ab}(KE)≈0, J_{ab}(PE)≈0, J_{ab}(SP)>0; J_{ab}>0)	(1. 8c)
Case IV	(J_{ab}(KE)≈0, J_{ab}(PE)≈0, J_{ab}(SP)<0; J_{ab}<0)	(1. 8d)

Cases I and II are understood intuitively by the symmetry of SOMO-SOMO contact. The effective exchange interaction between closely located radical groups is usually antiferromagnetic (J_{ab}<0) [4], since the KE interaction stabilizes the low spin (LS) state (Case I). However, if the mutual orientation of radical groups is controlled to reduce the KE term, the ferromagnetic interaction (J_{ab}>0) is expected at a short intermolecular distance (Case II) because of nonzero Coulombic exchange integral (J_{ab}(PE)=K_{ab}) as studied in the case of simple nitroxide pair model [1]. On the other hand, the SP term induced by the indirect interactions through bond and space becomes important when the distance between the two radical groups is large (Case III, IV). For example, β-phase of p-NPNN corresponds to the case III [5]. The sign of J_{ab}(SP) depends on the phase of spin alternation by the SP effect.

Ab initio configuration interaction (CI) method by use of the complete active space (CAS) selected on the basis of the occupation numbers of the UHF natural orbitals (UNO), *i. e.*, UNO CASCI, has been used to estimate the SOMO-SOMO direct interaction terms (KE and PE) [19, 20, 23, 24]. Semiempirical INDO method has been successfully employed to calculate J_{ab} values which include all terms in eq. (1. 7).

1. 4 MO methods

1. 4. 1 Hartree-Fock method

Hartree-Fock (HF) method plays an important role for theoretical explanations of chemistry. In addition, it is a starting point for more accurate approximations. Most of the computational methods of quantum chemistry are based on HF approximation.

In HF method, the wave function is expressed by one Slater determinant. The HF equation is mentioned as follows:

$$\left[h(1) + \sum \hat{J}_b(1) - \sum \hat{K}_b(1) \right] \chi_a(1) = \varepsilon_a \chi_a(1) \tag{1. 9}$$

This is the HF equation for electron 1. In eq. (1. 9),

$$h(1) = -\frac{1}{2}\nabla_1^2 - \sum_A \frac{Z_A}{r_{1A}} \qquad (1.\ 10)$$

is the electronic kinetic energy and electron-nuclear attraction energy of electron 1. $\hat{J}_b(1)$ and $\hat{K}_b(1)$ is the Coulombic operator and the exchange operator, respectively, and two electrons correlations are replaced with one electron potential in these operator. $\chi_a(1)$ is the spin orbital, and ε_a is the orbital energy.

1. 4. 2 INDO method

INDO (Intermediate Neglect of Differential Overlap) method is one of the semiempirical MO methods. In this method, one center two electrons integrals is obtained as

$$(ss \mid ss) = (ss \mid xx) = F^0$$

$$(xx \mid xx) = F^0 + \frac{4}{25}F^2$$

$$(xx \mid yy) = F^0 - \frac{2}{25}F^2$$

$$(xs \mid xs) = \frac{1}{3}G^1$$

$$(xy \mid xy) = \frac{3}{25}F^2 \qquad (1.\ 11)$$

where s, x and y express the s, $2p_x$ and $2p_y$ orbitals, respectively. F^0 are calculated from the Slater orbital, F^2 and G^1 are determined in semiempirical procedures. Two center integrals are ignored in INDO method.

1. 4. 3 Restricted and unrestricted spin orbital

In restricted spin orbital, α-spin and β-spin are in a same spatial orbital. On the other hand, they are in different spatial orbitals in unrestricted spin orbital as shown in **Fig. 1. 3**. HF method used restricted spin orbital is known as RHF method, and it with unrestricted spin orbital is known as UHF.

For open shell systems, because α-spin electron and β-spin electron are given different potential energies, unrestricted spin orbital gives a lower energy than restricted spin orbital. On the other hand, unrestricted spin orbital always overestimates the expectational values of

$\hat{S}^2$ because constituents of higher order are mixed. When the number of α-electrons N^α is larger than that of β-electrons N^β, the expectational value of $\hat{S}^2$ in UHF is mentioned as following equation:

$$\left\langle \hat{S}^2 \right\rangle_{UHF} = \left\langle \hat{S}^2 \right\rangle_{exact} + N^\beta - \sum_i^N \sum_j^N \left| S_{ij}^{\alpha\beta} \right|^2 \qquad (1.\ 12)$$

where,

$$\left\langle \hat{S}^2 \right\rangle_{exact} = \left(\frac{N^\alpha - N^\beta}{2} \right) \left(\frac{N^\alpha - N^\beta}{2} + 1 \right) \qquad (1.\ 13)$$

In spite of this weak point, UHF method, which is suitable for the calculations of unpaired electrons, is used in these studies of radicals.

1. 4. 4 Configuration interaction method

Configuration interaction (CI) method is a more accurate method based on HF approximation. CI wave function is mentioned as follows:

$$|\Phi\rangle = c_0 |\Psi_0\rangle + \sum_{ar} c_a^r |\Psi_{0a}^{\ r}\rangle + \sum_{\substack{a<b \\ r<s}} c_{ab}^{rs} |\Psi_{0ab}^{\ rs}\rangle + \sum_{\substack{a<b<c \\ r<s<t}} c_{abc}^{rst} |\Psi_{0\ abc}^{\ rst}\rangle + \cdots \qquad (1.\ 14)$$

where $|\Psi_0\rangle$ is the RHF wave function. In wave function $|\Psi_{0a}^{\ r}\rangle$, the electron in χ_a excite to χ_r.

According to eq. (1. 14), a full CI wave function contains all excited states. Though it is an exact solution when basis function is complete, full CI calculations are very difficult to carried out. There are $\binom{2K}{N}$ Slater determinants in 2K spin orbitals and N electron, and the calculations are not able to be done even though a small molecule is considered.

For complete active space (CAS) CI, a subset of the orbitals and electrons are selected, and full CI are carried out only in this subset. This subset is known as complete active space. CASCI method with n electrons and m orbitals is specified CASCI {n, m}. CASCI with SCF of a referential orbital is CASSCF. 2-electrons and 2-orbitals active space is illustrated in **Fig. 1. 4**.

1. 4. 5 Natural orbital

One electron density matrix of UHF wave function is mentioned as follows:

$$\rho(r_1, r_1') = N\int \Psi(r_1, r_2, \cdots, r_N)\Psi^*(r_1', r_2, \cdots, r_N)dr_2 \cdots dr_N \qquad (1.\ 15)$$

The sum of matrixes for α-spin and β-spin is diagonalized, eq. (1. 16) are obtained:

$$\rho_\alpha(r_1, r_1') + \rho_\beta(r_1, r_1') = \sum_i \xi_i \nu_i(r_1)\nu_i^*(r_1') \qquad (1.\ 16)$$

Spin orbital $\{\nu_i\}$ is known as natural orbital (NO), and ξ_i $(0 \le \xi_i \le 2)$ is known as occupation number.

NO is useful for CASCI and CASSCF calculations of radicals because the occupation number of NO contributed unpaired electron is almost equal to 1. CASCI with UHF natural orbital (UNO) and CASSCF with UNO is known as UNO CASCI and UNO CASSCF, respectively.

1. 4. 6 Density functional theory

The many fermion systems are treated the Hamiltonians developed with the Hohenberg-Kohn theorem. The total energy in the density functional theory (DFT) is mentioned as follows [25, 26]:

$$E_{el} = -\frac{1}{2}\sum_i \int \phi_i(r_1)\nabla^2\phi_i(r_1)dr_1 + \sum_A \int \frac{Z_A}{|R_A - r_1|}\rho(r_1)dr_1 + \frac{1}{2}\sum_i \int \frac{\rho(r_1)\rho(r_2)}{|r_1 - r_2|}dr_1 dr_2 + E_{XC}$$

$$\rho(r_1) = \sum_i \phi_i(r_1)\phi_i(r_1)$$

$$E = T(r) + V(r) + G(r) + E_{XC}(r) \qquad (1.\ 17)$$

where T(r), V(r), G(r) and $E_{XC}(r)$ are the electronic kinetic energy, the electron-nuclear attraction energy, the Coulombic repulsion energy between electrons and the exchange correlation energy, respectively. The total density ρ is given by the spin unrestricted approximation as

$$\rho = \rho^\alpha + \rho^\beta$$

$$\rho^\alpha = \sum\left|\phi_i^\alpha\right|^2,\ \rho^\beta = \sum\left|\phi_i^\beta\right|^2 \qquad (1.\ 18)$$

The spin orbitals ϕ_i^γ (γ = α, β) are determined by the spin unrestricted Kohn-Sham (UKS) equation

$$\left[-\frac{1}{2}\nabla^2 + \sum_A \frac{Z_A}{|R_A - r_i|} + \int \frac{\rho(r_2)}{|r_1 - r_2|}dr_2 + V_{XC}\right]\phi_i(r_1) = h_{KS}\phi_i(t_1) = \varepsilon_i\phi_i(r_1)$$

$$V_{XC}[\rho] = \delta E_{XC}[\rho]/\delta\rho$$

$$\hat{H}(UKS)\phi_i^\gamma = \varepsilon_i\phi_i^\gamma \qquad (1.\ 19)$$

There are several approximate correlation-correction functionals in DFT methods: Vosko-Wilk-Nusair (VWN) [27], Perdew's 1981 (PL) functionals [28], Perdew's 1986 (P86) [29], Lee-Yang-Parr (LYP) functional [30], etc. Because UKS B-LYP method gives reasonable spin densities for nitronyl nitroxide derivatives, LYP functionals are used for calculations of NN derivatives.

1. 5 Details of following chapters in part I

The purpose of this part is to investigate the intermolecular magnetic interaction in the crystalline phases of nitronyl nitroxide derivatives. For this purpose, the author carried out ab initio and semiempirical MO calculations for these derivatives.

In this chapter, the author briefly reviewed the organic magnets and the method of quantum chemical calculations.

In chapter 2, intermolecular interactions in α phase of HNN, which is the simplest NN derivatives, are calculated. Computational values are compared with an experimental value, and advantages of each methods are discussed.

In chapter 3, the calculations for J_{ab} of *p*-CNPNN are carried out. The important pairs for magnetic properties of *p*-CNPNN crystal and the important parts of *p*-CNPNN molecule are investigated, and 2D ferromagnetic interactions with antiferromagnetic interplane interactions are discussed.

In chapter 4, the author investigates intermolecular interactions of hydrogen bonded NN derivatives. Interactions in α and β phase crystals of HQNN and RSNN crystal are calculated, and the roles of hydrogen bonds are discussed.

Summary of the part I is described in chapter 5.

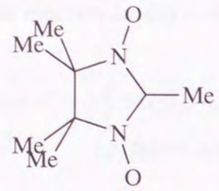

HNN

1

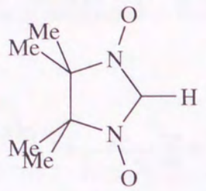

MeNN

2

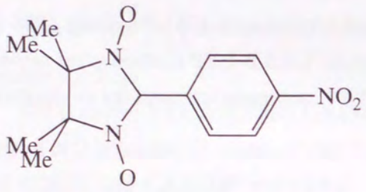

p-NPNN

3

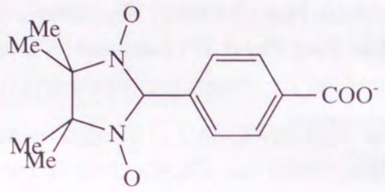

2 p-NNBA$^-$

4

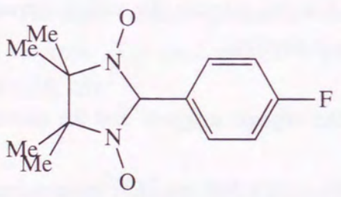

p-FPNN

5

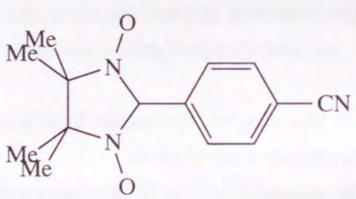

p-CNPNN

6

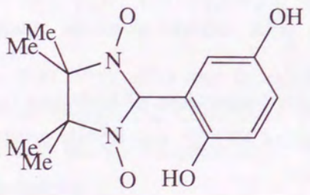

HQNN

7

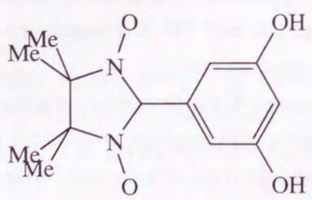

RSNN

8

Figure 1. 1 Various nitronyl nitroxide derivatives are illustrated.

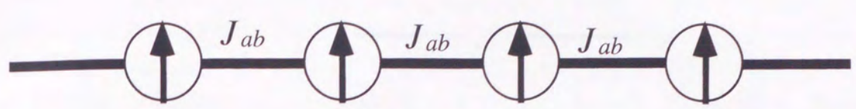

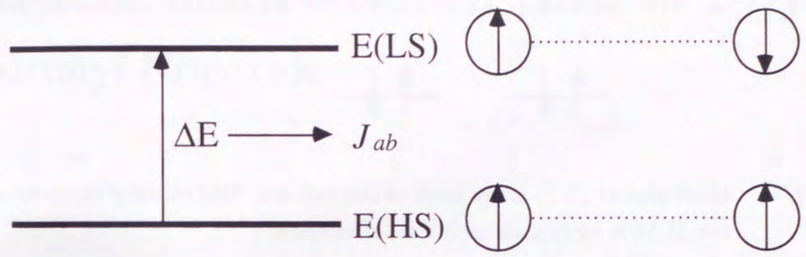

$J_{ab} > 0$ ferromagnetic interaction

$J_{ab} < 0$ antiferromagnetic interaction

Figure 1. 2 Intermolecular interactions (J_{ab}) between two spin sites are illustrated. The positive and negative J_{ab} values mean ferro- and antiferro- magnetic interactions, respectively.

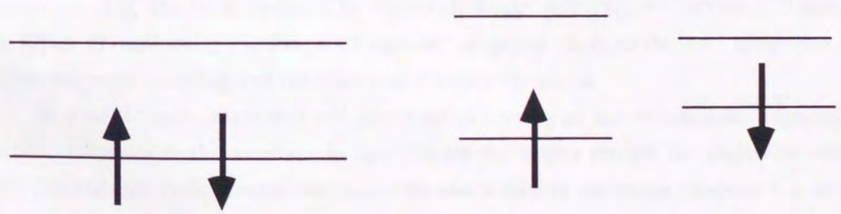

restricted spin orbital unrestricted spin orbital

Figure 1. 3 Restricted and unrestricted spin orbitals are shown. In unrestricted spin orbitals, α- and β- spins occupy the different spacial orbitals.

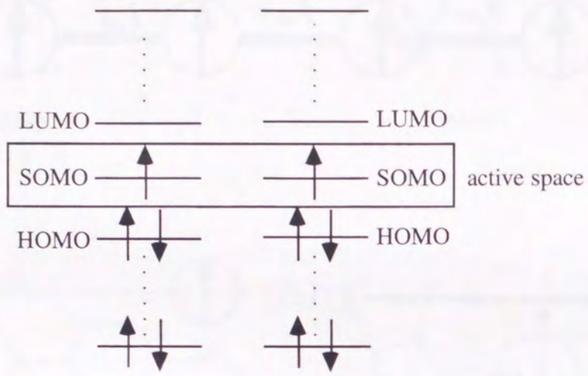

Figure 1. 4 Illustration of {2, 2} active space of two radicals. Two unpaired electrons and two SOMOs are considered in this active space.

Chapter 2

Magnetic Interactions in α phase of 2-Hydro Nitronyl Nitroxide

2. 1 Introduction

Recently, in a series of theoretical studies of ferromagnetic interaction in PNNO derivatives, it was shown that the ON-C-NO moieties play important roles for the sign and magnitude of the effective exchange interaction (J_{ab}) in the crystal [31]. Replacing the phenyl ring by a hydrogen atom is expected to introduce direct contacts between the ON-C-NO moieties.

Recently Kinoshita and co-worker reported the magnetic property of α phase 2-hydroxy nitronyl nitroxide (2-hydroxy-4, 4, 5, 5-tetramethyl-4, 5-dihydro-1*H*-imidazolyl-1-oxyl-3-oxide, abbreviated as HNN) [32, 33]. Because this compound has the simplest structure of all nitronyl nitroxide derivatives, investigations of HNN are interested. The whole temperature dependence of χ_p can be reproduced by the dimer model with J/k_B = -7.65 cm^{-1}. There are two types of molecular packings of nearest neighbor in α-HNN, and only one has antiferromagnetic coupling and the other one is negligibly small.

It is particularly interesting and important to investigate theoretically the origin of the magnetic behavior in this crystal. In this chapter the author reports the molecular orbital (MO) calculations to determine the intermolecular effective exchange integrals for several pair models whose geometries are extracted from the X-ray structure in the crystal.

2. 2 Crystal structure

Fig. 2. 1 displays the molecular packing of α-HNN. There is a noticeable chain structure along the *c* axis. Each chain contains two types of dimeric structure as shown in **Fig. 2. 2**. One of them is pair **A**, it has close spacing between ON-C-NO moieties. The other is pair **B** with the NO...HC contact. This contact is doubled as a result of the inversion symmetry at the center of the two molecules. Intrachain molecular coupling is pair **C**, and the distance between two molecules of pair **C** is longer than that of interchain dimeric pairs.

The theoretical calculations were performed for all possible pairs, **A** (**1**-**2**), **B** (**1**-**3**), **C** (**1**-**4**), **D** (**4**-**5**) and **E** (**4**-**6**) by use of the semiempirical, *ab initio* MO and DFT methods. 4-31G basis sets were used for these pairs, and 6-31G* basis sets were also used for simplified pair models.

2. 3 Calculations for HNN pair molecules

In order to elucidate the ferromagnetic property observed for the HNN crystal, semiempirical INDO and *ab initio* calculations are carried out for four pair models of HNN molecules. **Table 2. 1** shows the calculated J_{ab} values. Semiempirical INDO, DFT, UNO CASCI {2, 2} and UNO CASSCF {2, 2} methods can reproduce qualitatively the experimental results. The pair **A** in **Fig. 2. 2** which has close spacing between ON-C-NO moieties shows the largest J_{ab}. J_{ab} values of other pairs are much smaller than J_{ab} for **A**. These results suggests that dimeric antiferromagnetic interaction exists along the *c* axis and interaction between the chains is weak.

UNO CASCI {2, 2} and UNO CASSCF {2, 2} methods by use of two active UNOs and two unpaired electrons give suitable J_{ab} values for pair **A**, suggesting a large contribution of direct SOMO-SOMO coupling to the antiferromagnetic interaction of pair **A**.

2. 4 Calculations for the simplified pair models

To study possible mechanisms of the magnetic interaction in the HNN crystal in detail, theoretical calculations with various methods were performed for the simplified pair models of pair **A** and **B**.

The model $\mathbf{A}_1$ and $\mathbf{B}_1$ consist of two nitronyl nitroxides (ON-C-NO). **Table 2. 2** shows the J_{ab} values obtained by several computational methods. The following conclusions were drawn from **Table 2. 2**:

(i) **Fig. 2. 3** illustrates the results of model $\mathbf{A}_1$ and pair **A**. The results of calculations of model $\mathbf{A}_1$ and $\mathbf{B}_1$ almost can reproduce the results for pair **A** and **B**. These results suggest that ON-C-NO moieties play important roles for the magnetic interactions of pair **A** and **B**.

(ii) The conclusion (i) suggests that model $\mathbf{A}_1$ and $\mathbf{B}_1$ can be calculated by MO methods instead of pair **A** and **B**. For the model $\mathbf{A}_1$, calculational results using 4-31G and 6-31G* basis sets are compared and illustrated in **Fig. 2. 4**. These results resemble each other except for those of UNO CASCI {10, 10} method. Because UNO CASCI {10, 10} method gives unsuitable J_{ab} values compared with experimental result, it is negligible.

(iii) The results calculated by several methods for model $\mathbf{A}_1$ are shown in **Fig. 2. 5**. For these calculations, 4-31G basis sets were used for *ab initio* MO and DFT methods because of the conclusion (ii). INDO, UBLYP, UB3LYP, UNO CASCI {2, 2}, UNO CASSCF {2, 2}, UNO CASSCF {10, 10} methods give the reasonable J_{ab} values. The results of UNO CASCI {2, 2} and UNO CASSCF {2, 2} methods suggest a large contribution of direct SOMO-SOMO coupling to the ferromagnetic interaction.

2. 5 Conclusion

intermolecular interactions in α-HNN crystal

The pair **A** plays an important role in α-HNN crystal. The intermolecular interaction of pair **A** is maybe compared with the experimental one derived from magnetic susceptibility measurement by assuming the dimer model. In this pair, ON-C-NO moieties are significant for the intrapair interaction of pair **A**.

the validities of methods for calculations

UHF/4-31G method gave the unsuitable results because SP terms were overestimated by it. Because the wave function of UHF was inadequate, J_{ab} values calculated by UMP2 and UMP4 methods were much different from experimental value. Though UNO CASCI {6, 6} and UNO CASSCF {6, 6} methods gave unsuitable J_{ab} values, UNO CASSCF {10, 10} method gave reasonable results. From these results, more active spaces are desirable, however, it is difficult because of bounds of computers.

INDO, DFT and UNO CASSCF methods are suitable for HNN molecules. The validity of these methods are discussed also in following chapters.

Table 2. 1 Calculated J_{ab} values for several pairs of HNN.

	J_{ab}/cm^{-1}				
	A	**B**	**C**	**D**	**E**
INDO	-4.917	0.524	0.011	-0.016	0.050
UHF/4-31G	-66.727	6.258	0.292	-0.066	0.285
UHF/6-31G*	-60.315	4.416	0.261	-0.068	0.263
UBLYP/4-31G	-8.932	0.233	0.092	-0.953	0.255
UBLYP/6-31G*	-9.146	0.266			
UB2LYP/4-31G	-30.763	1.775	0.204	-0.009	0.426
UB3LYP/4-31G	-12.674	0.843	0.143		
UNO CASCI {2, 2}[a)]	-5.679	0.014	0.705	0.004	0.059
UNO CASSCF {2, 2}[a)]	-7.395	0.748	0.214	0.107	0.304
UNO CASCI {6, 6}[a)]	-51.413	-0.810	0.081	-0.091	0.131
UNO CASSCF {6, 6}[a)]	-23.966	-0.224	0.110	-0.011	0.165
UNO CASCI {10, 10}[a)]	-227.082	-3.259			
UNO CASSCF {10, 10}[a)]	-22.869				

a) 4-31G basis set was used.

Table 2. 2 Calculated J_{ab} values for simplified models for the pair **A** and **B**.

	J_{ab}/cm^{-1}			
	A	**A$_1$**	**B**	**B$_1$**
INDO	-4.917	-3.692	0.524	0.169
UHF/4-31G	-66.727	-63.902	6.258	7.059
UHF/6-31G*	-60.315	-62.677	4.416	4.759
UBLYP/4-31G	-8.932	-10.442	0.233	0.215
UBLYP/6-31G*	-9.146	-11.263	0.266	0.233
UB2LYP/4-31G	-30.763	-31.778	1.775	
UB3LYP/4-31G	-12.674	-13.244	0.843	0.521
UMP2/4-31G		-20.255		-0.826
UMP4/4-31G		-21.617		-1.540
UNO CASCI {2, 2}[a)]	-5.679	-5.261	0.014	0.067
UNO CASSCF {2, 2}[a)]	-7.395	-7.251	0.748	0.006
UNO CASCI {6, 6}[a)]	-51.413	-40.893	-0.810	-1.280
UNO CASSCF {6, 6}[a)]	-23.966	-25.478	-0.224	-0.457
UNO CASPT2 {6, 6}[a)]		-42.643		-1.975
UNO CASCI {10, 10}[a)]	-227.082	-216.916	-3.259	-18.773
UNO CASSCF {10, 10}[a)]	-22.869	-19.299		
UNO CASCI {2, 2}[b)]		-7.036		0.089
UNO CASSCF {2, 2}[b)]		-9.434		0.013
UNO CASCI {6, 6}[b)]		-46.186		-1.244
UNO CASSCF {6, 6}[b)]		-25.461		-0.411
UNO CASCI {10, 10}[b)]		-122.270		-12.069
UNO CASSCF {10, 10}[b)]		-21.684		

a) 4-31G basis set was used.
a) 6-31G** basis set was used.

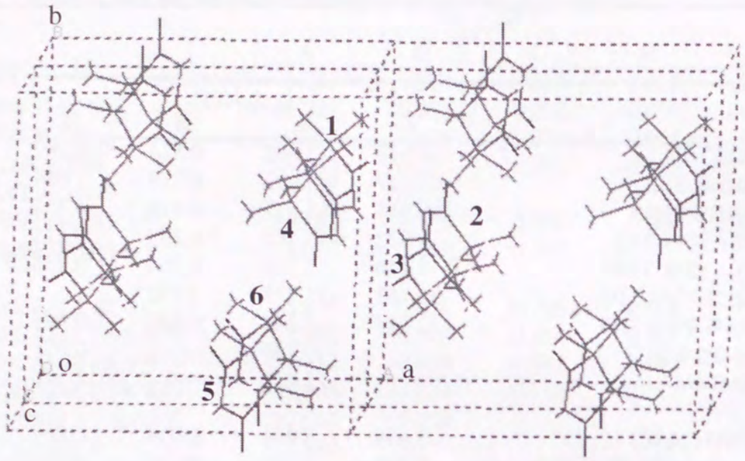

Figure 2. 1 Crystal structure of α-HNN are illustrated. In this crystal, there are two types of dimeric structure. One of them is pair **A** (**1**-**2**), and another is pair **B** (**1**-**3**).

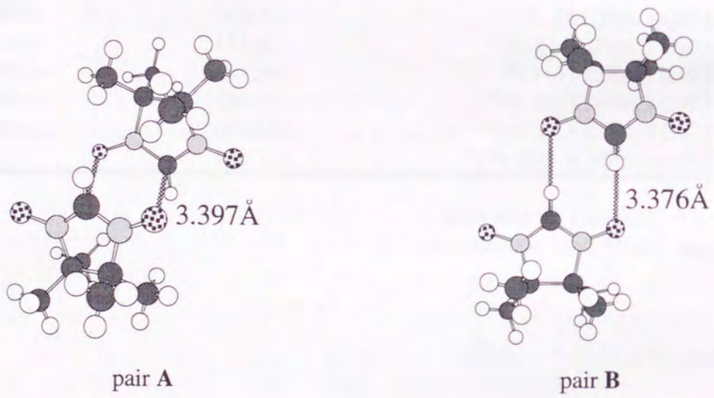

Figure 2. 2 Nearest neighbors of α-HNN.

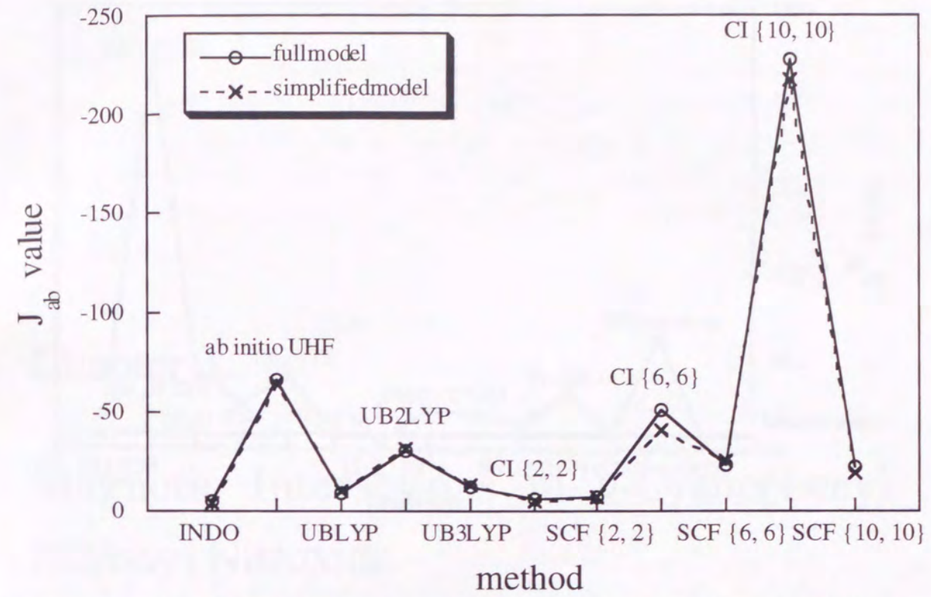

Figure 2. 3 Comparison with J_{ab} values of model **A** and pair $\mathbf{A}_1$ are illustrated. UNO CASCI and UNO CASSCF methods are abbreviated to "CI" and "SCF", respectively.

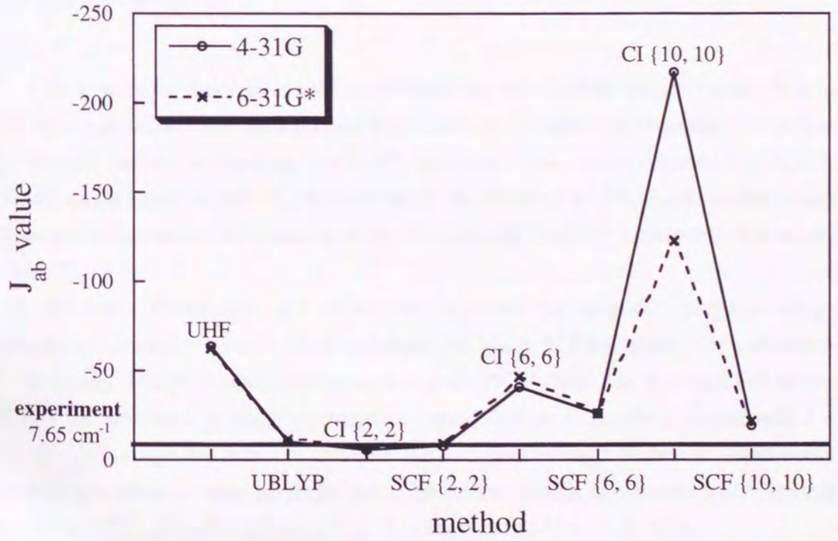

Figure 2. 4 Comparison with 4-31G basis sets and 6-31G* for model $\mathbf{A}_1$. "CI" and "SCF" are same as **Fig 2. 3**.

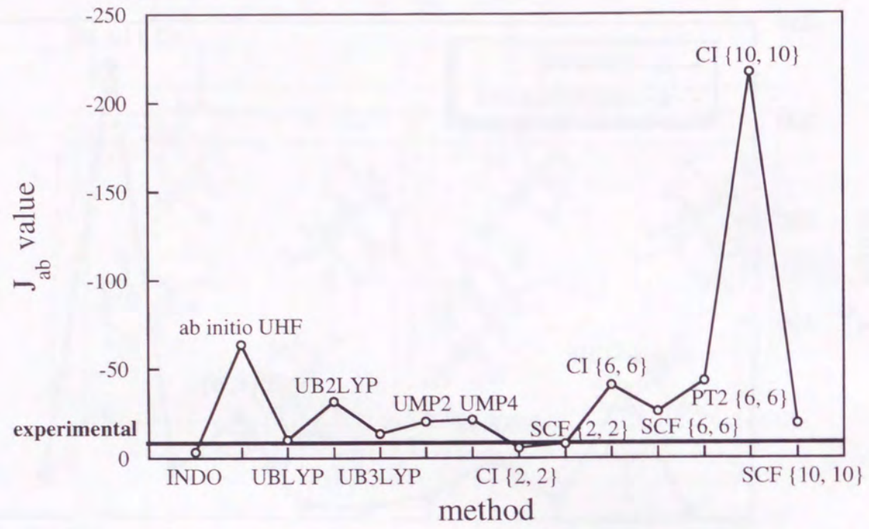

Figure 2. 5 J_{ab} values of model $\mathbf{A}_1$ calculated by several methods. "CI" and "SCF" are same as **Fig 2. 3**.

Chapter 3

Magnetic Interactions in *p*-Cyanophenyl Nitronyl Nitroxide

3. 1 Introduction

In a series of theoretical studies of ferromagnetic interaction in organic radical crystals, it was shown that the sign and magnitude of the effective exchange interaction (J_{ab}) strongly depend on stacking modes of radical molecules in the crystal [4, 5, 6, 31]. Recently many experimental efforts to construct the stacking modes which exhibit strong ferromagnetic interaction have been paid by synthesizing a variety of nitroxide derivatives [3, 34, 35].

Recently Hosokoshi and co-worker reported the magnetic property of *p*-cyanophenyl nitronyl nitroxide (2-(4'-cyanophenyl)-4, 4, 5, 5-tetramethyl-4, 5-dihydro-1*H*-imidazolyl-1-oxyl-3-oxide, abbreviated as *p*-CNPNN) [36]. The susceptibility above 4 K can be explained by the ferromagnetic square-lattice Heisenberg model with J = 0.52 cm^{-1}. It is suggested from the structure analysis that the origin of the two dimensional ferromagnetic behavior may be attributed to the intermolecular contacts between nitronyl nitroxide groups and cyanophenyl groups in a sheet parallel to the *ac*-plane.

It is particularly interesting and important to investigate theoretically the origin

of the two-dimensional magnetic behavior in this crystal. In this chapter the author reports the molecular orbital (MO) calculations to determine the intermolecular effective exchange integrals for several pair models whose geometries are extracted from the X-ray structure in the crystal.

3. 2 Crystal structure

Fig. 3. 1(a) illustrates the packing arrangement of *p*-CNPNN molecules (**1** through **6**) in the crystal and **Fig. 3. 1**(b) shows the geometry of *p*-CNPNN molecule. There are two crystallographically independent molecules. One of the molecules corresponds to **1**, **4** or **6** (group **I**) and the other to **2**, **3** or **5** (group **II**). Since disorder of the methyl groups in group **I** was suggested and correct geometry of the methyl groups was not determined, the geometry of the methyl groups in group **II** was used for group **I** in our MO calculations. The sheet structure parallel to the *ac*-plane is outstanding. Within the sheet, each molecule in **I** is surrounded by four molecules in **II** and *vice versa*. As shown in **Fig. 3. 2**, relatively short distances were found between the carbon atom of the cyano group and the terminal oxygen atom of the nitroxide group, *i. e.*, r2 along the a-axis and r2' along the c-axis. Close contact between the terminal oxygen atom of the nitroxide group and the carbon atoms of the phenyl group was also found. The molecular packing along the a-axis is very similar to that along the c-axis. From the crystal structure the magnetic interaction in the *ac*-plane is interested.

The theoretical calculations were performed for the pairs of *p*-CNPNN molecules, **A** (**1**-**2**), **BI** (**1**-**4**), **BII** (**2**-**3**), **C** (**1**-**5**) and **D** (**1**-**6**), in the crystal shown in **Fig. 3. 1** by use of semiempirical INDO and DFT methods. UNO CASCI and UNO CASSCF methods were also used for the simplified pair models.

3. 3 Calculations for *p*-CNPNN pairs

In order to study the magnetic property observed for *p*-CNPNN crystal, the semi-empirical INDO calculation was carried out for whole molecular skeleton (pairs **A**, **BI**, **BII**, **C** and **D**). **Table 3. 1** shows the calculated J_{ab} values. The INDO method gives reasonable values for J_{ab} as compared with the experiment, and DFT methods give qualitatively reasonable values [36]. The pairs **A** and **C** on the *ac*-plane show large

positive J_{ab} values. The reason of the large positive J_{ab} may be explained by short intermolecular distances for the pairs **A** and **C**. The INDO and DFT calculations suggests that pseudo-two-dimensional ferromagnetic interaction exists in the molecular sheet parallel to the *ac*-plane and interaction between the sheets (**BI** and **BII**) is weak. This result qualitatively explains the experimental result by Hosokoshi and co-worker.

3. 4 Calculations for simplified pair models

In order to elucidate the magnetic interaction path in the pairs described above, various computations were carried out for the simplified pair models.

3. 4. 1 Simplified models for the pairs **A** and **C**

Different simplified pair models shown in **Fig. 3. 3** were considered to designate the role of cyano, phenyl and methyl groups for the intermolecular magnetic interaction. $\mathbf{A}_1$ and $\mathbf{C}_1$ are the most simplified pair models, in which only the nitronyl nitroxide groups are considered. Cyano groups of **A** and **C** are replaced by hydrogen atoms in the pairs $\mathbf{A}_2$ and $\mathbf{C}_2$, whereas cyanophenyl groups are replaced by hydrogen atoms in the pairs $\mathbf{A}_3$ and $\mathbf{C}_3$. In the pairs, $\mathbf{A}_4$ and $\mathbf{C}_4$, methyl groups of **A** and **C** are replaced by hydrogen atoms.

Table 3. 2 shows J_{ab} values calculated for the simplified models by several computational methods. Large and positive values of J_{ab} were obtained by use of INDO and DFT methods for the model pairs, $\mathbf{A}_2$, $\mathbf{A}_4$, $\mathbf{C}_2$ and $\mathbf{C}_4$. These results indicate that cyanophenyl group contributes dominantly to the intermolecular ferromagnetic interaction in the pairs, **A** and **C**. Particularly the phenyl group seems to be important for the ferromagnetic interaction in the pairs, **A** and **C**. Direct interaction between nitronyl nitroxide groups is negligible as shown in the pair models, $\mathbf{A}_1$ and $\mathbf{C}_1$. It is note worthy that J_{ab} values calculated by UNO CASCI {2, 2} and UNO CASSCF {2, 2} methods predominantly reflect the direct SOMO-SOMO interactions, KE and PE terms in Eq. 1. Therefore, the ferromagnetic interactions in **A** and **C** pairs are classified into Case III.

3. 4. 2 Simplified models for the pairs **BI**, **BII** and **D**

The inter-sheet magnetic interaction was estimated by use of simplified models

of the pairs **BI** (**1**-**4**) and **BII** (**2**-**3**) shown in **Fig. 3. 1** and **Fig. 3. 4**. Model pairs $\mathbf{BI}_1$ and $\mathbf{BII}_1$ consist of two nitronyl nitroxide molecules. In $\mathbf{BI}_2$ and $\mathbf{BII}_2$ only the interacting components of *p*-CNPNN molecules are retained and terminal components are simplified, *i. e.*, atoms located between the two nitronyl nitroxide groups of the pairs are maintained.

Table 3. 3 shows that the direct interactions are negligible in the models $\mathbf{BI}_1$, $\mathbf{BII}_1$, $\mathbf{BI}_2$ and $\mathbf{BII}_2$ as indicated by UNO CASCI {2, 2} and UNO CASSCF {2, 2} methods. INDO method revealed a small antiferromagnetic interaction for model $\mathbf{BII}_2$ as in the case of **BII**. On the other hand, model $\mathbf{BI}_2$ have small ferromagnetic interaction as in the case of **BI**. These results suggest a weak magnetic interaction between the molecular sheets parallel to the *ac*-plane.

Finally the magnetic interaction in the pair **D** was examined. Simplified model pair $\mathbf{D}_1$ consists of two nitronyl nitroxide molecules, whereas hydrogen atoms of $\mathbf{D}_1$ were replaced by cyanophenyl groups in $\mathbf{D}_2$ as shown in **Fig. 3. 4**.

INDO, three types of DFT methods, UNO CASCI {2, 2} and UNO CASSCF {2, 2} gave negligibly small J_{ab} values, indicating the negligible magnetic interaction in the pair **D** compared with the ferromagnetic interactions in the pairs, **A** and **C**. Therefore, the ferromagnetic interaction in the molecular sheet parallel to the *ac*-plane is concluded to be quasi-square-lattice type, in accord with the experiment [36].

3. 5 Conclusion

Characteristic magnetic interaction in *p*-CNPNN crystal was studied by semiempirical and *ab initio* calculations. Effective exchange integral J_{ab} was calculated for several pair molecules in the crystal. Quasi-two-dimensional ferromagnetic interaction in the molecular sheet parallel to the *ac*-plane was revealed. The phenyl group of *p*-CNPNN molecule plays a dominant role for the ferromagnetic interaction. The methyl and cyano groups slightly contribute to cancel the ferromagnetic interaction. J_{ab} values, 0.541 and 0.301 cm^{-1}, in the molecular sheet (Table I) obtained by INDO method may be compared with the experimental one ($J = 0.52\ cm^{-1}$) derived from magnetic susceptibility measurement by assuming the square-lattice Heisenberg model [36].

Table 3. 1 J_{ab} values for the pairs of *p*-CNPNN molecules shown in **Fig. 3. 1**.

	J_{ab} /cm^{-1}				
methods	**A**	**BI**	**BII**	**C**	**D**
INDO/UHF	0.541	0.003	-0.003	0.301	0.000
UBLYP/4-31G	1.629	0.002	-0.002	0.884	
UB2LYP/4-31G	2.302	0.015	-0.009	0.705	
UB3LYP/4-31G	1.736	0.002	-0.004	0.827	
experiment (square-lattice Heisenberg model)[9]	0.52				

Table 3. 2 J_{ab} values for the simplified models of pairs, **A** and **C**, shown in **Fig. 3. 1**.

	J_{ab} /cm^{-1}				
methods	**A**	$\mathbf{A}_1$	$\mathbf{A}_2$	$\mathbf{A}_3$	$\mathbf{A}_4$
INDO/UHF	0.541	0.000	0.643	0.000	0.636
UBLYP/4-31G	1.629				1.659
UB2LYP/4-31G	2.302				2.947
UB3LYP/4-31G	1.736				2.017
UNO CASCI{2, 2}[a)]		0.000			0.019
UNO CASSCF{2, 2}[a)]		0.000			

a) 4-31G basis set was used.

	J_{ab} /cm^{-1}				
methods	**C**	$\mathbf{C}_1$	$\mathbf{C}_2$	$\mathbf{C}_3$	$\mathbf{C}_4$
INDO/UHF	0.301	0.000	0.331	0.000	0.374
UBLYP/4-31G	0.884				0.830
UB2LYP/4-31G	0.705				1.185
UB3LYP/4-31G					0.924
UNO CASCI{2, 2}[a)]		0.000			0.005
UNO CASSCF{2, 2}[a)]		0.000			

a) 4-31G basis set was used.

Table 3. 3 J_{ab} values for the simplified models of the pairs, **B** and **D**.

	J_{ab} /cm^{-1}								
methods	**BI**	**BI$_1$**	**BI$_2$**	**BII**	**BII$_1$**	**BII$_2$**	**D**	**D$_1$**	**D$_2$**
INDO/UHF	0.003	0.000	0.003	-0.003	0.000	-0.003	0.000	0.000	0.000
UBLYP/4-31G	0.002			-0.002					
UB2LYP/4-31G	0.015			-0.009					
UB3LYP/4-31G	0.002			-0.004					
UNO CASCI{2, 2}[a)]		0.000	0.000		0.000	0.000		-0.001	-0.001
UNO CASSCF{2, 2}[a)]		0.000	0.000		0.000	0.000			0.000

a) 4-31G basis set was used.

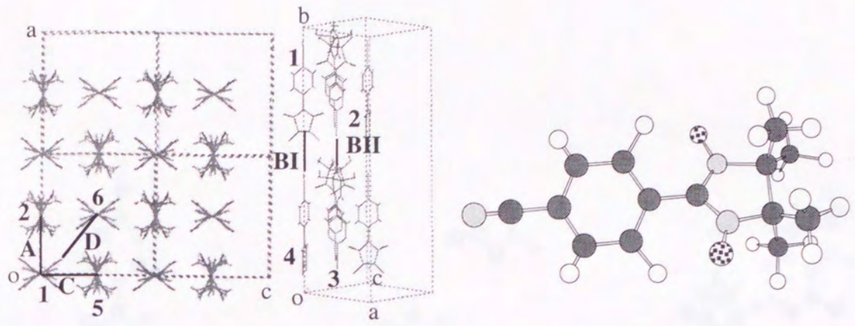

(a) (b)

Figure 3. 1 Crystal structure (a) and molecular geometry (b) of *p*-CNPNN.

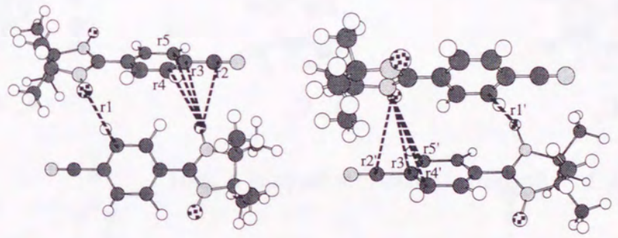

along a-axis (**A**) along c-axis (**C**)

r1: 3.49Å r2: 3.47Å r3: 3.47Å r4: 3.55Å r5: 4.13Å
r1': 3.45Å r2': 3.466Å r3': 3.433Å r4': 3.81Å r5': 3.82Å

Figure 3. 2 Pairs of *p*-CNPNN molecules along the a- and c-axes.

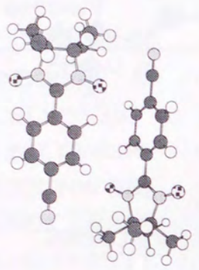

A, C

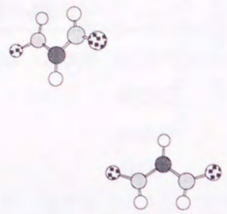

A_1, C_1

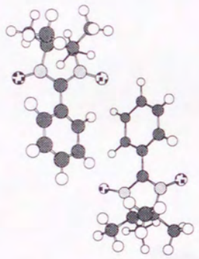

A_2, C_2

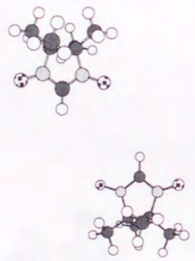

A_3, C_3

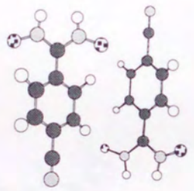

A_4, C_4

Figure 3. 3 Simplified models for the pairs **A** and **C**.

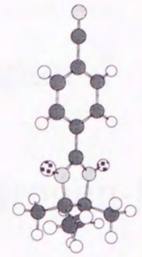

BI, BII

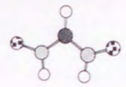

BI_1, BII_1

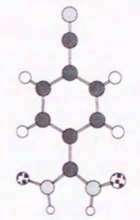

BI_2, BII_2

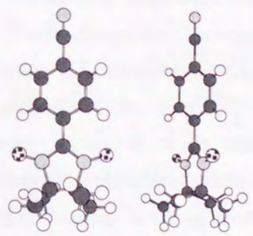

D

D_1

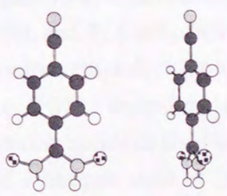

D_2

Figure 3. 4 Simplified models of the pairs, **B** and **D**

Chapter 4

Hydrogen-bonded Nitronyl Nitroxide

4. 1 Introduction

Several calculations suggested that molecular assembly and intermolecular magnetic interactions may be controlled by intermolecular hydrogen bonds [17, 21]. The purpose of this chapter is to elucidation of intermolecular magnetic interactions of hydrogen-bonded pairs of organic radical crystals.

Recently, Sugawara and co-worker reported the magnetic behavior of α and β phase of 2', 5'-dihydroxyphenyl nitronyl nitroxide (2-(2', 5'-dihydroxyphenyl)-4, 4, 5, 5-tetramethyl-4, 5-dihydro-1*H*-imidazolyl-1-oxy-3-oxide, abbreviated as HQNN), and 3', 5'-dihydroxyphenyl nitronyl nitroxide (2-(3', 5'-dihydroxyphenyl)-4, 4, 5, 5-tetramethyl-4, 5-dihydro-1*H*-imidazolyl-1-oxy-3-oxide, abbreviated as RSNN) [37-39]. α-HQNN crystal undergoes a ferromagnetic phase transition at low temperature and intermolecular hydrogen bond is formed between oxygen atom of nitronyl nitroxide (NN) group and hydrogen atom of hydroxyl group. The temperature dependence of the magnetic susceptibility of this crystal was well reproduced by the ST model with the $J/k_b = +0.65\ cm^{-1}$. The intermolecular hydrogen bond is also formed in β-HQNN crystal, the hydrogen bonded chain runs along the *a* axis. The experimental plot for this crystal indicated exhibiting an antiferromagnetic interaction, and the plot was found to be best fitted by the ST model with ferromagnetic interaction of $J/k_b = +3.5\ cm^{-1}$. In RSNN crystal, a double intermolecular hydrogen bond is formed between the oxygen atom of nitronyl nitroxide (NN) group and the hydrogen atom of the hydroxyl group. This crystal undergoes a ferromagnetic intrapair interactions and an antiferromagnetic interpair interactions at low temperature. The plot for RSNN was reproduced by the ST model with

the ferromagnetic interaction of $J/k_b = +7.0\ cm^{-1}$.

It is particularly interesting and important to investigate theoretically the origin of the magnetic interaction in these crystal to understand the role of the hydrogen bonds. In this chapter the author reports the molecular orbital (MO) calculations to determine the intermolecular effective exchange integrals for several pair models whose geometries are extracted from the X-ray structure in the crystal.

4. 2 α-HQNN

4. 2. 1 Crystal structure

Fig. 4. 1(a) illustrates the packing arrangement of HQNN molecules (**1** through **5**) in the crystal and **Fig. 4. 1**(b) shows the geometry of a HQNN molecule with numbering scheme. The following features are remarked from the X-ray structure analysis.

(i) The hydroxyl group (O(1')H) forms a strong intramolecular hydrogen bond (O(1')...O(1) : 2.507Å) with one of the NO groups (N(1)-O(1)). This hydrogen bond induces a remarkable deformation of the NN group. The bond lengths of N(1)-O(1) and C(1)-N(1) at the hydrogen-bonded side are 1.303 and 1.332Å, respectively, whereas those of N(2)-O(2) and C(1)-N(2) at the opposite side are 1.272 and 1.367Å, respectively.

(ii) The hydroxyl group O(1')H of molecule **1** also participates in an intermolecular hydrogen bond with the O(2')H group of the translated molecule (**2**) along the c-axis, resulting in a one-dimensional hydrogen-bonded chain along the c-axis. A similar one-dimensional chain runs parallel to the previous one related with inversion symmetry between the two facing molecules. Two NN groups related by inversion symmetry are located in proximity with the short NO...ON of distance 3.159Å presumably due to two bifurcated hydrogen bonds between the two hydroxyl groups as shown in **Fig. 4. 2** B. These two arrays form a herringbone type structure.

The theoretical calculations were performed for all possible pairs, **A** (**1**-**2**), **B** (**1**-**3**), **C** (**1**-**4**), **D** (**1**-**5**) and **E** (**2**-**5**) by use of the semiempirical INDO and DFT method [24]. *Ab initio* UNO CASCI and CASSCF calculations [23, 24] were also carried out for simplified pair models.

4. 2. 2 Calculations for HQNN pair molecules

In order to elucidate the ferromagnetic property observed for the α-HQNN crystal, the author carried out semiempirical INDO and DFT calculations for five pair models of HQNN molecules. **Table 4. 1** shows the calculated J_{ab} values. Semiempirical INDO and DFT methods can reproduce qualitatively the experimental results. The pair **B** in **Fig. 4. 2** which has bifurcated hydrogen bonds (OH...OH and OH...O-N) shows the largest J_{ab}. J_{ab} values of other pairs are smaller than a half of J_{ab} for **B**. One of the origins of this significant feature

may be attributed to the dependence of J_{ab} on the interatomic distance (R). The J_{ab} decreases exponentially with the increase of R [17, 18]. Other contributions will be discussed later.

4. 2. 3 Calculations for the simplified pair models

To study possible mechanisms of the ferromagnetic interaction in the α-HQNN crystal in detail, theoretical calculations with various methods were performed for the several simplified pair models.

(A) Simplified models for the pair **A**

The simplified pair models, $\mathbf{A}_1$ through $\mathbf{A}_5$ shown in **Fig. 4. 3** were considered. The model $\mathbf{A}_1$ consists of two nitronyl nitroxides (ON-C-NO) and the model $\mathbf{A}_2$ consists of two nitronyl nitroxides with hydroquinone moieties. In the model $\mathbf{A}_3$ hydroquinone moieties of **A** are replaced by hydrogen atoms, in $\mathbf{A}_4$ hydroxyl groups of **A** are replaced by hydrogen atoms and in $\mathbf{A}_5$ one of the methyl groups of **A** is replaced by hydrogen atom. The methyl group locates in close proximity to adjacent N-O group. Positions of the substituted hydrogen atoms were optimized by PM3 (semiempirical method). **Table 4. 2** shows the calculated J_{ab} values and gives the following results.

(i) INDO and DFT calculations suggest that the methyl group in close proximity to adjacent N-O group is significant for the intermolecular ferromagnetic interaction (positive J_{ab} value). Replacement of the methyl group by hydrogen atom leads to very weak antiferromagnetic interaction in $\mathbf{A}_5$ by INDO, UBLYP and UB3LYP.

(ii) UNO CASCI {2, 2} and UNO CASSCF {2, 2} methods by use of two active UNOs and two unpaired electrons give very small positive J_{ab} values, suggesting a small contribution of direct SOMO-SOMO coupling to the ferromagnetic interaction.

(B) Simplified models for the pair **B**

J_{ab} values were calculated for the simplified pair models, $\mathbf{B}_1$ through $\mathbf{B}_5$ shown in **Fig. 4. 4**. The models $\mathbf{B}_1$ and $\mathbf{B}_2$ are simplified in the same way as $\mathbf{A}_1$ and $\mathbf{A}_2$. For the model $\mathbf{B}_3$, hydroxyl groups linked to N-O radical group by bifurcated hydrogen bond in model **B** are replaced by hydrogen atoms. In the model $\mathbf{B}_4$ hydroxy ethylene groups linked to opposite N-O radical group by bifurcated hydrogen bond are attached to $\mathbf{B}_1$. The hydroxyl groups of $\mathbf{B}_4$ are replaced by hydrogen atoms in $\mathbf{B}_5$. **Table 4. 3** shows the J_{ab} values obtained by several computational methods. The following conclusions were drawn from **Table 4. 3**:

(i) All the methods give positive J_{ab} values for pairs $\mathbf{B}_2$ and $\mathbf{B}_4$, which have intermolecular hydrogen bonds, and negative J_{ab} values for pairs $\mathbf{B}_1$, $\mathbf{B}_3$ and $\mathbf{B}_5$, which do not have intermolecular hydrogen bonds. These results indicate that the intermolecular hydrogen bond plays an important role for the ferromagnetic interaction in the pair **B**.

(ii) Comparisons between *ab initio* and INDO results show that semiempirical INDO method gives smaller J_{ab} values than those of DFT methods.

Table 4. 3 suggests that the hydrogen bonds in model **B** play a dominant role for the intermolecular ferromagnetic interaction. For investigating this interaction more precisely

the hydroxyl groups of the model $\mathbf{B}_4$ were rotated simultaneously about the **Table 4. 4** J_{ab} vs. rotation angle of OH group respective C-O axis with rotation angle R (**Fig. 4. 5**). J_{ab} value was calculated by INDO method for every 30° of the rotation angle. **Table 4. 4** and **Fig. 4. 6** shows the J_{ab} values for the pair $\mathbf{B}_4$ with different angles. When the rotation angle is in between 120° and 240°, the J_{ab} value turns into negative. It is noted that break of the hydrogen bonding in the pair $\mathbf{B}_4$ leads to antiferromagnetic interaction.

(C) Simplified models for the pairs **C**, **D** and **E**

The simplified models $\mathbf{C}_1$, $\mathbf{D}_1$ and $\mathbf{E}_1$ shown in **Figure 4. 7** were considered. **Table 4. 5** shows the calculated J_{ab} values. These pairs are simplified in the same way as $\mathbf{A}_1$. All J_{ab} values calculated by the INDO method are small compared with the pairs **A** and **B** because of the long intermolecular distances.

4. 3 β-HQNN

4. 3. 1 Crystal structure

Fig. 4. 8 illustrates the packing arrangement of HQNN molecules (**1** through **4**) in the crystal. The following features are remarked from the X-ray structure analysis.

(i) The phenolic hydroxy group (O(1')H) shown in **Fig. 4. 1** (b) participates in the intramolecular hydrogen bond with the oxygen atom of the NN group (O(1')...O(1) : 2.616Å). The intramolecular distance is slightly longer than that of α-HQNN. As a result, the degree of bond alternation in the NN group is lessened to some extent, N(1)-O(1) and C(1)-N(1) at the hydrogen bonded side are 1.296 and 1.350Å, respectively, whereas those of N(2)-O(2) and C(1)-N(2) at the opposite side are 1.279 and 1.364Å, respectively.

(ii) The hydroxyl group O(2')H of molecule **1** also forms the intermolecular hydrogen bond with the oxygen atom O(2) of the NN group which does not participate in the intramolecular hydrogen bond in adjacent molecule **2** as **Fig. 4. 9**. The intermolecular distance between hydroxyl group and the NN group which forms intermolecular hydrogen bond is 2.777Å. The hydrogen bonded chain runs in a zigzag manner along the a-axis, and such chains stack along the c-axis. The HQNN molecules in the stack (**1** and **3**) are dimerized as shown Fig. **4. 8**. Within the dimer, HQNN has the inversion symmetry and the distance between two NN groups O(2)...C(1) is 3. 781Å. The distance between molecules **1** and **4** is 4.287Å.

The theoretical calculations were performed for all possible pairs, **A** (**1**-**2**), **B** (**1**-**3**), and **C** (**1**-**4**) by use of the semiempirical INDO, UBLYP, UB2LYP and UB3LYP methods [24]. UNO CASCI and CASSCF [23, 24] calculations are carried out for simplified models.

4. 3. 2 Calculations for HQNN pair molecules

In order to elucidate the magnetic property observed for the HQNN crystal, we carried

out semiempirical INDO and DFT calculations for three pair models of HQNN molecules. **Table 4. 6** shows the calculated J_{ab} values. Semiempirical INDO, UB2LYP/4-31G and UB3LYP/4-31G methods can reproduce the experimental results, qualitatively. The pair **B** in **Fig. 4. 8** which has short distance of two NN groups (NO…C) shows the largest J_{ab}. J_{ab} values of other pairs are smaller than a half of J_{ab} for **B**. INDO method gave smaller J_{ab} values than UB2LYP and UB3LYP methods. J_{ab} values of pair **A** which has the intermolecular hydrogen bond are slightly larger than the pair **C**. One of the origins of this significant feature may be attributed to the dependence of J_{ab} on the interatomic distance (R). The J_{ab} decreases exponentially with the increase of R [17, 18]. Other contributions will be discussed later.

4. 3. 3 Calculations for the simplified pair models

To study possible mechanisms of the magnetic interaction in the β-HQNN crystal in detail, theoretical calculations with various methods were performed for the several simplified pair models.

(A) Simplified models for the pair **A**

The simplified models $\mathbf{A}_1$ through $\mathbf{A}_5$ shown in **Fig. 4. 10** were considered. The model $\mathbf{A}_1$ consists of two nitronyl nitroxides (ON-C-NO), and the model $\mathbf{A}_2$ consists two nitronyl nitroxides and one hydroquinone moiety which is linked to the N-O radical group by the intermolecular hydrogen bond. In the model $\mathbf{A}_3$ the hydroxyl group participates in hydrogen bond in model $\mathbf{A}_1$ is replaced by hydrogen atom. In the model $\mathbf{A}_4$ and $\mathbf{A}_5$, hydroquinone moieties of $\mathbf{A}_1$ and $\mathbf{A}_2$ are replaced by 1-hydroxy butadiene group without break the intermolecular hydrogen bond, respectively. **Table 4. 7** shows the J_{ab} values obtained by several computational methods. The following conclusions were drawn from **Table 4. 7**:

(i) UB2LYP/4-31G, UNO CASCI{10, 10} and UNO CASSCF {10, 10} methods give positive J_{ab} values for model $\mathbf{A}_2$ and $\mathbf{A}_4$, which have intermolecular hydrogen bonds, and negative J_{ab} values for model $\mathbf{A}_5$ which does not have intermolecular hydrogen bonds. The model $\mathbf{A}_3$ and $\mathbf{A}_5$ have smaller J_{ab} values than $\mathbf{A}_2$ and $\mathbf{A}_4$ by INDO method. These results indicate that the intermolecular hydrogen bond plays an important role for the magnetic interaction in the pair **A**.

(ii) Comparisons among INDO, DFT and UNO CASSCF results show that semiempirical INDO method and UNO CASSCF method gives reasonable J_{ab} for the models which have hydrogen bonds. Though the J_{ab} value calculated by UB2LYP/4-31G method is reasonable, UB3LYP/4-31G and UBLYP/4-31G methods do not give reasonable J_{ab} values.

Table 4. 7 suggests that the hydrogen bonds in model **A** play a dominant role for the intermolecular ferromagnetic interaction. For investigating this interaction more precisely, the hydroxyl groups of the model $\mathbf{A}_4$ were rotated simultaneously about the respective C-O axis with rotation angle θ (**Fig. 4. 5**) same as α-HQNN in section 4. 2. J_{ab} value was calculated by INDO method for every 30° of the rotation angle. **Table 4. 8** and **Fig. 4. 11** shows the J_{ab} values for the model $\mathbf{A}_4$ with different angles. When the rotation angle of the

model $\mathbf{A}_4$ is in 120° and between 270° and 330°, the J_{ab} value turns into negative. It is noted that break of the hydrogen bonding in the pair $\mathbf{A}_4$ leads to antiferromagnetic interaction.

(B) Simplified models for the pair **B** and **C**

J_{ab} values were calculated for the simplified pair models, $\mathbf{B}_1$ and $\mathbf{C}_1$ shown in **Fig. 4. 12.** The models $\mathbf{B}_1$ and $\mathbf{C}_1$ is simplified in the same way as $\mathbf{A}_1$. **Table 4. 9** shows the J_{ab} values obtained by several computational methods. The following conclusions were drawn from **Table 4. 9**:

(i) All the methods give positive J_{ab} values for pairs $\mathbf{B}_1$ and $\mathbf{C}_1$. These results indicate that the ON-C-NO moieties play important roles for the magnetic interaction in the pair **B** and **C**.

(ii) UNO CASCI {2, 2} methods by using of two active UNOs and two unpaired electrons give reasonable J_{ab} values, suggesting large contribution of direct SOMO-SOMO coupling to the ferromagnetic interaction.

4. 4 RSNN

4. 4. 1 Crystal structure

Fig. 4. 13 (a) illustrates the packing arrangement of RSNN molecules (**1** through **5**) in the crystal. **Fig. 4. 13** (b) shows the geometry of a RSNN molecule with the numbering scheme. The following features are remarked from the X-ray structure analysis.

(i) Compared with α-HQNN, RSNN have no intramolecular hydrogen bond. Therefore, there is no bond alternation in the NN group, and the twist angle between the NN group and the phenyl ring (23.3 degrees) is smaller than that of HQNN.

(ii) The hydroxyl groups O(1')H and O(2')H of molecule **1**, **4** and **5** also participate in intermolecular hydrogen bonds with the oxygen atoms of NN groups of two adjacent molecules at the both sites, resulting in a one-dimensional hydrogen-bonded chain along the diagonal of ac-plane, as shown in **Fig. 4. 14.** The distances of the hydrogen bonds are the same on one side of the molecule (d_1 =1.84Å; between **1** and **4**), they are slightly longer on the other side (d2 = 1.89Å; between **1** and **5**). Two types of similar one-dimensional chains run parallel to the previous one related with inversion symmetry between the two facing molecules. The oxygen of the NN group (O(2)) is located close to the C(1) of the NN group of the dimeric counterpart with the intermolecular distance of 3.727Å as depicted in **1-2** of **Fig. 4. 13** (a). Since the overlap of the NN groups between pairs 1-3 is poor, the NN groups are located remote form each other.

The theoretical calculations were performed for all the possible pairs, **A**(**1**-**2**), **B** (**1**-**3**), **C** (**1**-**4**) and **D** (**1**-**5**), by using of the INDO, UBLYP, UB2LYP and UB3LYP methods [24]. *Ab initio* UNO CASCI and CASSCF calculations [23, 24] were also carried out for simplified pair models (see Figs 3, 4 and 6).

4. 4. 2 Calculations for RSNN pair molecules

In order to elucidate the magnetic property observed for the RSNN crystal, we carried out semiempirical INDO and *ab initio* calculations for four pair models of RSNN molecules. **Table 4. 10** shows the calculated J_{ab} values. Semiempirical INDO and DFT methods can reproduce qualitatively the experimental results for the pair **A** and **B**. The pair **A** which has close contact between each NN groups (N-O…C) shows the largest J_{ab}. J_{ab} values of the pair **B** are slightly smaller than those of the pair **A**. On the other hand, the pair **C** and **D** have small $|J_{ab}|$ values in comparison with those of the pair **A** and **B**. One of the origins of this significant feature may be attributed to the dependence of J_{ab} on the interatomic distance (R). The J_{ab} decreases exponentially with the increase of R [17, 18]. Other contributions will be discussed later.

4. 4. 3 Calculations for the simplified pair models

To study mechanisms of the magnetic interaction in RSNN crystal in detail, theoretical calculations with various methods are performed for the several simplified pair models.

(A) Simplified models for the pair **A**

The simplified pair models, $\mathbf{A}_1$ shown in **Fig. 4. 15** were considered. The model $\mathbf{A}_1$ consists of two nitronyl nitroxides (ON-C-NO). Positions of the substituted hydrogen atoms were optimized by PM3 (semiempirical method). **Table 4. 11** shows the calculated J_{ab} values and gives the following results.

(i) INDO and DFT calculations for model $\mathbf{A}_1$ can reproduce qualitatively the result of the full pair **A**. It suggests that NN groups of this pair are significant for the intermolecular ferromagnetic interaction (positive J_{ab} value).

(ii) UNO CASCI {2, 2} and UNO CASSCF {2, 2} methods by using of two active UNOs and two unpaired electrons give positive J_{ab} values, suggesting large contribution of direct SOMO-SOMO coupling to the ferromagnetic interaction.

(B) Simplified models for the pair **B**

J_{ab} values were calculated for the simplified pair models, $\mathbf{B}_1$ through $\mathbf{B}_3$ shown in **Fig. 4. 16**. The models $\mathbf{B}_1$ is simplified in the same way as $\mathbf{A}_1$. The model $\mathbf{B}_2$ consists of two nitronyl nitroxides with dihydroxyphenyl moieties, and the hydroxyl groups of $\mathbf{B}_2$ are replaced by hydrogen atoms in $\mathbf{B}_3$. **Table 4. 12** shows the J_{ab} values obtained by several computational methods. The following conclusions were drawn from **Table 4. 12**:

(i) All the methods give positive J_{ab} values for pairs $\mathbf{B}_2$ and $\mathbf{B}_3$, which have phenyl rings, and negligible J_{ab} values for pair $\mathbf{B}_1$, which does not have phenyl rings. These results indicate that the phenyl ring plays an important role for the ferromagnetic interaction in the pair **B**, and NN groups scarcely contribute to positive J_{ab} values.

(ii) Comparisons between the J_{ab} values of the model $\mathbf{B}_2$ and that of the model $\mathbf{B}_3$ show that hydroxyl groups do not play an important role for the intermolecular interaction in the pair **B**.

(C) Simplified models for the pairs **C** and **D**

The simplified models $\mathbf{C}_1$ through $\mathbf{C}_4$ and $\mathbf{D}_1$ through $\mathbf{D}_4$ shown in **Fig. 4. 17** are considered. **Table 4. 13** shows calculated J_{ab} values. The model $\mathbf{C}_1$ and $\mathbf{D}_1$ are simplified in the same way as $\mathbf{A}_1$, and the model $\mathbf{C}_2$ and $\mathbf{D}_2$ are simplified in the same way as $\mathbf{B}_2$. For the model $\mathbf{C}_3$ and $\mathbf{D}_3$, the hydroxyl groups linked to N-O radical group by hydrogen bond in $\mathbf{C}_2$ and $\mathbf{D}_2$ are replaced by hydrogen atoms. In the model $\mathbf{C}_4$ and $\mathbf{D}_4$, hydroxy butadiene groups linked to opposite N-O radical group by hydrogen bond are attached to $\mathbf{C}_1$ and $\mathbf{D}_1$.

(i) INDO and UNO CASSCF methods give negative J_{ab} values for model $\mathbf{C}_2$ and $\mathbf{C}_4$, which have intermolecular hydrogen bonds, and positive J_{ab} values for model $\mathbf{C}_3$ which does not have intermolecular hydrogen bonds. These results indicate that the intermolecular hydrogen bond plays an important role for the magnetic interaction in the pair **C**.

(ii) The absolute values of J_{ab} for the model $\mathbf{D}_2$ make a difference form that of $\mathbf{D}_4$. It suggests that the intermolecular hydrogen bonds are significant for the intermolecular interaction in pair **D**.

(iii) Comparisons among INDO, UBLYP/4-31G and UNO CASSCF results show that semiempirical INDO method gives reasonable J_{ab} values for all models, and UNO CASSCF method gives reasonable J_{ab} for the models which have phenyl rings.

(iv) All J_{ab} values of these models calculated by the INDO method are smaller than those of pairs **A** and **B**.

Table IV suggests that the hydrogen bonds in model **C** and **D** play a dominant role for the intermolecular ferromagnetic interaction. For investigating this interaction more precisely, the hydroxyl groups of the model $\mathbf{C}_4$ and $\mathbf{D}_4$ were rotated simultaneously about the respective C-O axis with rotation angle θ (**Fig. 4. 5**). J_{ab} value was calculated by INDO method for every 30° of the rotation angle. **Fig. 4. 18** and **Table 4. 14** shows the J_{ab} values for the model $\mathbf{C}_4$ and $\mathbf{D}_4$ with different angles. When the rotation angle of the model $\mathbf{C}_4$ is in between 30° and 240°, the J_{ab} value turns into positive. Regarding the model $\mathbf{D}_4$, J_{ab} value turns into negative with rotation angle 60°. It is noted that break of the hydrogen bonding in the model $\mathbf{C}_4$ leads to ferromagnetic interaction, and in the model $\mathbf{D}_4$ that leads to antiferromagnetic interaction. For the model $\mathbf{C}_4$, the rotation of hydroxyl group changes more sensitively the sign of J_{ab} values than the model $\mathbf{D}_4$. This implies that the pressure effect is an interesting experimental task in the future.

4. 5 Conclusion

4. 5. 1 α-HQNN

Ab initio and semiempirical calculations indicate that magnetic interaction through the

bifurcated hydrogen bonds in the pair **B** is dominant for the ferromagnetic property of α-HQNN crystal. The J_{ab} value of the pair **B** was almost three times larger than that of other pairs (**A**, **C**, **D** and **E**). The pair **B** has bifurcated hydrogen bonds and the simplified models of **B** without hydrogen bonds show negative J_{ab} values. The UNO CASSCF method with two SOMOs and two unpaired electrons {2, 2} demonstrates that the SOMO-SOMO potential exchange (PE) interaction is not important for the ferromagnetic interaction in the pair **B**.

The J_{ab} value of the pair **A** was positive in the case that all the methyl groups remain. Close contact between the methyl group and adjacent N-O radical group is important for the intermolecular ferromagnetic interaction rather than hydrogen bonding in the pair **A**.

4. 5. 2 β-HQNN

The J_{ab} values of the pair **B** were much larger than that of other pairs (**A** and **C**). The UNO CASCI {2, 2} and UNO CASSCF {2, 2} results show that the SOMO-SOMO potential exchange (PE) interaction is dominant for the intermolecular ferromagnetic interactions of pair **B** and **C**.

The pair **A** has hydrogen bonds and the simplified models of **A** without hydrogen bonds show smaller J_{ab} values than models with hydrogen bonds. The UNO CASCI {2, 2} demonstrates that the SOMO-SOMO potential exchange (PE) interaction is not important for the magnetic interaction in the pair **A**.

4. 5. 3 RSNN

The J_{ab} values of the pair **A** were much larger than that of pair **C** and **D**. The UNO CASSCF {2, 2} result shows that the SOMO-SOMO potential exchange (PE) interaction is dominant for the intermolecular ferromagnetic interactions of pair **A**, while the through-bond interaction is predominant in the pair **B**.

Ab initio and semiempirical calculations indicate that the hydrogen bonds are dominant for the intermolecular magnetic interactions. The J_{ab} values of the simplified models without hydrogen bond are much different from the full pair **C** and **D**. The UNO CASSCF method with two SOMOs and two unpaired electrons {2, 2} demonstrates that the SOMO-SOMO potential exchange (PE) interaction is not important for the ferromagnetic interaction in the pair **C** and **D**.

4. 5. 4 Role of hydrogen bond

The simplified model $\mathbf{B}_4$ of α-HQNN, the model $\mathbf{A}_4$ of β-HQNN, The model $\mathbf{C}_4$ and $\mathbf{D}_4$ of RSNN gave a useful guide for understanding of the role of the hydrogen bond: the sign of J_{ab} value depends on the rotation angle of the hydroxyl groups.

The J_{ab} values of β-HQNN and RSNN change more sensitively the model $\mathbf{B}_4$ of α-HQNN around 0°. In the RSNN, the dependence of J_{ab} values on rotation angles of the

model C_4 was larger than that of D_4. Assuming that the rotation of the hydroxyl group is caused by the pressure effect, the influence of this effects for the β-HQNN and RSNN crystals are expected to be larger than that of α-HQNN.

Table 4. 1 J_{ab} values for the pairs shown in **Fig. 4. 1**.

	J_{ab} /cm^{-1}				
methods	**A**	**B**	**C**	**D**	**E**
INDO/UHF	0.013	0.041	-0.003	0.010	0.008
UBLYP/4-31G	0.145	1.396	0.114	0.033	0.033
UB2LYP/4-31G	0.156	1.409	0.081	0.072	0.162
UB3LYP/4-31G	0.178	1.464	0.122	0.037	0.108

Table 4. 2 J_{ab} values for the simplified models of the pair **A**.

	J_{ab} /cm^{-1}					
methods	**A**	**A$_1$**	**A$_2$**	**A$_3$**	**A$_4$**	**A$_5$**
INDO/UHF	0.013	0.000	-0.001	0.009	0.005	-0.004
UBLYP/4-31G	0.145		-0.099	0.129		
UB2LYP/4-31G	0.156		0.009	0.127		
UB3LYP/4-31G	0.178		-0.011	0.129		
UNO CASCI{2, 2}[a)]		0.003	0.006			
UNO CASSCF{2, 2}[a)]		0.002	0.002			

a) 4-31G basis set was used.

Table 4. 3 J_{ab} values for the simplified models for the pair **B**.

	J_{ab} /cm^{-1}					
methods	**B**	**B$_1$**	**B$_2$**	**B$_3$**	**B$_4$**	**B$_5$**
INDO/UHF	0.041	-0.030	0.121	-0.138	0.141	-0.505
UBLYP/4-31G	1.396				3.862	-7.218
UB2LYP/4-31G	1.409				3.430	-5.973
UB3LYP/4-31G	1.464				3.900	-4.641
UNO CASCI{2, 2}[a)]		-1.554	0.142		0.148	-1.002
UNO CASSCF{2, 2}[a)]		-1.036	0.014		0.016	-1.848

a) 4-31G basis set was used.

Table 4. 4 J_{ab} vs. rotation angle of OH group.

θ	J_{ab} (INDO)	θ	J_{ab} (INDO)
0°	0.141	180°	-0.545
30°	1.179	210°	-0.530
60°	7.088	240°	-0.061
90°	4.339	270°	4.288
120°	-0.055	300°	7.028
150°	-0.529	330°	1.172

Table 4. 5 J_{ab} for the simplified models for the pairs **C**, **D** and **E**

	J_{ab} /cm^{-1}					
methods	**C**	**C$_1$**	**D**	**D$_1$**	**E**	**E$_1$**
INDO/UHF	-0.003	0.000	0.010	0.000	0.008	0.000
UBLYP/4-31G	0.114		0.033		0.033	
UB2LYP/4-31G	0.081		0.072		0.162	
UB3LYP/4-31G	0.122		0.037		0.108	
UNO CASCI{2,2}[a)]		0.000		0.000		0.000
UNO CASSCF{2,2}[a)]		0.000				

a) 4-31G basis set was used.

Table 4. 6 J_{ab} values for the pairs shown in **Fig. 4. 8**.

	J_{ab} /cm^{-1}		
methods	**A**	**B**	**C**
INDO/UHF	0.102	0.959	0.065
UBLYP/4-31G	0.000	-0.585	0.191
UB2LYP/4-31G	0.544	7.243	0.252
UB3LYP/4-31G	0.279	4.633	0.198

Table 4. 7 J_{ab} values for the simplified models of the pair **A**.

	J_{ab} /cm^{-1}					
methods	**A**	**A$_1$**	**A$_2$**	**A$_3$**	**A$_4$**	**A$_5$**
INDO/UHF	0.102	0.000	0.112	0.012	0.151	0.032
UBLYP/4-31G	0.000					-0.090
UB2LYP/4-31G	0.544				0.944	-0.723
UB3LYP/4-31G	0.279				-0.006	-0.250
UNO CASCI{2, 2}[a)]					0.004	0.004
UNO CASCI {10, 10}[a)]					0.109	-0.049
UNO CASSCF {10, 10}[a)]					0.061	-0.004

a) 4-31G basis set was used.

Table 4. 8 J_{ab} vs. rotation angle of OH group.

θ	J_{ab} (INDO)	θ	J_{ab} (INDO)
0°	0.102	180°	0.045
30°	0.096	210°	0.044
60°	0.147	240°	0.021
90°	0.039	270°	-0.049
120°	-0.003	300°	-0.541
150°	0.014	330°	-0.475

Table 4. 9 J_{ab} for the simplified models for the pairs **B** and **C**

	J_{ab} /cm^{-1}			
methods	**B**	**B$_1$**	**C**	**C$_1$**
INDO/UHF	0.959	1.837	0.065	0.088
UBLYP/4-31G	-0.585	8.830	0.191	1.005
UB2LYP/4-31G	7.243	13.859	0.252	0.850
UB3LYP/4-31G	4.633	12.207	0.198	1.105
UNO CASCI {2,2}[a)]		0.392		0.054
UNO CASCF {2, 2}		13.232		1.064
UNO CASSCF {6, 6}		5.812		0.008

a) 4-31G basis set was used.

Table 4. 10 J_{ab} values for the pairs shown in **Fig. 4. 13**.

	J_{ab} /cm^{-1}			
methods	**A**	**B**	**C**	**D**
INDO/UHF	0.782	0.613	-0.010	0.065
UBLYP/4-31G	2.718	2.693	-0.086	-0.046
UB2LYP/4-31G	5.532	4.154	0.138	0.443
UB3LYP/4-31G	4.971	3.449	0.048	0.219

Table 4. 11 J_{ab} values for the simplified models of the pair **A**

	J_{ab} /cm^{-1}	
methods	**A**	**A$_1$**
INDO/UHF	0.782	1.518
UBLYP/4-31G	2.718	8.473
UB2LYP/4-31G	5.532	7.623
UB3LYP/4-31G	4.971	9.870
UMP2/4-31G		1.978
UNO CASCI{2, 2}[a)]		1.349
UNO CASSCF{2, 2}[a)]		13.694
UNO CASSCF{6, 6}[a)]		2.484
UNO CASSCF{10, 10}[a)]		2.271

a) 4-31G basis set was used.

Table 4. 12 J_{ab} values for the simplified models for the pair **B**

	J_{ab} /cm^{-1}			
methods	**B**	**B$_1$**	**B$_2$**	**B$_3$**
INDO/UHF	0.613	0.000	1.460	1.590
UBLYP/4-31G	2.693	0.000	4.882	3.672
UB2LYP/4-31G	4.154	0.000	10.434	7.455
UB3LYP/4-31G	3.449	0.002	6.755	4.900
UNO CASCI{2, 2}[a)]			0.032	0.005
UNO CASSCF{2, 2}[a)]			2.031	1.941
UNO CASSCF{6, 6}[a)]			1.337	0.709

a) 4-31G basis set was used.

Table 4. 13 J_{ab} for the simplified models for the pairs **C** and **D**

	J_{ab} /cm^{-1}				
methods	**C**	**C$_1$**	**C$_2$**	**C$_3$**	**C$_4$**
INDO/UHF	-0.010	0.000	-0.010	0.025	-0.066
UBLYP/4-31G	-0.086		0.064	-0.033	0.816
UB2LYP/4-31G	0.138		0.274	-0.050	1.683
UB3LYP/4-31G	0.048		0.149	-0.007	1.314
UNO CASSCF{2, 2}[a)]			-0.005	0.025	-0.005
UNO CASSCF{6, 6}[a)]			-0.007	-0.031	

a) 4-31G basis set was used.

	J_{ab} /cm^{-1}				
methods	**D**	**D$_1$**	**D$_2$**	**D$_3$**	**D$_4$**
INDO/UHF	0.065	0.000	0.075	0.035	0.314
UBLYP/4-31G	-0.046		0.209	0.155	1.369
UB2LYP/4-31G	0.443		0.522	0.090	2.692
UB3LYP/4-31G	0.219		0.334	0.160	2.176
UNO CASCI {2, 2}[a)]			0.008	-0.022	0.007
UNO CASSCF{2, 2}[a)]			-0.005	0.080	-0.007
UNO CASCI{6, 6}a)			0.178	-0.306	0.582
UNO CASSCF{6, 6}[a)]			0.017	0.044	0.231
UNO CASCI{10, 10}[a)]			0.017	-0.237	

a) 4-31G basis set was used.

Table 4. 14 J_{ab} vs. rotation angle of OH group.

pair **C**

θ	J_{ab} (INDO)	θ	J_{ab} (INDO)
0°	-0.066	180°	0.162
30°	0.914	210°	0.121
60°	0.614	240°	0.087
90°	0.219	270°	-0.148
120°	0.170	300°	-1.732
150°	0.182	330°	-1.833

pair **D**

θ	J_{ab} (INDO)	θ	J_{ab} (INDO)
0°	0.314	180°	0.262
30°	0.274	210°	0.270
60°	-0.057	240°	0.280
90°	0.275	270°	0.241
120°	0.291	300°	0.204
150°	0.272	330°	0.309

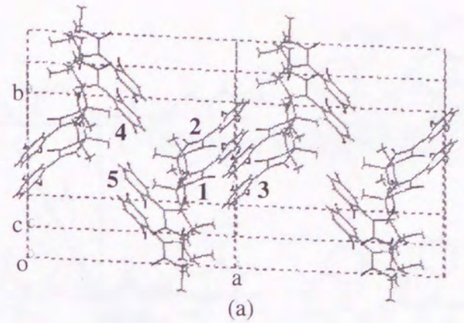

(a)

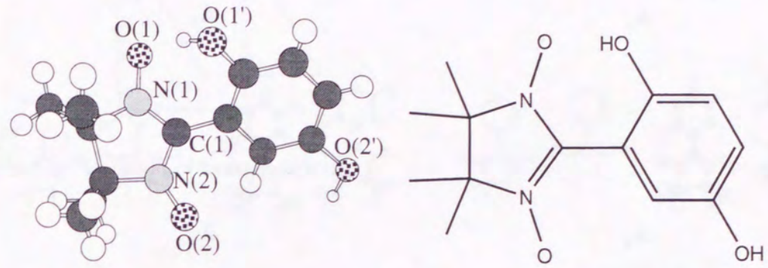

(b)

Figure 4. 1 Crystal structure (a) and molecular geometry (b) of α-HQNN.

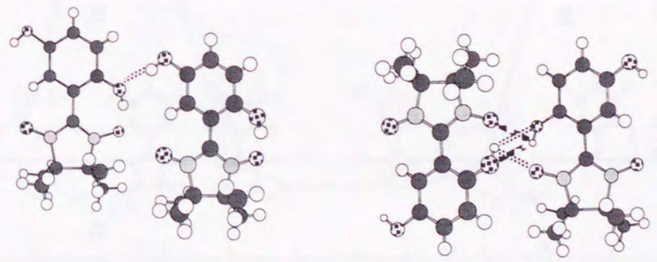

A **B**

Figure 4. 2 Pairs which have intermolecular hydrogen bonds.

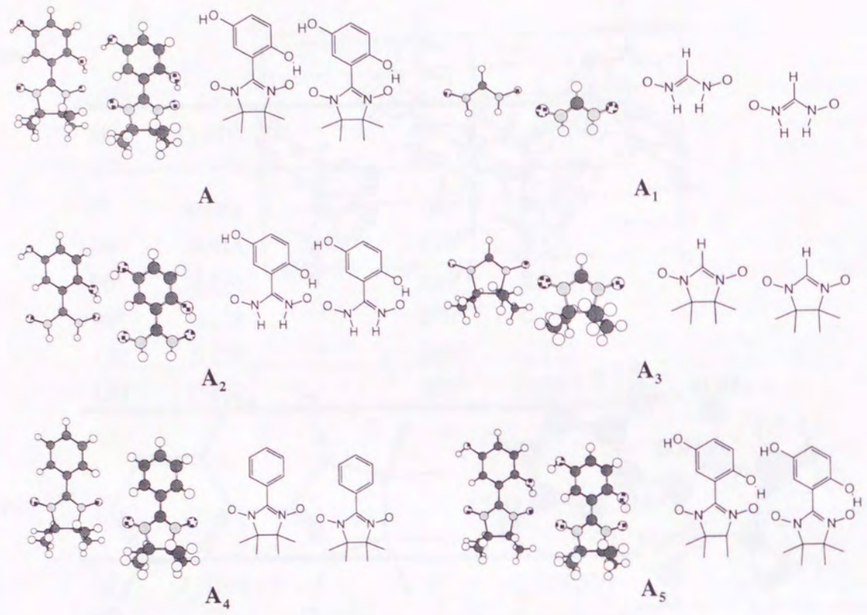

Figure 4. 3 Different simplified pair models for **A** in Figure 4. 2.

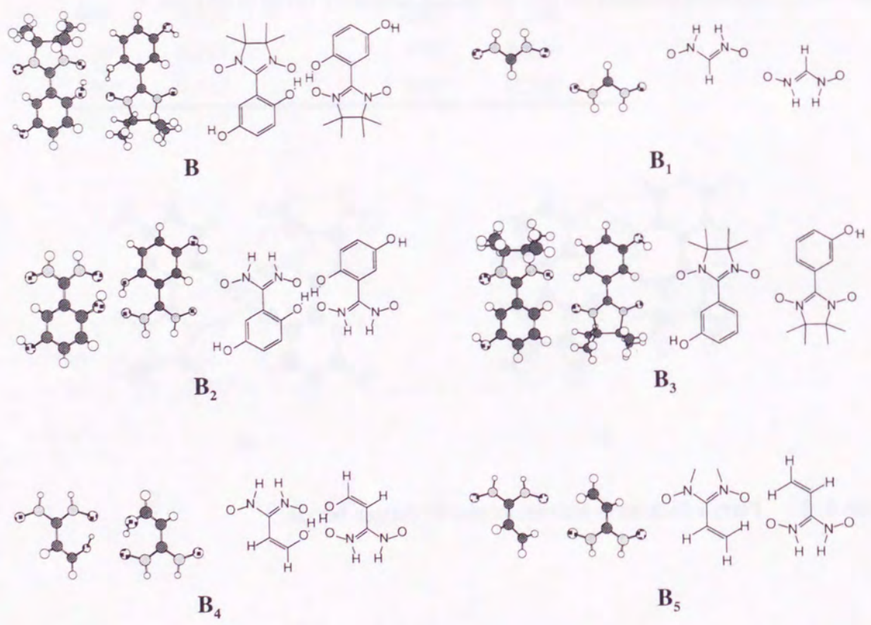

Figure 4. 4 Different simplified pair models for **B** in Figure 4. 2.

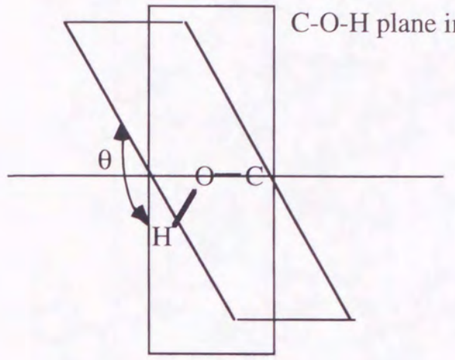

Figure 4. 5 Rotation of hydroxyl group.

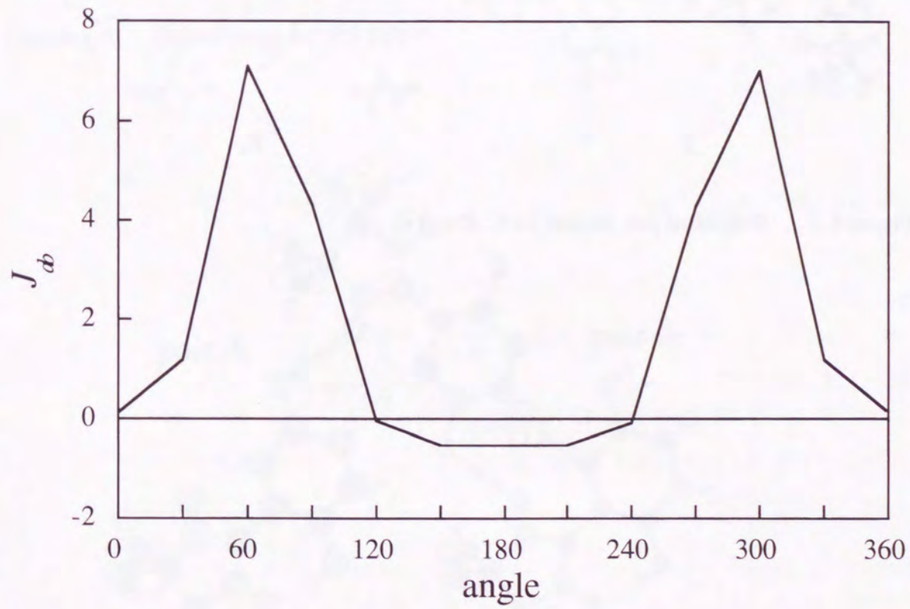

Figure 4. 6 J_{ab} vs. rotation angle of OH group.

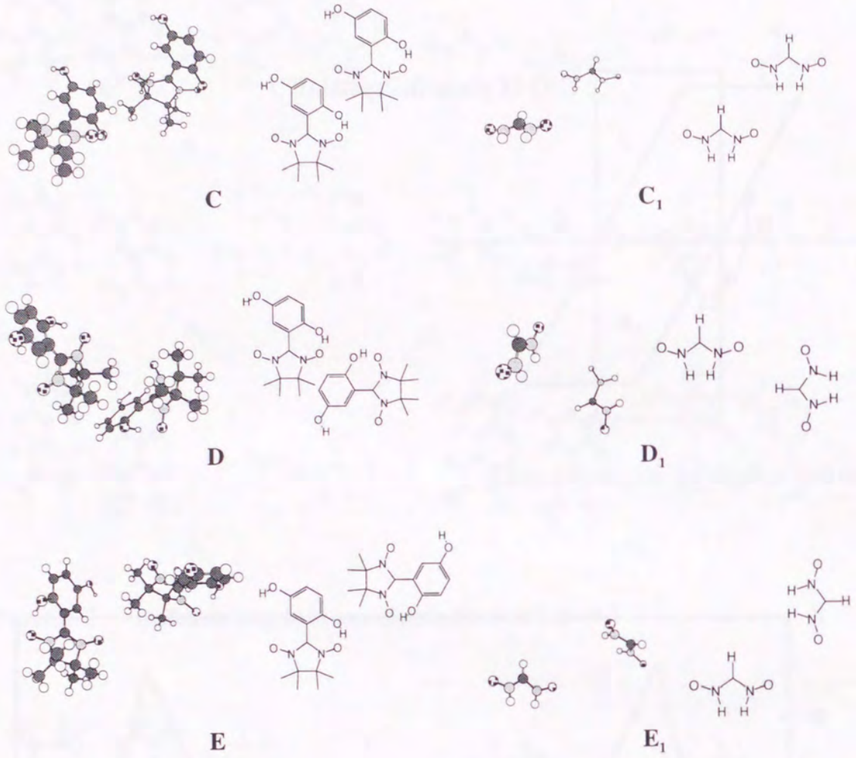

Figure 4. 7 Simplified pair models for **C**, **D** and **E**.

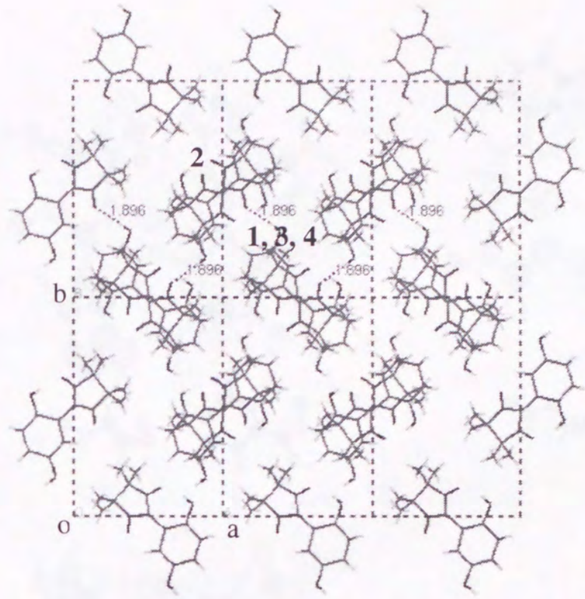

Figure 4. 8 Crystal structure of β-HQNN.

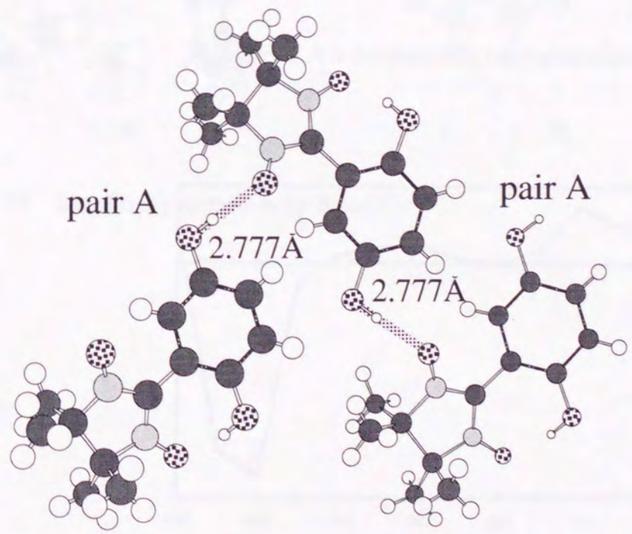

Figure 4. 9 Hydrogen bonded chain along the a-axis.

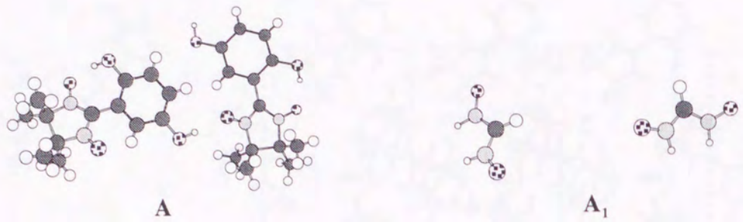

A

A_1

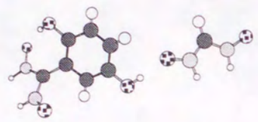

A_2

A_3

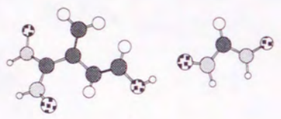

A_4

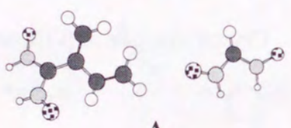

A_5

Figure 4. 10 Different simplified pair models for A in Fig. 4. 9.

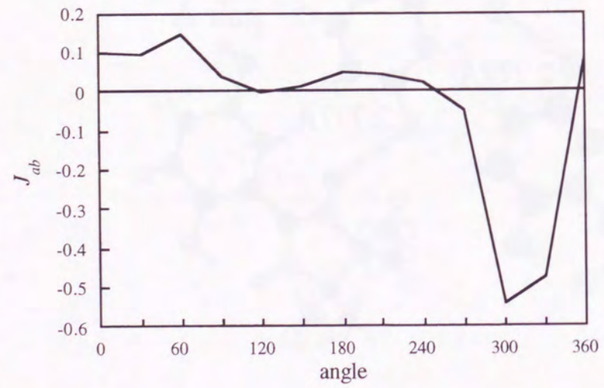

Figure 4. 11 J_{ab} vs. rotation angle of OH group.

A

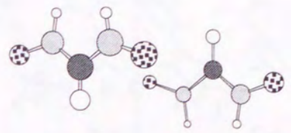

A_1

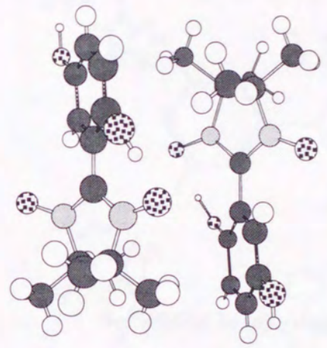

B

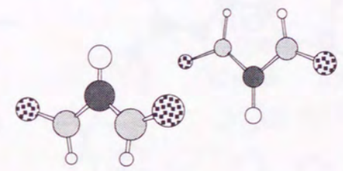

B_1

Figure 4. 12 Simplified pair models for **B** and **C**.

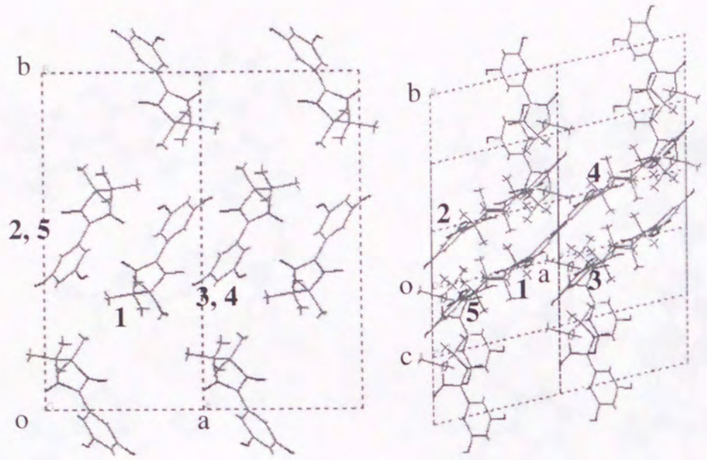

(a)

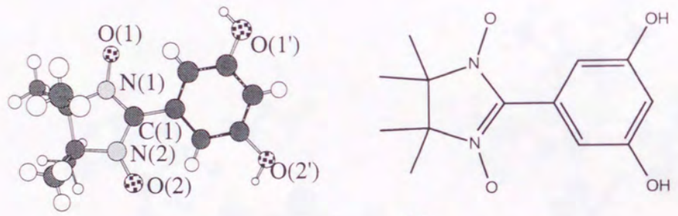

(b)

Figure 4. 13 Crystal structure (a) and molecular geometry (b) of RSNN.

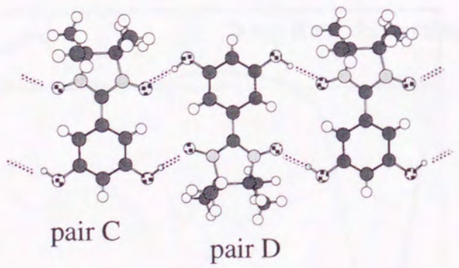

Figure 4. 14 The hydrogen bonded chain.

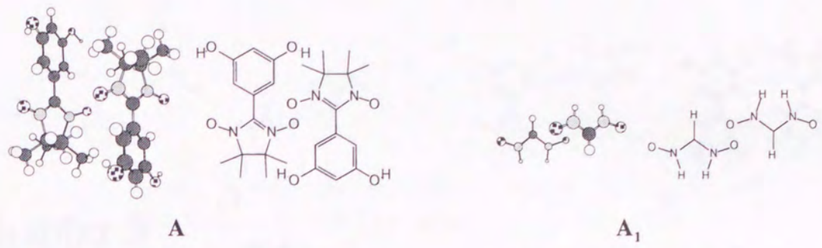

Figure 4. 15 Simplified pair models for **A**

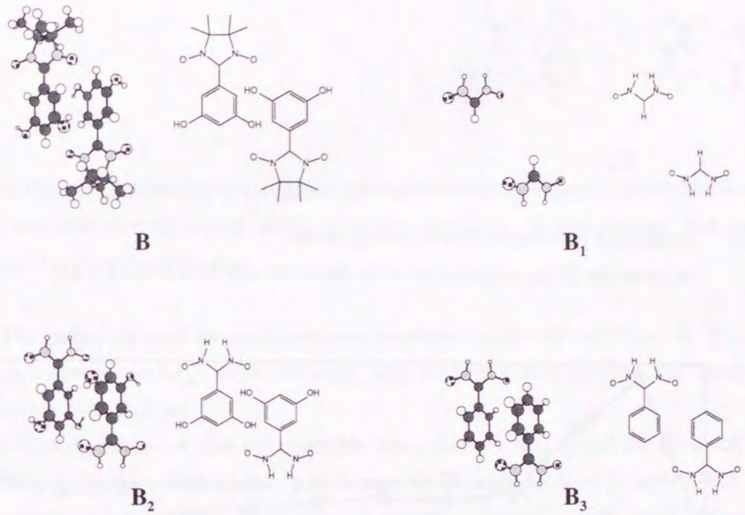

Figure 4. 16 Different simplified pair models for **B**.

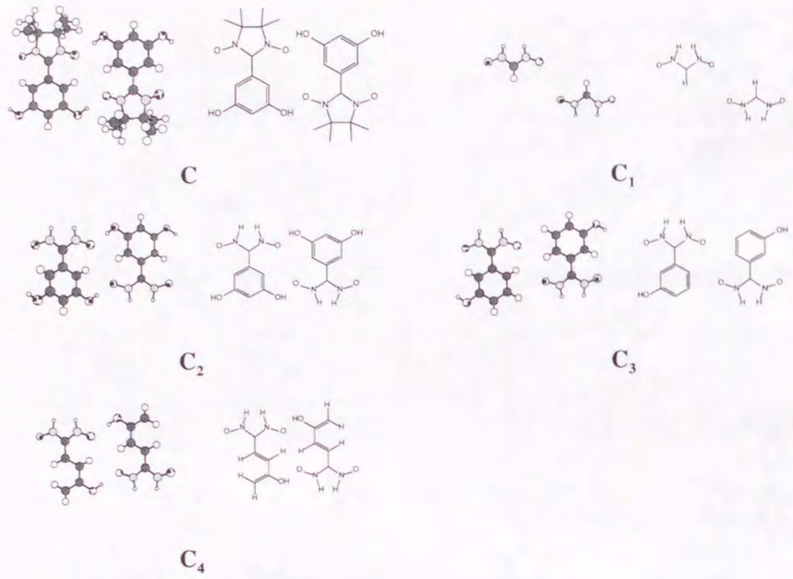

Figure 4. 17 Simplified pair models for **C** in **Fig. 4. 14**.
(models for **D** are constructed with the same way as models for **C**)

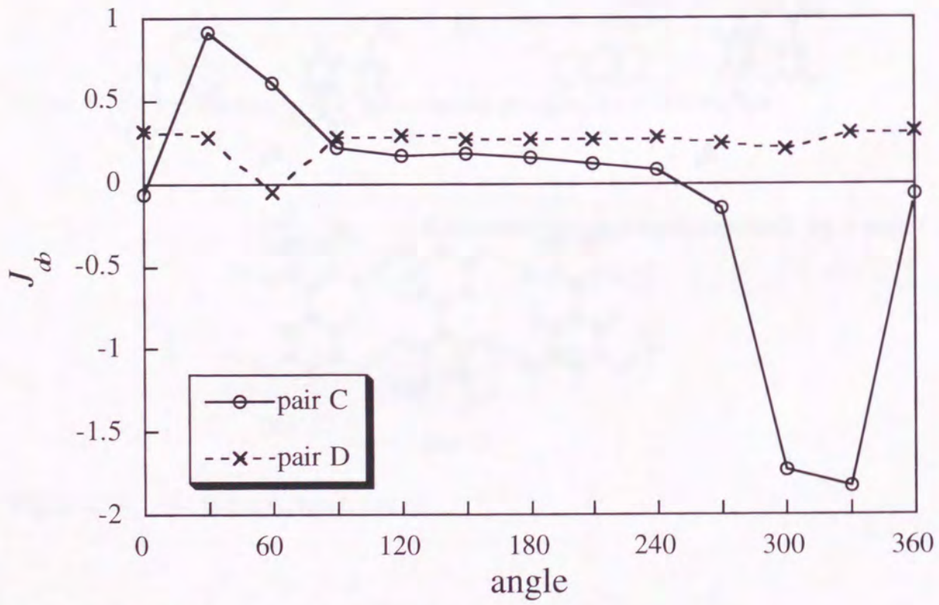

Figure 4. 18 J_{ab} vs. rotation angle of OH group.

Chapter 5

Concluding Remarks in Part I

In this part, the author investigated the intermolecular magnetic interactions of various nitronyl nitroxide derivatives by using quantum chemistry. In this chapter, the author will summarize the results of this part.

The author adopted the computational schemes mentioned in chapter 1. The effective exchange interactions (J_{ab}) were derived, and magnetic interactions are characterized quantitatively by J_{ab} values.

About J_{ab} values of nitronyl nitroxide derivatives, it was found the absolute values of SOMO-SOMO directly interactions (pair **A** of α-HNN and pair **B** of β-HQNN and pair **A** of RSNN) were much larger than those through the phenyl rings (pair **A** and **C** of *p*-CNPNN) and hydrogen bonds (pair **B** of α-HQNN, pair **A** of β-HQNN and pair **C** and **D** of RSNN), and the intermolecular interactions through the phenyl rings were larger than those through the hydrogen bonds.

For the hydrogen bonded pairs, the rotations of hydroxyl groups derived the change of J_{ab} values. It suggests that the pressure effect of these derivatives are expected. Assuming that the rotation of the hydroxyl group is caused by the pressure effect, the influence of this effects for the β-HQNN and RSNN crystals are larger than that of α-HQNN.

About calculational methods, semiempirical INDO methods reproduced qualitatively experimental results for these derivatives. On the other hand, it was found that *ab initio* UHF methods are not reasonable for not only quantitative but also qualitative calculations of intermolecular interactions because they overestimates the spin polarization effects. About DFT methods, UB2LYP and UB3LYP methods were able to reproduce qualitatively

experimental results for nitronyl nitroxide derivatives.

For CASCI and CASSCF methods, 2-orbitals and 2-electrons active space({2, 2}) was not enough to calculate the intermolecular magnetic interactions because CASCI and CASSCF with {2, 2} active space are able to calculate only the SOMO-SOMO potential exchange interactions. Interactions through the phenyl groups and hydrogen bonds were especially not obtained reasonable values. It is considered that 6-orbitals and 6-electrons ({6, 6}) or more are required for these calculations.

For the molecular pair models of α-HNN, 4-31G and 6-31G* basis sets were used. J_{ab} values calculated with them were similar to each other. It suggests that 4-31G basis sets are enough to calculate qualitatively reasonable intermolecular interactions for nitronyl nitroxide derivatives.

For all derivatives, calculational results reproduced the experimental results. It was found that the two sites model based on Heisenberg Hamiltonian is effective for the calculations of intermolecular magnetic interactions of organic radical crystals.

PART II

Calculations of Magnetic Properties of Model Systems by the Genetic Algorithm

Chapter 1

Genetic Algorithms

1.1 History and development

An important problem in computational chemistry is the determination of global energy minima of large molecular clusters. This task becomes more difficult as the number of dimensions and, hence, the number of local minima, grows. Within the past decade many optimization methods have been developed. These methods have both strong and weak points for each problem.

In general, optimization methods can be categorized as either deterministic or stochastic. When the number of degrees of freedom are increased, deterministic methods become difficult to search global minima, exponentially. On the other hand, the stochastic methods produce candidates of global minima in a probabilistic steps. Though these methods can give the solutions rapidly, they can not avoid local minima, frequently.

Genetic algorithms (GA's) classify one of stochastic methods. These algorithms are based on neo-Darwinism, and they imitate the biological evolution process. GA's are robust optimization methods, therefore they adapt to several problems.

In 1960's, Holland proposed GA's as learning methods they can adapt wide variety of environments [40]. His studies are the groundwork of GA's, especially in machine learning [41]. After his works, Goldberg applied GA's to various problems, i. e., search, machine learning and optimization [42]. His book had a great influence on other scientists, and GA's became popular optimization methods for not only the mathematical problems, i. e. traveling salesman problem [43-49], scheduling problem [50-54], knapsack problem [55, 56], but also for chemistry, physics, engineering, etc.

Recently, GA's have been used for many chemical problems, conformational analysis [57-60], alloy systems [61], protein folding [62-69], geometry optimization [70-76] and molecular design [77]. The searches for the global minima of Ising spin glass [9-12] and thermodynamical calculations [78] of Ising spin clusters are one of them. Though there are some studies for these problems, fixed $\pm J$ values were used in these studies and experimental or calculated J_{ab} values were not adopted.

In Ising model spin networks, when the number of spin sites are increased, the number of spin states and local minima of energies are exponentially increased. Thus, efficient optimization methods are indispensable to solve these problems. Simulated annealing methods [79-82] and neural network calculations [7] are well-known heuristics methods, however, they sometimes provide local minima for large systems. On the other hand, GA's are frequently able to escape local minima, and they are one of the fittest methods for these purposes.

In Part I of this thesis, intermolecular magnetic interactions were treated by using of *ab initio* and semiempirical MO methods. In the following chapters, the author mentions GA's for the purpose of investigation of magnetic behavior of spin networks connected by magnetic interactions calculated by *ab initio* and semiempirical MO methods.

1.2 Outlines of procedures

GA's imitate the biological evolution process [40]. A population has many individuals, and 'fitter' individuals for environments survive from current generation to next generation in higher probability. That is called "selection" or "reproduction". When a generation change, individuals in a next generation is formed by "crossover" and "mutation" operator. In **Fig. 1. 1**, flow chart of GA's are shown.

To carry out GA's, it is necessary that solutions of problems code to chromosomes ("coding"). In biological creatures, an individual frequently have some chromosomes. On the other hand, in GA's, an individual mostly have only one chromosome to describe its property. A chromosome contains many genes which are described any symbol. "1" and "0" are frequently used for this purpose, though genes are sometimes expressed by real numbers or any other symbols. The location of a gene is called "locus". The chromosomes in GA's are shown in **Fig. 1. 2**.

The procedures of GA's are mentioned as follows.

At first, a population of first generation are made. The individuals in it are mostly produced randomly.

In the selection phase, fitness of all individuals are given by using of fitness functions. Fitter individuals survive with higher probability, as shown in **Fig. 1. 3**. This resembles natural selection called "survival of the fittest". Scaling procedures are occasionally desirable before selection.

In crossover phase, two individuals are selected as parents. These two individuals

breed two children by following procedures: the chromosomes of parents are divided into two or many parts at the same points. The chromosomes of children are formed by complementary subsets of parental chromosomes, as shown in **Fig. 1. 4**. These children take the place of their parents.

The mutation operator is very simple. Some individuals are randomly selected. In these individuals, some loci are also randomly selected, and genes of these loci change in certain probabilities, as shown in **Fig. 1. 5**. These probabilities are almost fixed values, but sometimes they are defined to mutation functions.

These three operator, "selection", "crossover" and "mutation" are very important procedures in GA's. A selection is indispensable to optimization, and a mutation is key operator for keeping variety of individuals. A crossover operator is characteristic procedure of GA's. Because children inherit properties from both of parents, GA's are able to give reasonable solutions in early generation.

1. 3 Details of following chapters in part II

To the purpose of studies of Ising model spin networks by using GA's, the author carried out from the fundamental studies to the applications to real materials for these GA's. The contents of each chapter in this part is as follows.

In this chapter, basic informations of GA's were described. It was mentioned that GA's are robust for widely environments.

In the chapter 2, procedures of GA's for Ising model spin networks are illustrated. Pure GA methods are described, and particular operations for Ising problems are proposed.

In the chapter 3, theoretical background of GA's are described. Some terms are defined, and schema theorem and building block hypothesis are mainly illustrated.

In the chapter 4, pure GA calculations are carried out for Ising spin clusters. The behaviors of several operators are investigated. These calculations are preparations of following studies.

In the chapter 5, hybrid GA's for Ising model are developed. These methods are able to give the ground state of spin clusters.

In the chapter 6, thermodynamical calculations are carried out by using GA's. Particular operators are introduced, and the comparison with classical Metropolis's methods is conducted.

In the chapter 7, GA's are adopted to real compounds. The magnetic behavior of Mn_{12} cluster are investigated by using interactions assumed from experimental results. The intermolecular magnetic interactions of α-HQNN obtained in part I are used, and magnetic behaviors of α-HQNN clusters are also calculated.

Finally, summary of part II is mentioned in the chapter 8.

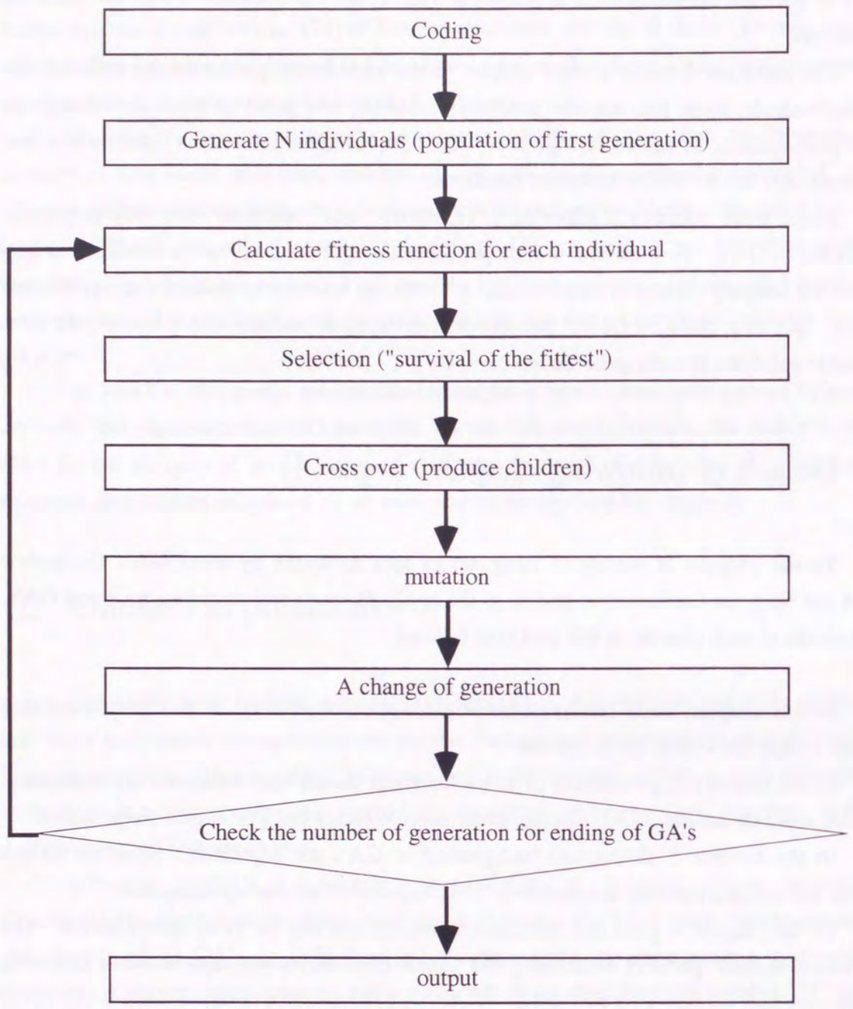

Figure 1. 1 Flow chart of GA's for Ising model spin networks.

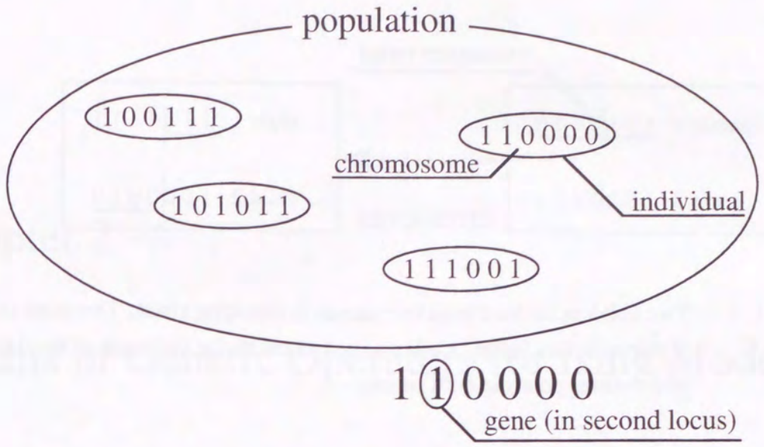

Figure 1. 2 Some individuals are included in a population, and individuals are described by chromosomes. In this figure, chromosomes are expressed by bitstrings. A chromosome have some genes. In this figure, one bit of bitstring means one gene. The location of a gene is called "locus".

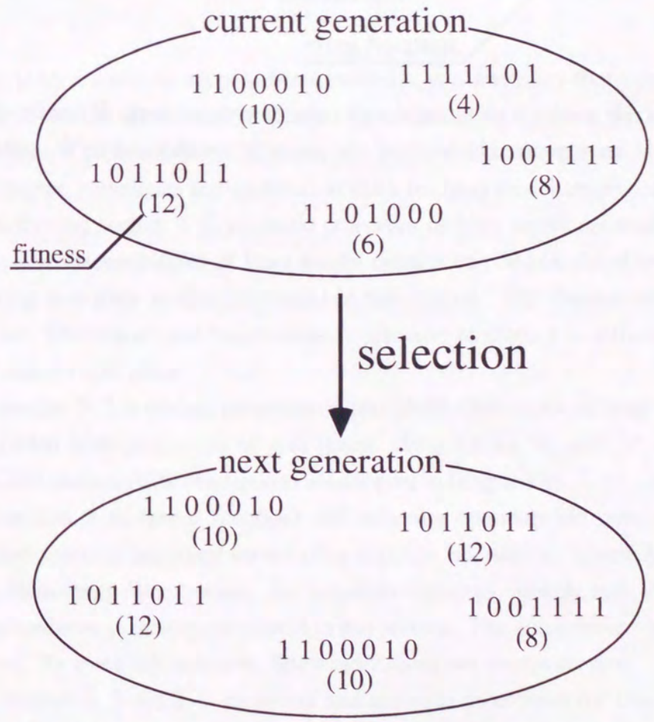

Figure 1. 3 Individuals which have larger fitness remain and increase in larger probability. They replace individuals which have smaller fitness.

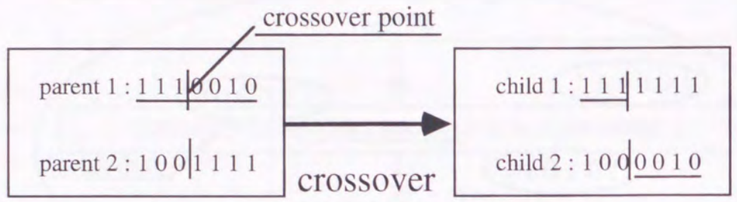

Figure 1. 4 Two children are bred from two parents in crossover phase. One point crossover is shown in this figure. Children are formed by the exchange of the right parts of crossover points in both parents.

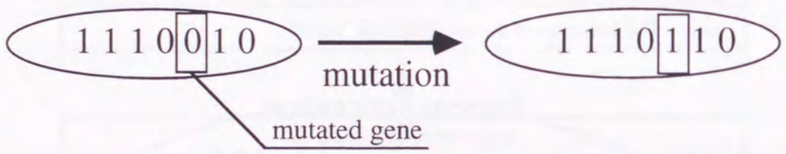

Figure 1. 5 In mutation phase, randomly selected genes change. When the chromosomes are expressed by bitstring, the genes "1" are changed to "0", and *vice versa*.

Chapter 2

Details of Genetic Operators for Ising Model

2. 1 Introduction

Though GA's are able to adopt various problems, it is necessary that parameters and operators of GA's are set up for each problem. An optimization for Ising model cluster is standard optimization problem. Some characteristic steps and parameters are introduced to GA's. In this chapter, parameters and operators of GA's for Ising model are provided.

In the following section 2. 2, magnetic properties of Ising model are described. The magnetizations and susceptibilities of Ising model clusters can be calculated by the use of spin states. Ising spin glass is also mentioned in this section. The characteristics of spin glass clusters are "frustration" and "randomness". Because of them, it is difficult to search for the ground state of spin glass.

In the section 2. 3, a coding procedure is provided. Genotypes of Ising model spin networks are coded from phenotype of spin states. Two alleles "1" and "0" are used in chromosomes, and characteristic descriptions are adopted to Ising model.

In the section 2. 4, fitness functions and selection operators are provided. These functions and operators are important for selecting superior individuals. Fitness functions are obtained from Heisenberg Hamiltonian. For selection operators, roulette rule, which is one of stochastic procedures, is mainly mentioned in this section. The elitist preserving selection is also described. By using this selection, fittest individuals can always survive.

In the sections 2. 5 and 2. 6, crossover and mutation procedures for Ising model are proposed. These are similar to simple GA, except for using multi-points crossover operators. A mutation depending on energies of spin states are also proposed. This mutation is important

for thermodynamical calculations discussed in chapter 6.

Finally, in the section 2. 7, other parameters and operators are described. The author mentions population sizes of GA's and a conditions for finish the program, etc.

2. 2 Magnetic properties of Ising model

Ising model is very useful to study magnetism. In this model, there are spin sites on the fixed lattice points, and interactions exist between two spin sites. Spin sites have two states; up-spin and down-spin.

Ising Hamiltonian is expressed as

$$H = -\sum J_{ij} s_i s_j \qquad (2.\ 1)$$

where J_{ij} is the magnetic interaction and ±1/2 is adopted for s_i and s_j. +1/2 and -1/2 expresses up-spin and down-spin, respectively. The positive J_{ij} means ferromagnetic interaction, and the negative one means antiferromagnetic interaction, same as J_{ab} mentioned in part I.

A ferromagnet and an antiferromagnet are illustrated in **Fig. 2. 1**. In ferromagnets, all interactions between two spin sites are ferromagnetic, and in antiferromagnets all interactions are antiferromagnetic. A model of clusters which include randomly located ferromagnetic interactions and antiferromagnetic interactions are shown in **Fig. 2. 2**. There are no state which can satisfy all interactions in this cluster. This is known as "frustration", and the cluster which has frustration and randomness is known as "spin glass". The energy does not change when up-spins replace to down-spins and down-spins replace up-spins in * marked 4 spins of this cluster. Thus, because various spin states have same or almost same energies for the spin glass clusters, the search for the ground state is the very difficult problem.

In Ising model, the locations of spin sites are fixed, only spin states change. In this model, magnetization M is calculated as follows:

$$M = \frac{1}{N}\left|\sum_i \langle s_i \rangle\right| \qquad (2.\ 2)$$

where, N is the number of spin sites.

On the other hand, the susceptibility χ in equilibrium states is calculated using the average of squared magnetizations and the squared average of magnetizations:

$$\chi = \frac{1}{NT}\sum_{i \neq j}\left(\langle s_i s_j \rangle - \langle s_i \rangle \langle s_j \rangle\right) \qquad (2.\ 3)$$

where, T means the temperature.

2. 3 Coding for Ising model

A coding procedure is first step of GA's. Spin states of Ising spin clusters are transformed into chromosomes made from genes. Using these chromosomes, genetic operators proposed in following sections can operate.

In general, various symbols are used for genes. For example, in biological creatures, physical characteristics can be described from four symbols, G, C, A and T. In GA's, "1" and "0" are frequently used for genes, and chromosomes are expressed by binary bitstrings. In GA's, except for "1" and "0", genes are occasionally described by real numbers, structural formulas of molecules, etc.

For Ising model spin networks, binary bitstrings are used. Descriptions for Ising clusters are simple. Spin sites of the network are numbered randomly. According to these numbers, "1" and "0" are arranged in bitstrings to generate chromosomes; up-spins are described by "1", and down-spins are "0", shown in **Fig 2. 3**.

Because S=1/2 Ising model are treated, the energy does not change by replacing up-spins with down-spins. For example, the chromosome '1 0 0 1' express the same state as '0 1 1 0' , as shown in **Fig 2. 4**. In this thesis, the first gene of chromosomes is constant "1" unless there are particular descriptions (in the above example, '1 0 0 1' are adopted) .

2. 4 Fitness function and selection

2. 4. 1 Fitness function

In GA's, fitness for all individuals are given by fitness functions. The fitness is the degree of tendencies of survivals in environment. In GA's, it expresses the validity of solutions for given problems.

The fitness for Ising model spin networks is in proportion to energies calculated by Ising model Hamiltonian in eq. (2. 1). In this thesis, the fitness of an individual x is defined by following equation:

$$f(x) = \sum_{i>j} J_{ij} s_i s_j \qquad (2.\ 4)$$

where, J_{ij} is magnetic interactions calculated by *ab initio* or semiempirical MO methods. s_i = 1/2 (up-spin) when the gene is 1, s_i = -1/2 (down spin) when the gene is 0.

Eq. (2. 4) means that the individuals which have larger fitness are more suitable for

this problem, it is different from energies mentioned in eq. (2. 1), in which smaller values mean more stable states, because fitness is related in a probability of survival of an individual.

2. 4. 2 Scaling

Fitness calculated by eq. (2. 4) is sometimes unsuitable for selection operators because of too large or too small values. When the spin state is not the global minimum, fitness frequently becomes negative value. To improve the fitness, the scaling is indispensable procedure before selection phase. For Ising model, two types of scaling are adopted in this thesis.

One of them is a linear scaling, shown in eq. (2. 5) and **Fig 2. 5**.

$$g(x) = a \cdot f(x) + b \tag{2. 5}$$

where a and b are real constant, $f(x)$ is the fitness of an individual x obtained by eq. (2. 4) before scaling, and $g(x)$ is the scaled fitness of x. The gradient and the segment of eq. (2. 5) are determined to be convenient for each problem.

Another type of scaling is the exponential scaling:

$$g(x) = e^{\beta f(x)} \tag{2. 6}$$

where $f(x)$ and $g(x)$ are similar to linear scaling. This scaling is base on Boltzmann distribution, negative fitness can change to positive by this scaling.

2. 4. 3 Roulette rule

After fitness is obtained for all individuals in a current generation, "survival of the fittest" is carried out. In this procedure, individuals survive or disappear according to fitness. Roulette rule is frequently used for this purpose [40]. The probability of survival for individual x_i is calculated by:

$$p_i = \frac{f(x_i)}{\sum_{i=1}^{N} f(x_i)} \tag{2. 7}$$

where p_i is the probability of survival for individual x_i, N is the number of individuals in a population (abbreviated to "population size") . In **Fig. 2. 6**, roulette rule is illustrated. N individuals are selected by N times trial of roulette. In this thesis, roulette rule is only

adopted as stochastic selection operator using fitness.

2. 4. 4 Elitist preserving selection

The global minima occasionally perish after many generation changes by roulette rule. To avoid this extinction, elitist preserving selection is frequently used together with other selection operators [83].

In this selection, one or some fittest individuals in a current generation unconditionally survive to next generation without crossover, mutation and any other operations. This selection have to be adopted carefully, because GA's possibly fall into local minima.

2. 5 Crossover

As mentioned above, crossover operators play the most important roles in GA's. By these operators, GA's are able to search various spin states, efficiently.

Crossover is carried out after roulette rule selection. Two individuals are randomly selected as parents, and chromosomes of these parents are divided into two or many parts at one or many points with a probability of crossover (abbreviated to p_c). These points are called "crossover points", and number of them is expressed as CP. Children are formed by alternate construction of divided parts of parents, see in **Fig. 2. 7**. These children take the place of their parents in the certain proportion. This proportion is called "generation gap" abbreviated as G. In this thesis, G=1 is fixed, it is known as "discrete generation model".

2. 5. 1 One-point and multi-points crossover

The one-point crossover is the most simple rule of crossover operators. A crossover point is randomly selected in the same point of two parental chromosomes, and chromosomes of parents are divided into left and right parts. Children are bred by an exchange of the right parts between parents, see in **Fig. 2. 7** (a).

By the one-point crossover, first gene always belong to left part, and last gene is always in right part, as shown in **Fig. 2. 7** (a). Because the generated child chromosomes strongly depend on arrangement of genes by one-point crossover, it is possibly unsuitable for optimization.

Multi-points crossovers operate same way of the one-point crossover. Crossover points, which are CP in number, are randomly selected, and parental chromosomes are divided into CP+1 parts. To form children, these parts of one parent and the other are alternately connected, as shown in **Fig. 2. 7** (b). Uniform crossover is one of the multi-points crossover. For uniform crossover, CP is not fixed and arbitrary chosen [84].

2. 5. 2 $\overline{x}$ crossover

As mentioned in section 2. 3, there are two genotypes for one spin state in GA's for Ising model. According to this property, new type of crossover are proposed. If the only one of these chromosomes is in a population, both of two genotypes are adopted in crossover phase, so-called $\overline{x}$ crossover.

In crossover phase, when the two parental chromosomes x and y are selected, x and y are divided into two parts x_1-x_2 and y_1-y_2, respectively. In all of these parts, replacing "1" with "0" (up-spins with down-spins) generates $\overline{x}_1$, $\overline{x}_2$, $\overline{y}_1$ and $\overline{y}_2$, as shown in **Fig. 2. 8**. Children are constructed from both original and replaced parts, possible children are following eight individuals:

x_1-y_2, x_1-$\overline{y}_2$, $\overline{x}_1$-y_2, $\overline{x}_1$-$\overline{y}_2$
y_1-x_2, y_1-$\overline{x}_2$, $\overline{y}_1$-x_2, $\overline{y}_1$-$\overline{x}_2$

On the other hand, because x and $\overline{x}$ have same energies, x_1-y_2 and $\overline{x}_1$-$\overline{y}_2$ are also decoded to same spin states. Thus, half of eight chromosomes are omitted, and following four individuals survive:

x_1-y_2, x_1-$\overline{y}_2$
y_1-x_2, y_1-$\overline{x}_2$

N individuals are selected in selection phase though the population size temporarily increases. Thus, the population size is always maintained.

2. 6 Mutation

2. 6. 1 General algorithm of mutation

Mutation operators are indispensable to GA's for the purpose of keeping varieties of individuals. General algorithm of mutation is as follows: the individuals selected with probability of mutations (p_m), and randomly selected genes of the individuals change, see in **Fig. 1. 5**. The genes "1" are mutated to "0", and "0" to "1". This operation means that up-spins are flipped to down-spins, *vice versa.*

2. 6. 2 Mutation depending on energies

In the general mutation, physical properties of spin states are not considered. Thus, if randomly mutation cause the increase of energies of the individual, it become the unfit

individual and perishes rapidly in selection phase, and varieties of individuals decrease. To avoid this problem, the probability of mutation of each individual is determined by following equation:

$$p_m = e^{\beta \Delta E} \tag{2. 8}$$

where,

$$\begin{aligned} \Delta E &= f_{current}(x) - f_{mutate}(x) && \left(f_{current}(x) > f_{mutated}(x)\right) \\ &= 0 && \left(f_{current}(x) \le f_{mutated}(x)\right) \end{aligned} \tag{2. 9}$$

where $f_{current}(x)$ and $f_{mutate}(x)$ are the non-scaled fitness of the individual x before and after mutation, respectively. β is the constant value related with temperature:

$$\beta = \frac{1}{kT} \tag{2. 10}$$

This type of mutation is similar to Metropolis Monte Carlo calculations [85] and simulated annealing, and it is illustrated in **Fig. 2. 9**.

2. 7 Other parameters and operators

The principal operators of GA's, selection, crossover and mutation, were provided in previous sections. In this section, other parameters and operators are described.

The length of chromosome (expressed as "n") is determined as the number of spin sites. Population size N is the number of individuals in one generation. It grows larger, superior individuals can be obtained.

Temperature T is used for β of exponential scaling described in eq. (2. 6) and mutation depending on energies mentioned in eq. (2. 10).

The ending condition of GA's is judged by the number of generations. When the calculation reaches for decided number of generations (k_{max}), the program is ended. k_{max} is required to be sufficiently large to give global minima.

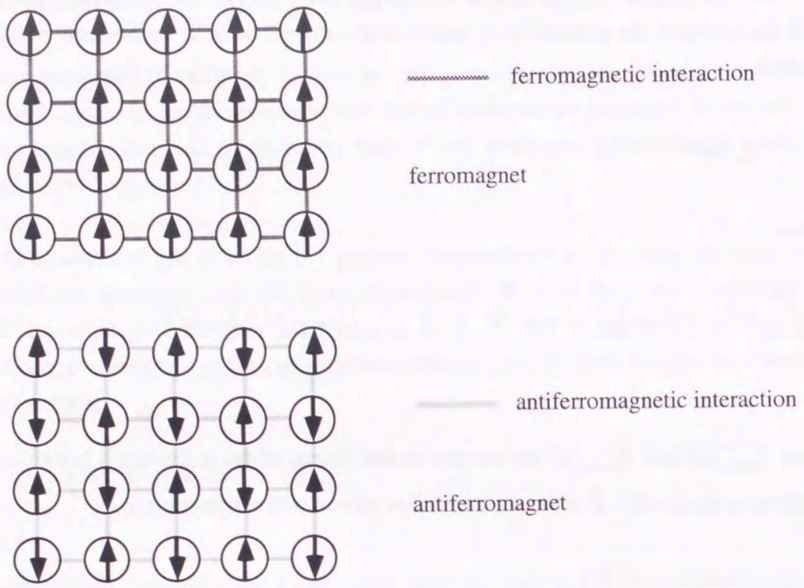

Figure 2. 1 Ising models of a ferromagnet and an antiferromagnet are illustrated.

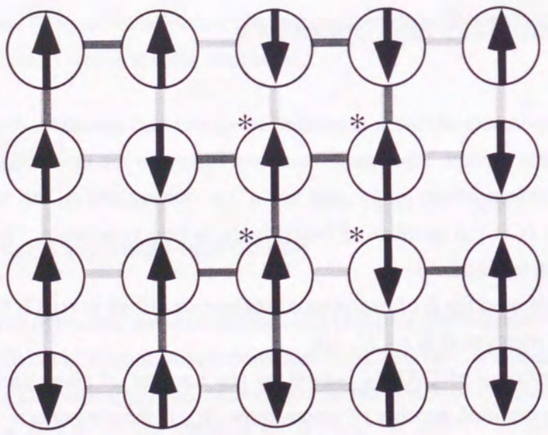

Figure 2. 2 Ising spin glass is illustrated. In this cluster, because ferromagnetic and antiferromagnetic interactions randomly exist, "frustration" is occurred.

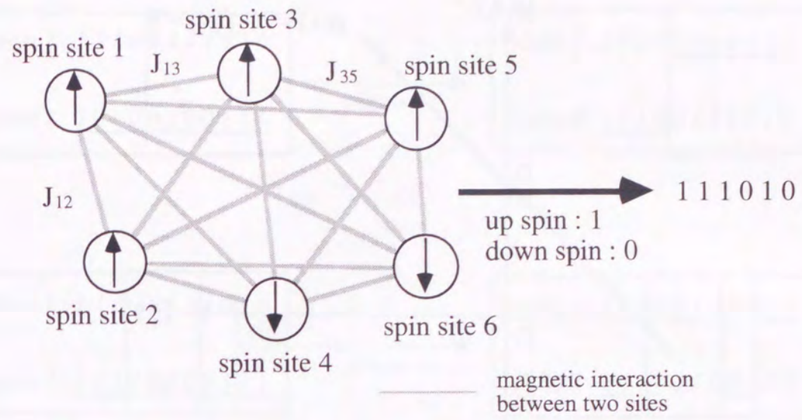

Figure 2. 3 Coding from spin states to chromosomes. Up-spins are expressed "1", and down-spins are "0".

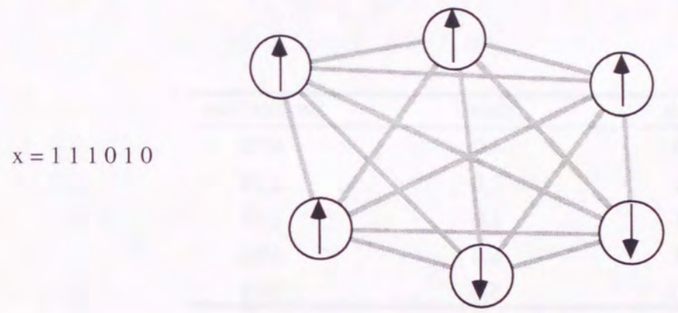

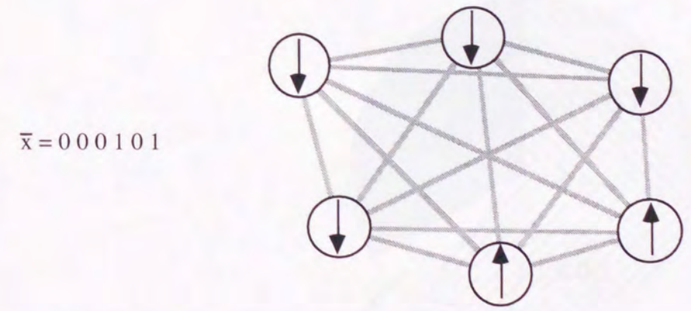

Figure 2. 4 Chromosome x and its inverse chromosome $\bar{x}$. Both of them have the same energies in Ising model.

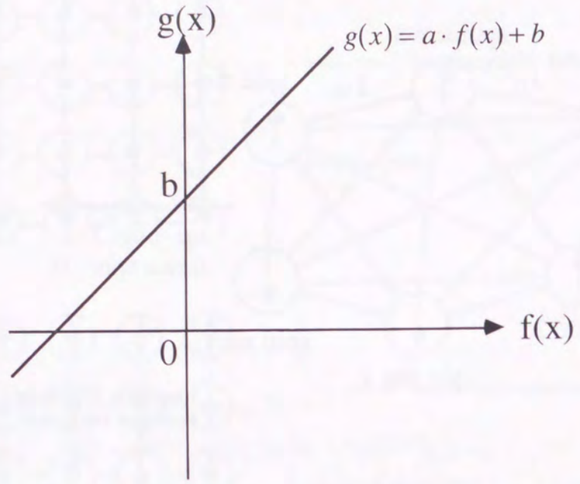

Figure 2. 5 The linear scaling is illustrated. Segments and gradients are determined in order to improve the fitness. Scaled fitness are always positive for all individuals.

individuals	fitness	probabilities
1 1 1 0 1 0	4.0	4/18
1 0 0 0 0 1	2.0	2/18
1 1 1 0 0 1	1.0	1/18
1 0 0 1 1 1	6.0	6/18
1 1 0 1 1 0	5.0	5/18

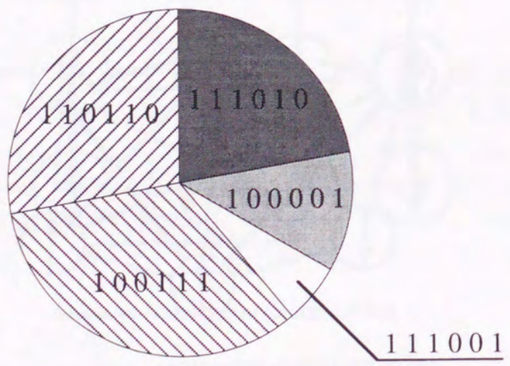

Figure 2. 6 The roulette rule is illustrated. The probability of survival is determined by proportion to fitness.

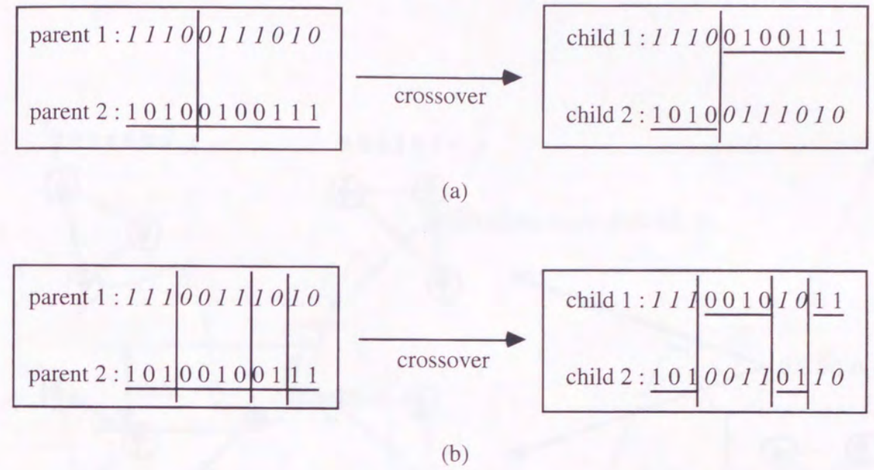

Figure 2. 7 (a) one-point crossover and (b) multi-points crossover (in this figure, three-points crossover) . In this figure, "*parts of parent 1*" and "parts of parent 2" breed two children.

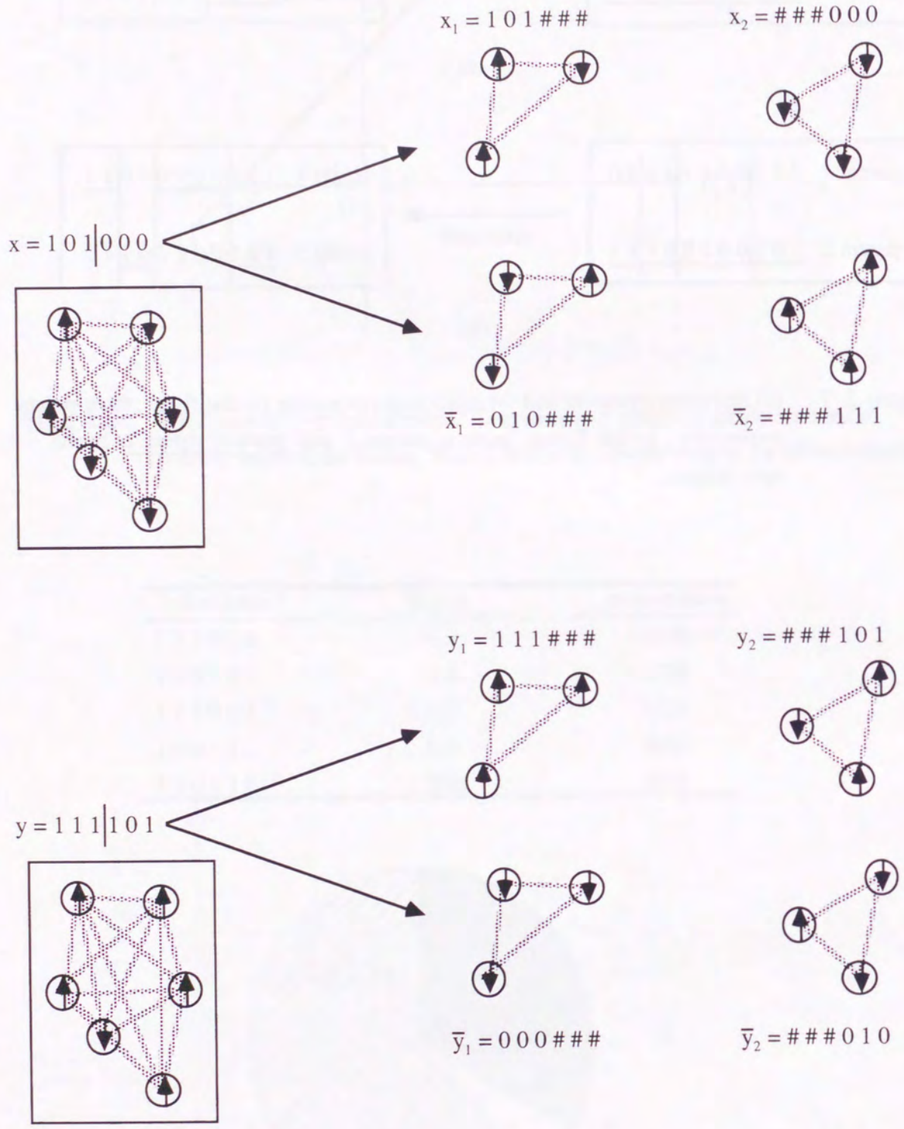

Figure 2. 8 Parental chromosomes are divided two parts and generate two replaced parts.

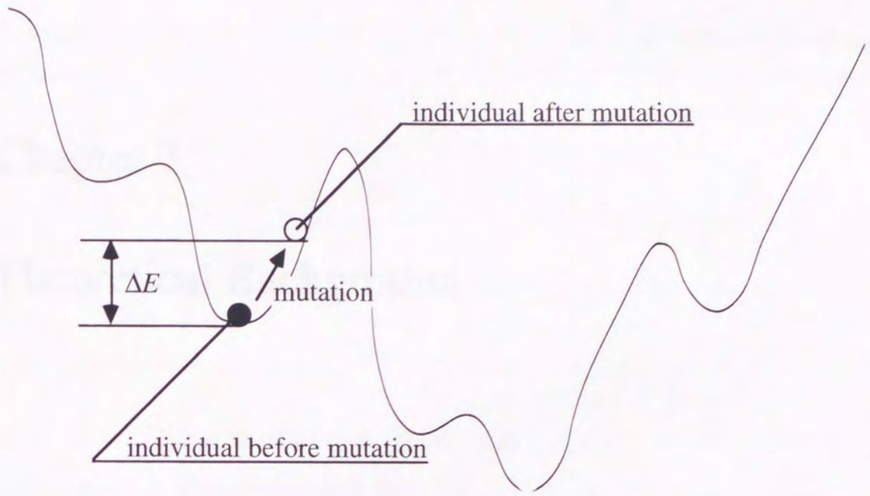

Figure 2. 9 The mutation depending on the energies. Probability of mutation p_m is determined by the difference of energies before and after mutation, $p_m = e^{\beta\Delta E}$.

Chapter 3

Theoretical Background

3.1 Introduction

Holland mentioned the theoretical background of GA's [40]. He introduced a concept of "schema", and it plays the most important role for GA's theory. Schemata can be regarded as parts of individuals. GA's can not give reasonable solutions for given problems unless suitable schemata are piled up. The searches by using GA's are carried out by a lot of combination of schemata. Reasonable solutions are only obtained by appropriate explorations of schemata. Recently, various GA's have been used, all of them are based on the Holland's theories.

In this chapter, theoretical background of GA's are mentioned. The schema theorem and the building block hypothesis are mainly described, and validity of GA's for Ising problems is discussed.

In the following section 3. 2, some important terms are introduced. Above all, "hamming distance" is indispensable to not only schema, but also improvements of GA's. Schemata for binary bitstrings are also provided.

In the section 3. 3, the number of schemata is discussed. Individuals transform by using genetic operators. The changes of individuals go with change of the number of schemata. When superior schemata can survived, suitable individuals can grow. The change of the number of schemata is expressed by the schema theorem. The implicit parallelism and the building block hypothesis are also mentioned in this section.

3. 2 Terms for schema

3. 2. 1 Hamming distance

For the investigation of GA's, differences between two individuals need to be measured. A hamming distance is used for this purpose.

When two individuals a and b are given by binary bitstrings expressed by eq. (3. 1),

$$a=\langle a_n a_{n-1}\cdots a_1\rangle,\ b=\langle b_n b_{n-1}\cdots b_1\rangle\ \ (a_i,b_i\in\{0,1\}) \tag{3. 1}$$

the hamming distance $d(a,b)$ is defined by eq. (3. 2).

$$d(a,b)=\sum_{i=1}^{n}|a_i-b_i| \tag{3. 2}$$

When two individuals are different from each other at only one gene, the hamming distance between them is only 1. If the difference between two chromosomes is larger, the hamming distance also grow larger. It is indispensable that the neighbor (small hamming distance) individuals around fittest solution have large fitness, because global minima are obtained from neighbor individuals.

In Ising model, large hamming distance does not always mean large difference of two individuals. As shown in **Fig. 3. 1** (a), though two individuals have largest hamming distance which is equal to length of chromosome n, they describe same spin state. On the other hand, shown in **Fig. 3. 1** (b), small hamming distance always mean small difference of two individuals, GA's are expected to give reasonable results for Ising model.

3. 2. 2 Schema of bitstring

Schemata can be regarded as parts of individuals. Assuming that individuals are the sets whose elements are genes, schemata are able to be looked upon as subsets. To make schemata, some genes are picked up from a chromosome, partially. The uncared loci are described * ("don't care symbol"). For example, all of 1**0, ***1, 1*00 and 1011 are schemata. All of 1000, 1001, 1100 and 1101 belong to schema 1*0*.

In the schema H, the number of loci which do not contain * are called the order of schema H, and expressed by o(H). For example, o(H) = 5, when the schema H=**110*1*1.

The length from first defined locus to last defined locus is called "defining length" and expressed by $\delta(H)$. The schema H defined same as above mentioned, $\delta(H)$ = 6.

3. 3 The number of schemata

3. 3. 1 The number of schemata and implicit parallelism

In GA's whose individuals made by "1" and "0", the number of schemata have following properties. In this section, the length of chromosome is n, and population size is N.

(1) The number of schemata for one individual is equal to 2^n.

Because a locus in a schema can be occupied either "*" or the defined gene.

(2) The number of schemata in a population is at most $N2^n$.

Property (1) leads to property (2). It is frequently much smaller because of overlap.

(3) The number of schemata which is made by "0", "1" and "*" is equal to 3^n.

Because the number of loci is n, and three symbols are used.

When individuals are randomly generated (the genes are decided "1" or "0" with the same probability), the expectation value of the number of schemata in a population is expressed by eq. (3. 3).

$$\sum_{i=0}^{n}{}_nC_i 2^i\left(1-\left(1-(1/2)^i\right)^N\right) \tag{3. 3}$$

The number of schemata whose orders o(H) = i is ${}_nC_i 2^i$. Where, one certain schema H whose o(H) = i is considered. It occurs with a probability $(1/2)^i$ that a randomly generated individual belong to schema H. It happens with a probability $\left(1-(1/2)^i\right)^N$ that all of N individuals do not belong to schema H. Thus, It occurs with a probability $1-\left(1-(1/2)^i\right)^N$ that at least one individual belong to schema H. When this probability multiplied by ${}_nC_i 2^i$, eq. (3. 3) are obtained.

When the N individuals are treated, less than $N2^n$ schemata are also treated in parallel. Because of this property, not only N individuals but also $N2^n$ schemata are able to operate to search for global minima in GA's. This property is called "implicit parallelism" [42]. In **Fig. 3. 2**, implicit parallelism is illustrated.

3. 3. 2 Evaluation for schemata

Schemata can be evaluated by similar procedure to fitness for individuals. The evaluated value of the schema H in generation k is calculated as follows.

$$f(H,k)=\frac{1}{|H(k)|}\sum_{x\in H(k)} f(x) \tag{3. 4}$$

where, $f(H,k)$ is the evaluated value (fitness of the schema), $|H(k)|$ is the number of individuals which belong to schema H in generation k. According to eq. (3. 4), $f(H,k)$ is the average of the fitness of all individuals which belong to schema H. The variation of schemata by genetic operators depend on this evaluated value.

3. 3. 3 Schema theorem

Genetic operators have influences on the number of individuals which belong to one certain schema. The number of them increases or decreases according to the evaluated value of the schema.

(i) selection

In this thesis, the roulette rule are adopted as selection operators. $m(H,k)$ is defined the number of individuals which belong to schema H in generation k. The evaluated value of H is described by $f(H,k)$, and the average of fitness for all individuals in a population is $\bar{f}(k)$. After operating roulette rule selection, the expectation value of the number of survival individuals which belong to schema H is equal to eq. (3. 5):

$$m(H,k+1)_{selection}=m(H,k)\frac{f(H,k)}{\bar{f}(k)} \tag{3. 5}$$

(ii) crossover

In one-point crossover, an individual which belongs to schema H is broken with probability $p_c\delta(H)/(n-1)$. On the other hand, the new individuals belong to schema H might be generated by crossover. And when the both of two parents belong to schema H, *m(H, k+1)* does not decrease because both of two children also belong to schema H. Considering these conditions, the number of individuals belong to schema H is described as follows:

$$m(H,k+1)_{crossover}\geq\left(1-\frac{p_c\delta(H)}{n-1}\right)\times m(H,k+1)_{selection} \tag{3. 6}$$

In the same way, by CP-points crossover,

$$m(H,k+1)_{crossover}\geq\left(1-p_c\frac{{}_nC_{CP}-{}_{n-1-\delta(H)}C_{CP}}{{}_{n-1}C_{CP}}\right)\times m(H,k+1)_{selection} \tag{3. 6}'$$

(iii) mutation

An individual belongs to schema H after mutation with probability $(1-p_m)^{o(H)}$. Because the probability of mutation (p_m) is enough small, $(1-p_m)^{o(H)}$ is able to be approximated to $1-p_m o(H)$. Similarly to crossover, because *m(H, k+1)* possibly increase by mutation operators, the probability is mentioned as follows:

$$p(H,k+1)_{mutation}\geq 1-p_m o(H) \tag{3. 7}$$

According to these equations, the following theorem is introduced by one-point crossover [40],

$$m(H,k+1)\geq m(H,k)\frac{f(H,k)}{\bar{f}(k)}\left(1-\frac{p_c\delta(H)}{n-1}-p_m o(H)\right) \tag{3. 8}$$

and CP-points crossover [86]:

$$m(H,k+1)\geq m(H,k)\frac{f(H,k)}{\bar{f}(k)}\left(1-p_c\frac{{}_nC_{CP}-{}_{n-1-\delta(H)}C_{CP}}{{}_{n-1}C_{CP}}-p_m o(H)\right) \tag{3. 8}'$$

This theorem is known as "schema theorem". The number of individuals which belong to schema H in next generation is calculated by this theorem, however, it is not easy to use for elucidation of GA's because calculation of $\bar{f}(k)$ is generally difficult.

3. 3. 4 Building block hypothesis

According to schema theorem, the mechanism of generating superior individuals by GA's is introduced as a following hypothesis:

building block hypothesis

In GA's, optimized individuals are generated by the schemata mentioned after:

(1) The defining lengths are short.
(2) The evaluated values are large.

To this hypothesis, it is found that the following mentioned coding is indispensable.

(1) The individuals which have similar phenotypes also have similar genotypes.
(2) Each locus do not have large interference.

For Ising model, this hypothesis can be satisfied. As mentioned in section 3. 2. 1, when two chromosomes have small hamming distance, they are always have a small difference. And, because the locus number is defined randomly, the interference of loci is enough small that GA's can operate well. Building block hypothesis in Ising model is shown in **Fig. 3. 3**.

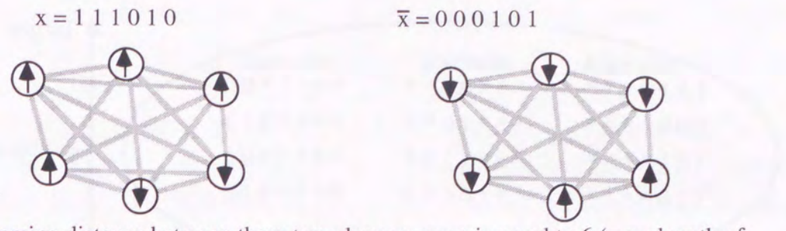

Hamming distance between these two chromosomes is equal to 6 (= n : length of chromosome).

(a)

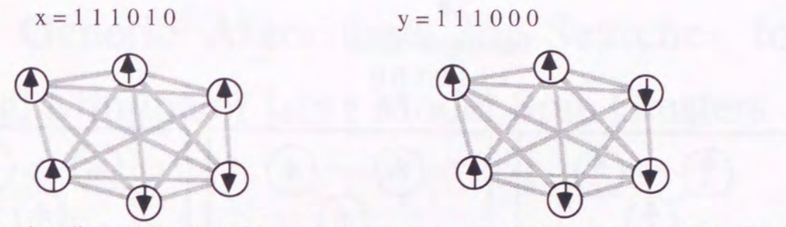

Hamming distance between these two chromosomes is equal to 1, and there is only one different spin between these two spin states.

(b)

Figure 3. 1 Hamming distances for Ising model. (a) largest hamming distance n means same spin state. (b) smaller hamming distance (< n/2) always means more similar spin states.

the variation of an individual

1 1 0 0 ⟶ 1 1 0 1

effected schemata by this variation

* * * 0, * * * 1,
1 * * 0, 1 * * 1,
* 1 * 0, * 1 * 1,
* * 0 0, * * 0 1,
1 1 * 0, 1 1 * 1,
1 * 0 0, 1 * 0 1,
* 1 0 0, * 1 0 1,
1 1 0 0, 1 1 0 1

Figure 3. 2 Implicit parallelism is illustrated. When an individual change, at most 2^n schemata (in this figure, 8 schemata) are treated.

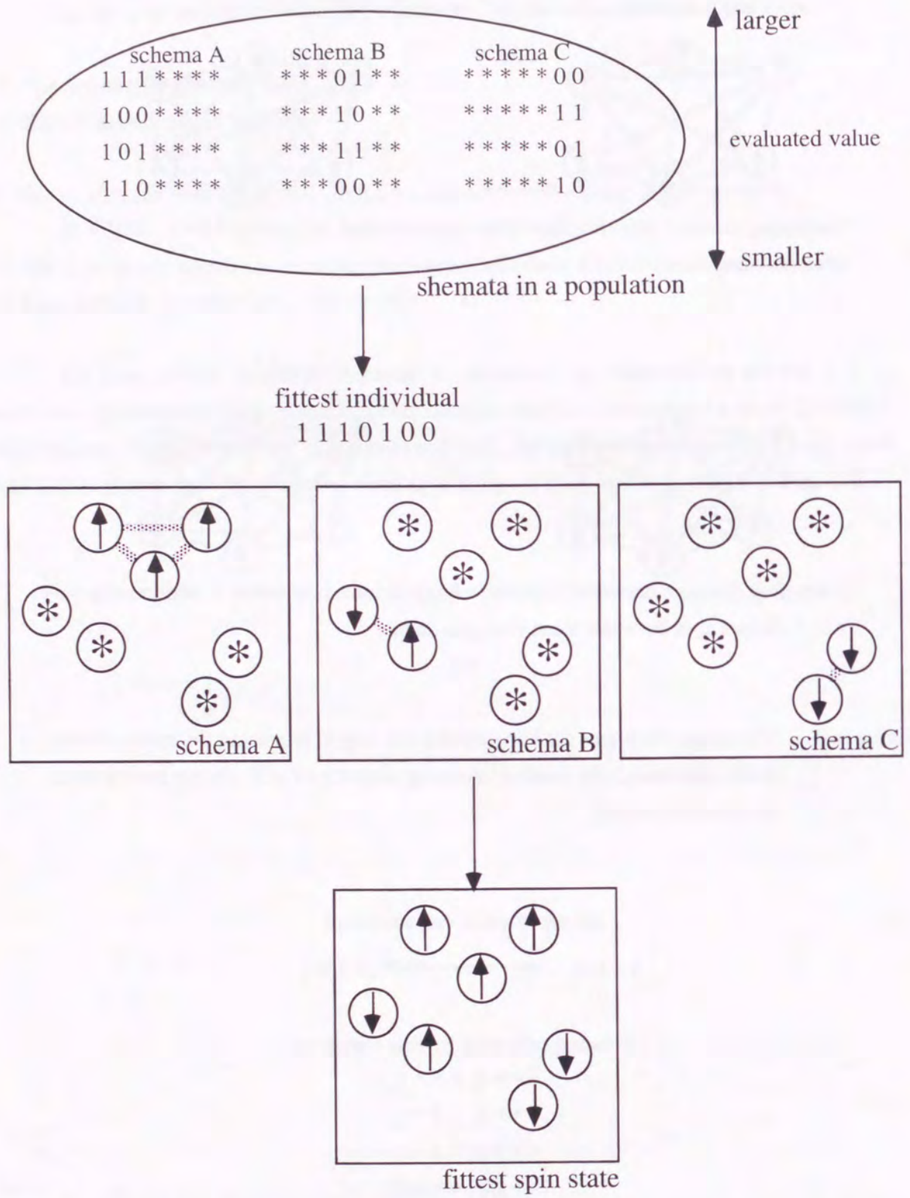

Figure 3. 3 Building block hypothesis for Ising model. The fittest spin state is obtained by combination of small spin clusters.

Chapter 4

Pure Genetic Algorithms for Searches for Global Minima of Ising Model Spin Clusters

4. 1 Introduction

Recently, searches for the global minima of 2D or 3D lattice Ising models which contain fixed $\pm J$ values by using of GA's were carried out [9-12]. On the other hand, there were no studies on GA's with calculated J values. In this chapter, the author discusses GA's with the random located spins and J values calculated by *ab initio* MO methods. The hydrogen atoms clusters are treated, and the interactions between two sites are calculated by UHF/4-31G method. Only pure GA's are discussed in this chapter, however, many improvements of GA's are proposed.

In the following section 4. 2, simple genetic algorithm (S-GA) is mentioned. This is the simplest method, and all algorithms are based on it. The results of calculations of S-GA are compared with results of random search. Two types of coding are adopted for S-GA.

In the section 4. 3, elitist preserving selection and two scalings are carried out. Elitist preserving selection is not stochastic procedure, therefore, it has some advantages and disadvantages. On the other hand, scaling of fitness functions are also discussed. Linear scaling and exponential scaling are adopted, and the roles of some parameters are discussed.

In the section 4. 4, the improvements of crossover are carried out. The roles of two parameters are investigated, and particular crossover operator of Ising model is adopted. Crossover is a characteristic procedure of GA's, and validity of GA's depend on the approach of crossover. Improvements of this operator are expected to play important roles of GA's.

In section 4. 5, mutation which depends on energies is provided. This type of mutation plays an important role in following chapter 5 and 6. The procedures and results of searches

for global minima by this mutation are illustrated in this section.

In section 4. 6, the other operators and parameters are considered. In GA's, though selection, crossover and mutation are principal operators, better solutions can be obtained by the improvements of other operator, occasionally. In this section, it is adopted that randomly generated individuals replace natural individuals. On the other hand, dependence of validity of solutions on the number of spin sites is investigated. The number of spin states exponentially increase with growth of the number of spin sites. The behavior of GA's for this problem is discussed.

Summery of this chapter is described in section 4. 7.

4. 2 Two types of simple genetic algorithms

4. 2. 1 Simple genetic algorithm

Simple genetic algorithm (S-GA) contains only basic genetic operators. Chromosomes are expressed by bitstring constructed by "0" and "1". Roulette rule is adopted, one-point crossover and normal mutation are used. Any other genetic operators are not used in S-GA.

S-GA are carried out for 15 sites spin networks (n=15) and 19 sites networks (n=19). There are 2^{15} (15 sites) and 2^{19} (19 sites) spin states in these systems, the energy of each spin state can be calculated in the bounds of computers. To compare these energies, all of 2^{15} or 2^{19} spin states can be given the ranking of stability, each other. Because the chromosome of S-GA can decode to spin state, all chromosomes can be given the ranking in all possible spin states. The validity of GA's is defined as ranking of the best chromosome. 100 types of clusters are calculated, and the average of validities is obtained. When networks contain at most 20 spin sites, this evaluational approach can be adopted the other types of GA's.

In this section, the linear scaling is adopted, and a=1 in eq. (2. 5). The segment of this function is defined from the smallest fitness in the population. In this scaling, minimum scaled fitness is equal to 0, see **Fig. 4. 1**.

In S-GA, CP=1 is defined. In this calculation, p_c =0.5, p_m=0.01 and N=100 are adopted. The number of generation is 200 and 300 for 15- and 19-sites clusters, respectively.

4. 2. 2 Fixed and non-fixed first locus

In Ising model, the energy does not change by replacing up-spins with down-spins, as shown in **Fig. 2. 4**. Thus, "1" can be adopted in first loci of chromosomes, constantly. With this procedure, the number of spin states become 2^{14} (15 sites) and 2^{18} (19 sites), calculational time become shorter.

Though calculations become easy by fixed first locus procedure, varieties of schemata decrease. To escape this problem, other type of S-GA, in which 0 is also adopted in the first loci of chromosomes, is also considered. These two types of S-GA's are carried out for 15

and 19 sites spin networks. In non-fixed first locus calculation, the stabilities are probably twice as large as those of S-GA with fixed first locus, and they are reevaluated by the same procedures of fixed first locus algorithm.

4. 2. 3 Results and discussions

The stabilities, convergent generations and probabilities to reach the global minima given by S-GA's are shown in **Table 4. 1** and **4. 2**. For search of 15 sites spin networks, both of S-GA's are not more suitable than random search. However, for 19 sites networks, the probability to reach the global minima by GA's is as large as that of random search. It suggests that GA's are expected to be more suitable for larger networks.

The results of S-GA with the non-fixed first locus shown in **Table 4. 2** are better than those of fixed S-GA for both of 15 sites and 19 sites networks. The difference between the results of two S-GA's for 19 sites is smaller than that for 15 sites. The fixed S-GA is expected to work as well as non-fixed S-GA when the cluster size is enough large. Because the calculational time of non-fixed S-GA is much larger than fixed S-GA, fixed one is used in the following sections in this chapter.

Though S-GA is the most simple of all GA's, it can be used as well as random search. For the purpose to obtain better solutions, improvements of operators and parameters are necessary to GA's.

4. 3 Several selections

4. 3. 1 Elitist preserving selection

Elitist preserving selection is used with S-GA. In this method, when the fittest individual does not survive, it replaces the unfit individual in next generation. Thus, by this selection, the fittest individual always survives. Parameters are the same as S-GA in section 4. 2. 2.

4. 3. 2 Several scalings

For the scaling methods, linear scaling and exponential scaling are used. The segments of linear scaling change with the fixed gradient a=1, shown in **Fig. 4. 2**. p_c, p_m, N and n are the same as those of S-GA. On the other hand, k_{max} is over 1000, and CP=8 is adopted. CP=1 is too small to obtain suitable individuals, it is discussed in following section 4. 5. With exponential scaling, 15 sites and 19 sites networks are calculated. β of eq. (2. 6) is defined as 1/T, and 1.0×10^{-5}K to 1.0×10^{5}K are adopted as T. CP=8 for 15-spin networks and CP=10 for 19-spin networks are used.

4. 3. 3 Results and discussions

elitist preserving selection

The stabilities, convergent generations and probabilities to reach the global minima for adding the elitist preserving selection are shown in **Table 4. 3** and **Fig. 4. 3**. S-GA with elitist preserving selection give much better solutions than S-GA, because the fit schemata remain by elitist preserving procedure. S-GA converges faster than S-GA with elitist preserving, because S-GA falls into local minima in early generation. When two GA's give same solution, the behavior of each algorithm is shown in **Fig. 4. 3**. According to **Fig. 4. 3**, the stabilities calculated by S-GA with elitist preserving selection monotonically decrease, and the global minima are obtained more efficiently than S-GA.

It suggest that elitist preserving selection is valid to the purpose of search the global minima.

linear scaling

The dependence of stabilities, convergent generations and probabilities to reach the global minima on segments of linear scaling is shown in **Table 4. 4** and **Fig. 4. 4**. Stabilities and probabilities toto reach reach the global minima do not depend on segments. On the other hand, convergent generations increase when the segments become larger, because the difference among fitness of individuals are decrease when segments grow larger.

exponential scaling

In **Table 4. 5** and **Fig. 4. 5** and **Fig. 4. 6**, the dependence of stabilities, convergent generations and probabilities to reach the global minima on temperature of exponential scaling is shown. Higher temperatures give more stable states and larger probabilities to reach the global minima. On the other hand, GA's converge too early to give global minima in low temperature.

By this scaling, the difference of fitness between fit and unfit individuals are overestimated. When temperature become higher, the overestimation become smaller, and GA's with exponential scaling give more reasonable results than those with linear scaling. On the other hand, GA's are similar to random search in too high temperatures, because the differences of fitness among all individuals become too small to use roulette rule.

4. 4 Several crossovers

Mentioned in section 4. 2, S-GA is almost not suitable for Ising model. Selection operators were improved in previous sections 4. 3, however, the validity is not sufficiently better than those of random search. Thus, it is necessary that crossover and mutation operators are improved.

There are two main parameters for crossover operators. One is the number of crossover

points (expressed by CP), the other is the probability of crossover (expressed by p_c). In this section, two parameters change, and new crossover operator is introduced.

4. 4. 1 Methods and procedures

(A) Investigations of role of the number of crossover points

At first, the roles of the number of crossover points are investigated. The number of crossover points is 1 in S-GA. In this section, CP=1 to 12 and uniform crossover are adopted for 15-spin clusters, and CP=1 to 16 and uniform crossover are adopted for 19 sites networks. The other parameters are equal to S-GA with using the elitist preserving selection mentioned in section 4. 3. 1.

(B) Investigations of the role of the probability of crossover

In GA's of this thesis, the p_c is important because it also plays a role of generation gap. Thus, the discussion of behaviors of p_c is indispensable, and p_c=0.1 to 1.0 are adopted. CP=8 (for 15-spin clusters) and CP=10 (for 19-spin clusters) are used in these algorithms. Other parameters are defined as the same as (A).

(C) $\overline{x}$ crossover

In (A) and (B), the improvements of parameters are carried out. In the next step, the new operator is adopted to obtain much more reasonable results. It is $\overline{x}$ crossover, proposed in section 2. 5. 2. By this crossover, both x and $\overline{x}$ are considered. It is expected that better solutions are given, because more types of schemata are considered. The $\overline{x}$ crossover strengthen the "implicit parallelism".

In these calculations, CP=8, p_c=0.5 and k_{max}=200 and 1000 (for 15-spins), and CP=10, p_c=0.5, k_{max}=200, 300, 1000, 1500 and 2000 (for 19-spins) are adopted. Other parameters are defined same values as S-GA.

4. 4. 2 Results and discussions

(A) Investigations of role of the number of crossover points

The dependence of stabilities, convergent generations and probabilities to reach the global minima on CP is shown in **Table 4. 6**, **Fig. 4. 7** and **Fig. 4. 8**. Stabilities, convergent generations and probabilities to reach the global minima are not different from several numbers of crossover points without CP=1 and 2 in 15 sites spin networks. It suggests that any number of crossover points can be adopted except for very small numbers. For 19 sites clusters, results do not depend on the numbers of crossover points with all CP.

(B) Investigations of role of the effects of the probability of crossover

The dependence of stabilities, convergent generations and probabilities to reach the global minima on p_c is given in **Table 4. 7**, **Fig. 4. 9** and **Fig. 4. 10**. For 15-spin clusters,

more stable solutions are obtained in more early generations by larger p_c, and the global minima are more probably obtained. The results indicate that higher probability gives better solutions, more rapidly. For 19-spin clusters, though the higher p_c gives better solutions similar to 15-spins, the result are saturated around p_c=0.5.

(C) $\bar{x}$ crossover

The stabilities, convergent generations and probabilities to reach the global minima for adding $\bar{x}$ crossover are shown in **Table 4. 8**, **Table 4. 9** and **Fig. 4. 11**. Though $\bar{x}$ crossover requires more generations than S-GA, it can give the better solutions for both 15 and 19 sites network. It works as well as random search for 15 sites, and it works much better than random search for 19 sites. It is expected to work better for larger systems.

Because $\bar{x}$ crossover preserves the variety of a schemata, the "bottleneck problem" are avoided. For example, even though all individuals become having same chromosome x, new type of children can be generated because $\bar{x}$ is also considered, see in **Fig. 4. 12**. According to **Table 4. 9** and **Fig. 4. 11**, GA's are able to search new solutions, endlessly. It suggests that more generations can give better solutions.

4. 5 Mutation depending on energies

4. 5. 1 Methods and procedures

In previous sections 4. 4, the improvements of crossover operators were treated. The validity of GA's turns better than that of S-GA, however, not much better than that of random search. In this section, mutation operators are improved.

This improved mutation depends on energy values described in eq. (2. 8), (2. 9) and (2. 10), and it is similar to Metropolis method. In a standard mutation, individuals are selected according to p_m, and only one randomly selected locus is mutated. On the other hand, all individuals and all loci are possibly considered in this mutation. At first, one locus are randomly selected. ΔE is calculated, and mutation is adopted with the probability calculated by eq. (2. 8). In each individual, n trials are carried out, nN mutations are tried in one generation.

Parameters are defined same as S-GA, except for p_m. $T = 1.0 \times 10^{-5}$ K to 1.0×10^{5} K is adopted in eq. (2. 10). Elitist preserving selection is not used, because global minima are expected to be obtained in very early generations by this algorithm. 10 types of 100-spin clusters are also calculated, CP=50 is adopted for these clusters.

4. 5. 2 Results and discussions

The dependence of stabilities, convergent generations and probabilities to reach the global minima on temperature of this mutation is shown in **Table 4. 10**. In this mutation, the

probabilities of mutation (p_m) are larger than that of standard mutation, whose p_m = 0.01. It gives much better results than other pure GA's because of high p_m. Many spin states resembled with one state can be searched by this mutation. This type of improvement is also discussed in following chapter 5.

For 100 sites, too high and too low temperature give worse solutions than the other temperatures. Temperature become higher, the more mutations are carried out. When temperature become lower, less mutations are done. The results suggests that too much or too little mutations are not desirable.

4. 6 Other parameters

4. 6. 1 Replacement by the randomly generated individuals

methods and procedures

In GA's, though variety of individuals is preserved in the early generations, all individuals become having similar schemata in the late generations. This is similar to "bottleneck problem" of the theory of the evolution. To escape this "bottleneck problem", individuals are replaced by randomly generated individuals in late generations. It is expected that this type of GA's can endlessly search new solutions similar to $\bar{x}$ crossover. The algorithm of it is follows: when the fittest individuals are not change for 20 generations, 10% of fitter individuals remain, and 90% of individuals are replaced by randomly generated individuals. The other procedures are same as S-GA with elitist preserving selection.

results and discussions

The stabilities, convergent generations and probabilities to reach the global minima for adding the replacement are shown in **Table 4. 11**. GA's with this replacement are much more suitable for search for global minima than S-GA, and give better solutions than random search. GA's are generally suitable for larger systems, this type of GA's are also suitable for small clusters, i. e. 15 sites.

4. 6. 2 Investigations of roles of the number of spin sites

methods and procedures

The complexity of calculations increases the order of 2^n in direct method of search for global minima of Ising model spin networks. In this section, effects of the number of spin sites are discussed by using S-GA with elitist preserving selection.

results and discussions

The dependence of stabilities, convergent generations and probabilities to reach the global minima on the number of spin sites is shown in **Table 4. 12** and **Fig. 4. 13**. The

stabilities exponentially increase when the number of spin sites increase. However, convergent generations linearly increase and probabilities to reach the global minima also linearly decrease. Thus, GA's are expected to give reasonable solutions for large systems.

4. 7 Conclusion

In this study, it was found that some of the pure GA's are able to give reasonable results for search for global minima of Ising model spin networks. Though S-GA is not suitable for this problem, GA's can be easily improved by changes of operators and parameters. These improvements can be divided into three classes.

The first is the improvements for preserving varieties of individuals. The exponential scaling in high temperature, an increase in the number of crossover points, an increase in the probability of crossover, $\overline{x}$ crossover and the replacement by the randomly generated individuals are classed in this category. The variety of individuals is very important for GA's. When the variety becomes narrow, all individuals rapidly become having same chromosomes. These improvements preserve the variety of schemata, and they strengthen the "implicit parallelism". Especially, $\overline{x}$ crossover and the replacement by the randomly generated individuals work well. These two procedures can keep the variety through the first generation to last generation, and they can give the global minima for all clusters in enough big generations.

The second is the tightening up the rule of "survival of the fittest". The exponential scaling in low temperature and elitist preserving selection belong to this class. In GA's, it is necessary that fitter individuals survive with more probability and breed more children. When improvements of this type are adopted, fitter individuals rapidly multiply and they become difficult to die. Thus, better solutions are obtained in early generation. On the other hand, the variety of individuals tend to become narrow. According to the calculational results of the exponential scaling in low temperature, stabilities of solutions are frequently worse than the ten times of those of high temperature. It suggests that though these improvements are useful to simplify the algorithms, they are unsuitable for highly accurate calculations.

The last is the using together with local search. Mutation depending on energies is the improvement of this class. GA can search widely, and improvements of this class can locally search in detail. This combination is expected to give reasonable results. The improvements of this type play important roles for GA's, and they are discussed in next chapter.

These three types of improvements are expected to derive more reasonable solutions when they are used together with each other.

Table 4. 1 The stabilities, convergent generations and probabilities to reach the global minima calculated by S-GA are illustrated. (100 trials)

	15	19
average of stabilities	9.96	91.49
convergent generation	32.65	55.03
probability to reach the global minima	0.24	0.10
(probability in random search)	(0.704988)[1)]	(0.108136)[2)]

1) 200 generations
2) 300 generations

Table 4. 2 The stabilities, convergent generations and probabilities to reach the global minima calculated by S-GA with non-fixed first locus. (100 trials)

	15	19
average of stabilities	11.08	178.92
(converted stabilities)	(6.04)	(89.96)
convergent generation	28.07	51.88
probability to reach the global minima	0.27	0.09
(probability in random search)	(0.704988)[1)]	(0.108136)[2)]

1) 200 generations
2) 300 generations

Table 4. 3 The stabilities, convergent generations and probabilities to reach the global minima calculated by S-GA with elitist preserving selection. (100 trials)

	15	19
average of stabilities	5.80	48.02
convergent generation	48.59	75.17
probability to reach the global minima	0.43	0.19
(probability in random search)	(0.704988)	(0.108136)

Table 4. 4 The dependence of stablities, convergent generations and probabilities to reach the global minima on the segment of linear scaling. (300 trials)

scaled minimum fitness	stabilities	generation	probability
0	4.4667	82.5900	0.4800
1	4.4767	86.1900	0.4967
10	6.0233	137.6233	0.4633
100	6.1100	171.7767	0.4367
1000	4.3900	162.0500	0.5233
10000	4.6033	222.6633	0.4667

Table 4. 5 The dependence of stabilities, convergent generations and probabilities to reach the global minima on temperature of exponential scaling.

15 sites:

temperature/K	stabilities	generation	probability
1.0×10^{-5}	28.61	21.55	0.19
1.0×10^{-4}	32.87	25.96	0.24
1.0×10^{-3}	40.98	22.50	0.18
1.0×10^{-2}	26.34	26.98	0.15
1.0×10^{-1}	40.05	27.66	0.20
1.0	29.41	37.85	0.12
1.0×10^{1}	29.96	36.18	0.16
1.0×10^{2}	19.84	48.73	0.26
1.0×10^{3}	9.10	43.84	0.37
1.0×10^{4}	4.72	52.29	0.43
1.0×10^{5}	3.65	70.97	0.39
1.0×10^{6}	3.60	79.53	0.60
1.0×10^{7}	3.73	92.10	0.52
1.0×10^{8}	3.10	107.09	0.54
1.0×10^{9}	4.65	100.96	0.43
1.0×10^{10}	3.61	82.24	0.53

19 sites:

temperature/K	stabilities	generation	probability
1.0×10^{-5}	273.08	42.12	0.08
1.0×10^{-4}	372.36	42.19	0.10
1.0×10^{-3}	256.65	42.49	0.04
1.0×10^{-2}	459.51	43.47	0.04
1.0×10^{-1}	255.67	43.00	0.06
1.0	293.62	47.03	0.06
1.0×10^{1}	373.22	53.87	0.04
1.0×10^{2}	283.98	75.06	0.06
1.0×10^{3}	130.26	97.74	0.10
1.0×10^{4}	43.08	84.63	0.10
1.0×10^{5}	38.94	110.50	0.19
1.0×10^{6}	21.29	126.79	0.18
1.0×10^{7}	19.47	136.56	0.18
1.0×10^{8}	33.46	144.89	0.26
1.0×10^{9}	36.92	140.96	0.18
1.0×10^{10}	20.57	144.47	0.21

Table 4. 6 The dependence of stabilities, convergent generations and probabilities to reach the global minima on CP.

15 spin sites (average of 400 trials)

CP	stabilities	generation	probability
1	6.0025	48.1575	0.4000
2	5.9475	38.6000	0.4325
3	5.2975	41.3300	0.4325
4	4.4525	43.1875	0.4325
5	5.3075	40.8200	0.4475
6	4.9050	46.0250	0.4575
7	5.4775	37.9150	0.4250
8	5.0400	44.4925	0.5025
9	5.5925	38.8050	0.4725
10	5.2375	46.2775	0.4275
11	4.6150	45.1725	0.4275
12	5.0625	41.2400	0.4250
Uniform	5.3150	50.3650	0.4750

19 spin sites (average of 100 trials)

CP	stabilities	generation	probability
1	48.02	75.17	0.19
2	48.01	80.79	0.15
3	21.84	75.59	0.17
4	44.87	73.50	0.19
5	47.51	69.36	0.17
6	60.46	64.55	0.18
7	26.12	65.69	0.23
8	37.50	64.21	0.18
9	30.40	68.87	0.16
10	30.19	77.23	0.22
11	42.66	46.88	0.19
12	35.94	65.16	0.22
13	55.42	63.26	0.21
14	35.41	72.65	0.16
15	42.04	67.19	0.24
16	35.04	67.74	0.18
Uniform	27.33	72.11	0.17

Table 4. 7 The dependence of stabilities, convergent generations and probabilities to reach the global minima on p_c. (100 trials)

15 sites:

probabilities of crossover	stabilities	generation	probability of reach the global minima
0.1	9.70	47.43	0.35
0.2	8.06	40.95	0.40
0.3	6.39	45.35	0.39
0.4	5.46	40.48	0.41
0.5	4.96	40.25	0.42
0.6	5.38	35.88	0.47
0.7	4.90	37.31	0.48
0.8	4.44	32.65	0.38
0.9	4.39	24.43	0.45
1.0	4.08	26.50	0.48

19 sites:

probabilities of crossover	stabilities	generation	probability of reach the global minima
0.1	53.99	77.73	0.16
0.2	56.49	93.85	0.21
0.3	27.49	83.23	0.19
0.4	30.46	66.32	0.22
0.5	19.99	70.36	0.25
0.6	31.33	68.35	0.20
0.7	25.13	67.14	0.17
0.8	17.68	74.33	0.30
0.9	26.56	57.52	0.20
1.0	19.42	65.96	0.23

Table 4. 8 Comparison with the results of $\bar{x}$ crossover and S-GA.

15 spin sites (100 trials)

	S-GA	$\bar{x}$ crossover (k_{max} = 200)
stability	9.96	2.30
convergent generation	32.65	59.94
probability to reach the global minima	0.24	0.68
(probability in random search)	(0.704988)	(0.704988)

19 spin sites (100 trials)

	S-GA	$\bar{x}$ crossover (k_{max} = 300)
stability	91.49	9.93
convergent generation	55.03	124.70
probability to reach the global minima	0.10	0.34
(probability in random search)	(0.108136)	(0.108136)

Table 4. 9 The dependence of stabilities, convergent generations and probabilities to reach the global minima on k_{max} of $\bar{x}$ crossover.

15 spin sites (100 trials)

max generation	stabilities	generation	probability
200	2.30	59.94	0.68 (0.704988)
1000	1.15	128.00	0.91 (0.997765)

19 spin sites (100 trials)

max generation	stabilities	generation	probability
200	15.47	87.85	0.31 (0.073456)
300	9.93	124.70	0.34 (0.108136)
500	9.11	177.33	0.50 (0.173649)
1000	4.58	319.23	0.60 (0.317143)
1500	3.89	425.71	0.68 (0.435721)
2000	2.33	531.89	0.73 (0.533707)

Table 4. 10 The dependence of stabilities, convergent generations and probabilities to reach the global minima on temperature of the mutation depending on energies.

15 spin sites (100 trials)

kT/K	stabilities	generation	probability
1.0×10^{-5}	1.00	2.09	1.00
1.0×10^{-4}	1.00	2.37	1.00
1.0×10^{-3}	1.00	2.04	1.00
1.0×10^{-2}	1.00	2.27	1.00
1.0×10^{-1}	1.00	2.17	1.00
1.0	1.00	2.09	1.00
1.0×10^{1}	1.00	2.29	1.00
1.0×10^{2}	1.00	2.09	1.00
1.0×10^{3}	1.00	2.17	1.00
1.0×10^{4}	1.00	2.02	1.00
1.0×10^{5}	1.00	2.36	1.00

19 spin sites (100 trials)

kT/K	stabilities	generation	probability
1.0×10^{-5}	1.03	4.31	0.97
1.0×10^{-4}	1.03	4.40	0.97
1.0×10^{-3}	1.03	5.32	0.97
1.0×10^{-2}	1.03	4.50	0.97
1.0×10^{-1}	1.06	4.09	0.99
1.0	1.01	6.49	0.99
1.0×10^{1}	1.01	5.08	0.99
1.0×10^{2}	1.07	4.24	0.97
1.0×10^{3}	1.03	4.81	0.97
1.0×10^{4}	1.03	4.34	0.97
1.0×10^{5}	1.03	5.13	0.98

100 sites

cluster	1	2	3	4	5	6	7	8	9	10
	-19145.	-77840.	-35123.	-93122.	-53566.	-109617.	-84324.	-136180.	-55238.	-63559.
10^{-5}	.464977	.646797	2.012291	3.064633	3.133081	.680619	.972871	.146079	.605005	.955392
10^{-4}	.437909	.338805	.490387	3.350229	1.084064	.528278	.810394	.565702	2.190759	1.235387
10^{-3}	.511224	.815508	1.433930	2.932413	1.607760	1.236288	.866622	1.083804	1.738865	1.431875
10^{-2}	.543931	1.527401	2.151353	3.582563	2.067740	1.219559	1.065161	1.708057	1.599230	1.187711
10^{-1}	.647560	1.428357	2.145068	4.035167	3.485444	1.033149	.966737	2.075819	2.296205	1.333507
1.0	.813544	1.482537	1.586258	4.111130	2.790128	.837388	.097609	2.080859	1.636931	1.500009
10^{1}	.334764	1.009497	2.192497	3.340926	2.834002	1.289996	1.055811	1.644722	2.325788	1.010827
10^{2}	.487025	1.997845	2.616287	2.800214	2.387979	1.137707	.934168	1.551475	1.528797	1.494546
10^{3}	.437909	.338805	.490387	3.350229	1.084064	.528278	.810394	.565702	2.190759	1.235387
10^{4}	.464977	.646797	2.012291	3.064633	3.133081	.680619	.972871	.146079	.605005	.955392
10^{5}	.780314	.293920	.515926	.935229	.816537	.562803	.385726	1.400052	1.157759	1.347250

Table 4. 11 The stabilities, convergent generationes and probabilities to reach the global minima calculated by GA with replacement by randomly generated individuals.

	15	19
average of stabilities	1.60	7.94
convergent generation	62.74	112.69
probability to reach the global minima	0.75	0.41
(probability in random search)	(0.704988)[1)]	(0.108136)[2)]

1) 200 generations

2) 300 generations

Table 4. 12 The dependence of stabilities, convergent generations and probabilities to reach the global minima on the number of spin sites.

the number of spin sites	stabilities	generation	probability (random search)
11	1.65	14.88	0.77 (1.000000)
12	1.90	20.02	0.67 (0.999943)
13	2.24	25.67	0.61 (0.992429)
14	3.65	27.21	0.51 (0.912975)
15	5.87	37.60	0.43 (0.704988)
16	7.36	38.17	0.36 (0.456845)
17	13.68	49.75	0.25 (0.263008)
18	22.82	68.46	0.29 (0.141517)
19	48.01	80.79	0.15 (0.073456)

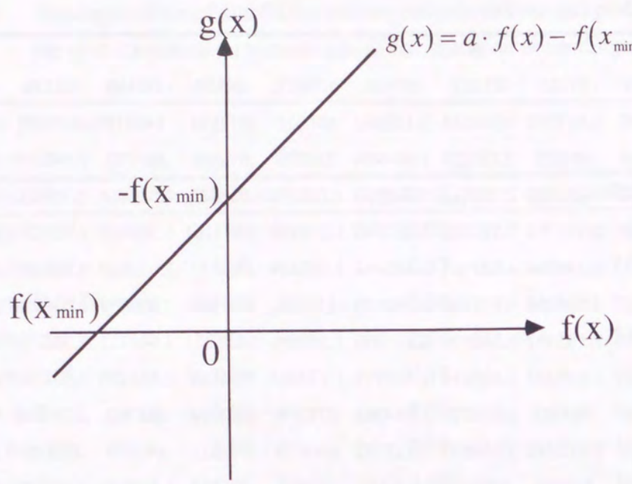

Figure 4. 1 Scaling adopted in S-GA. A minimum fitness before scaling is $f(x_{min})$, and after scaling $g(x_{min})$ is equal to 0.

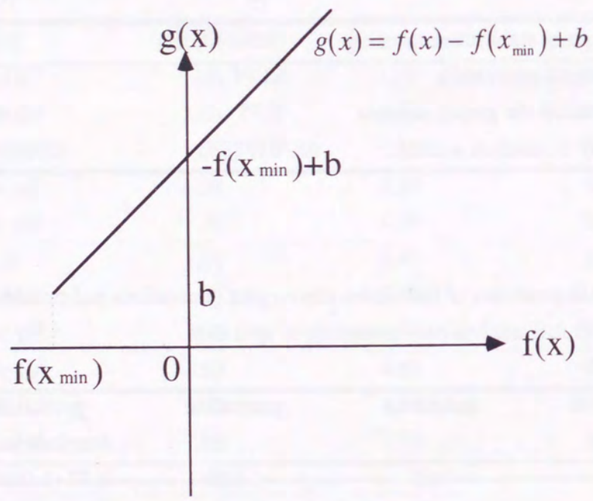

Figure 4. 2 Linear scaling which have several segments b.

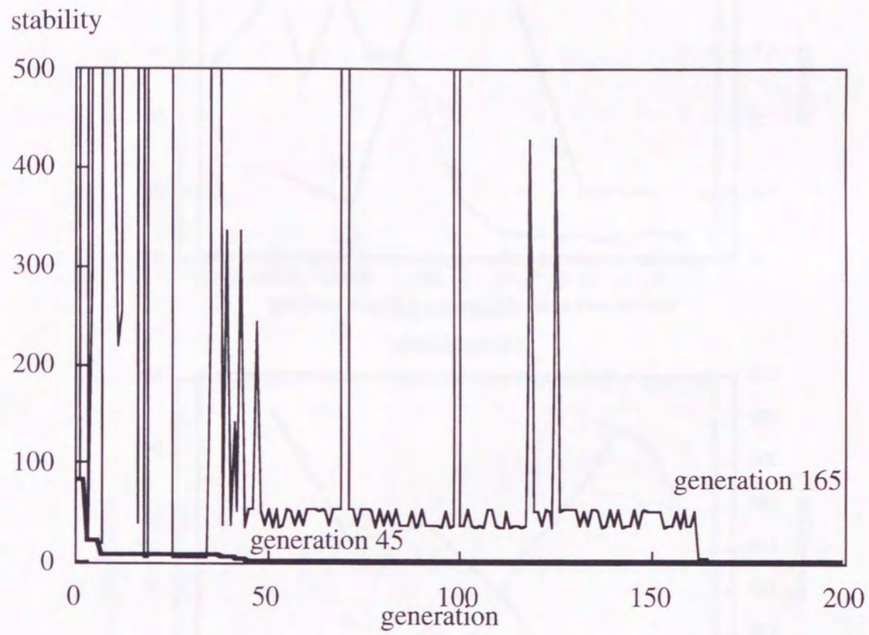

Figure 4. 3 Stabilities transition by changes of generation compare between S-GA and S-GA with elitist preserving selection.

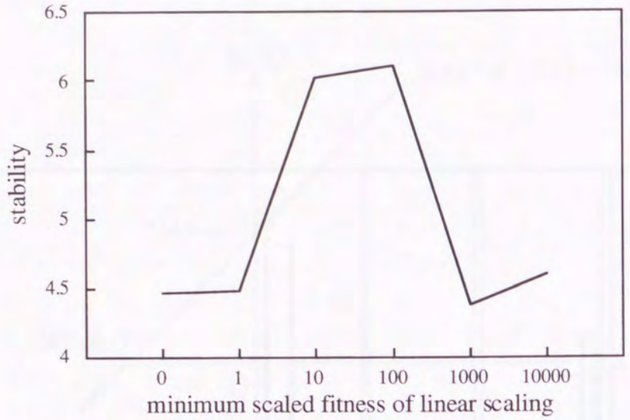

(a) stabilities

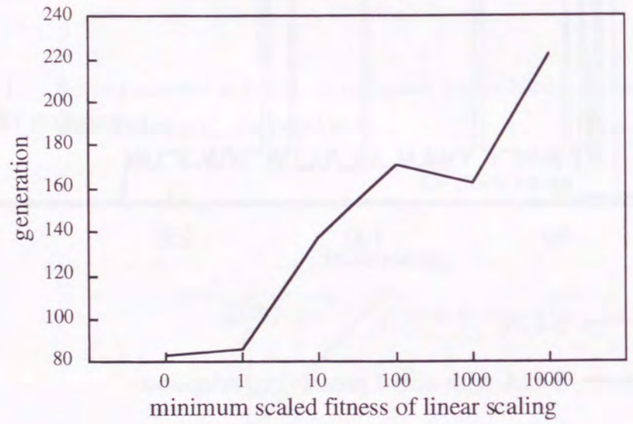

(b) convergent generation

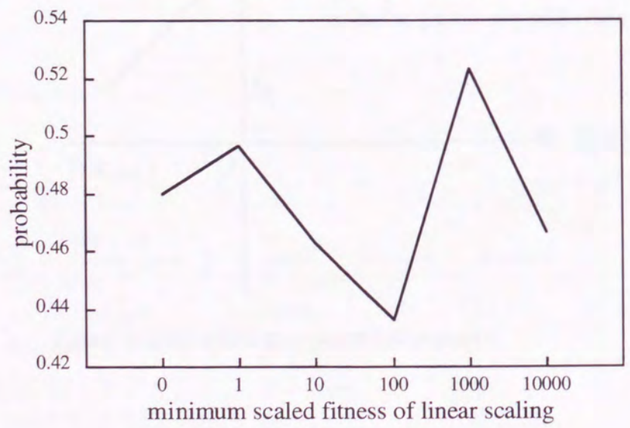

(c) probabilities to reach the global minimum

Figure 4. 4 The dependence of stabilities, convergent generations and probabilities of reach the global minima on the segment of linear scaling in 15 sites network.

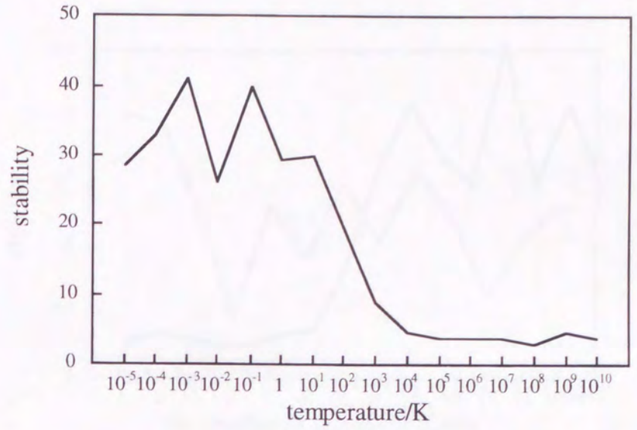

(a) stabilities

(b) convergent generation

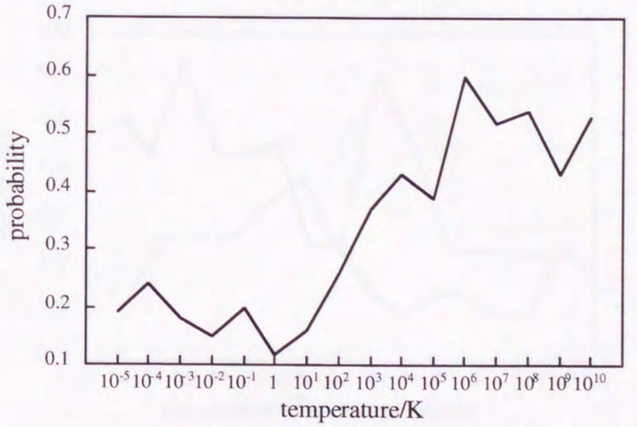

(c) probability to reach global minima

Figure 4. 5 The dependence of stabilities, convergent generations and probabilities of reach the global minima on the temperature of exponential scaling in 15 sites network.

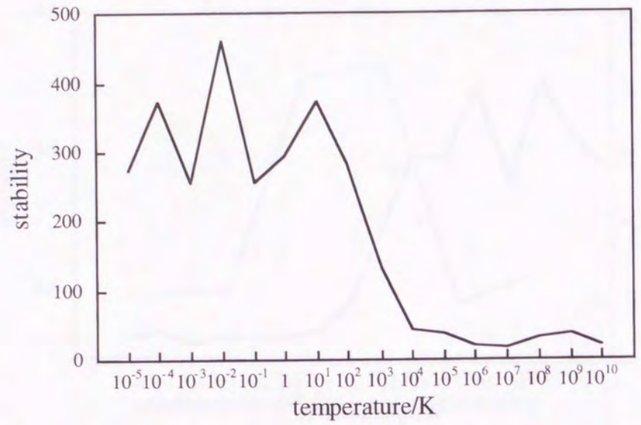

(a) stabilities

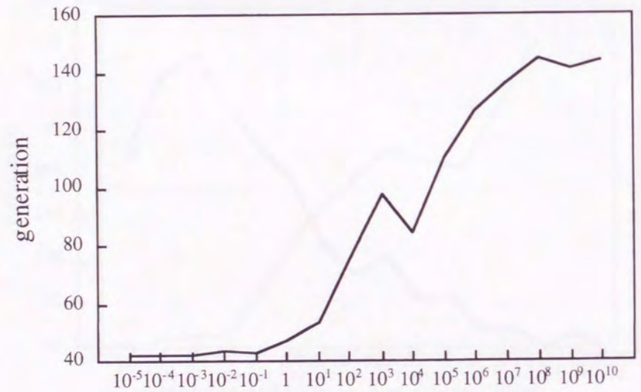

(b) convergent generation

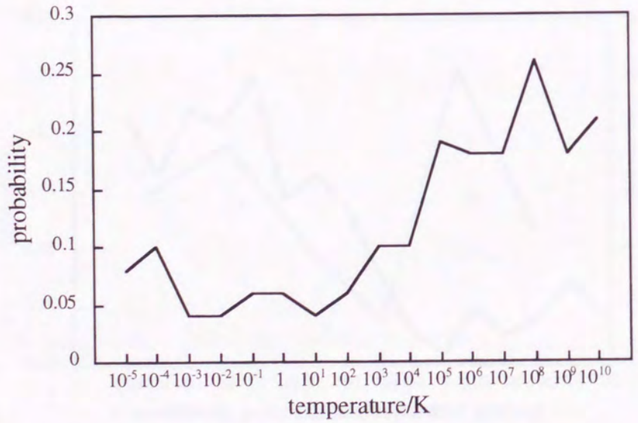

(c) probability to reach global minima

Figure 4. 6 The dependence of stabilities, convergent generations and probabilities of reach the global minima on the temperature of exponential scaling in 19 sites network.

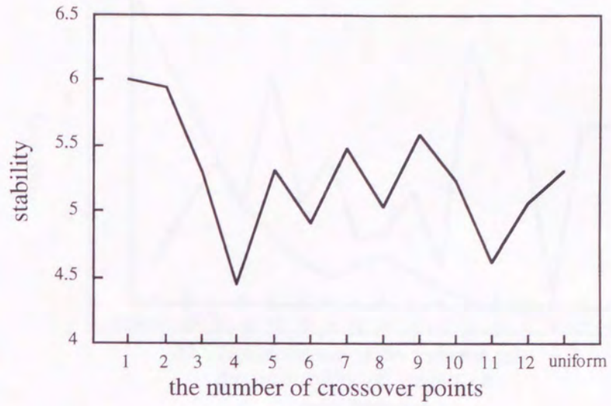

(a) stabilities

(b) convergent generation

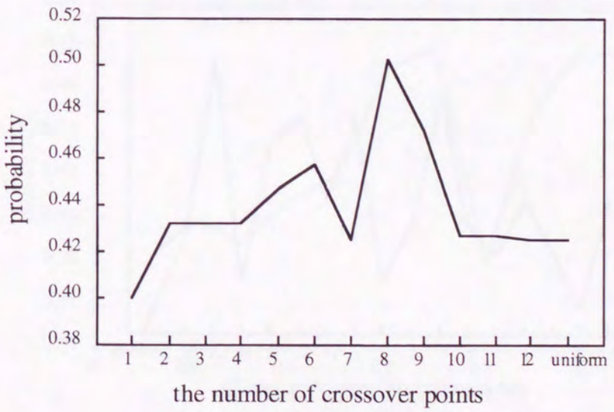

(c) probability to reach the global minima

Figure 4. 7 The dependence of stabilities, convergent generations and probabilities of reach the global minima on CP in 15 sites network is illustrated.

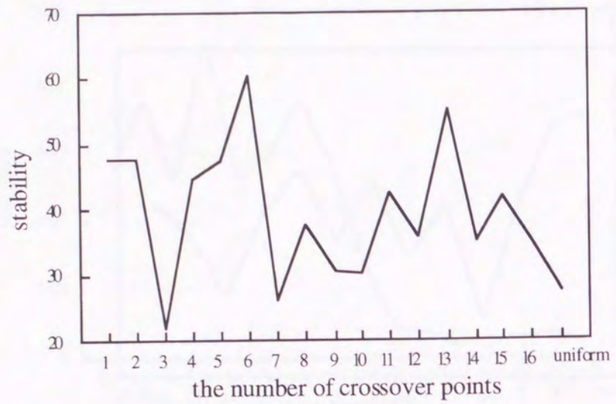

(a) stabilities

(b) convergent generation

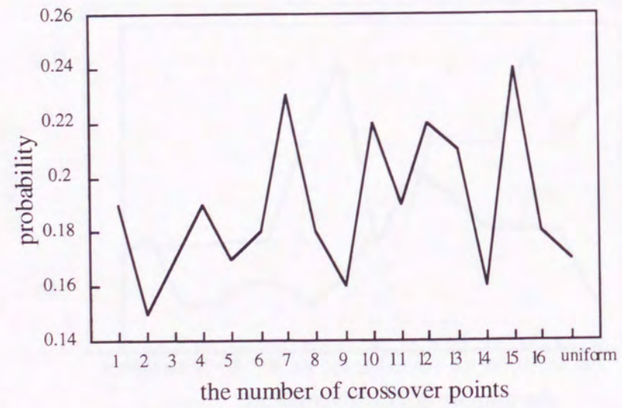

(c) probabilities to reach the global minima

Figure 4. 8 The dependence of stabilities, convergent generations and probabilities of reach the global minima on CP in 19 sites network is illustrated.

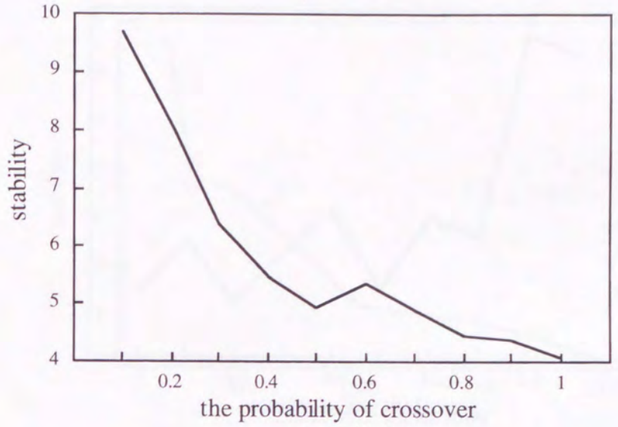

(a) stabilities

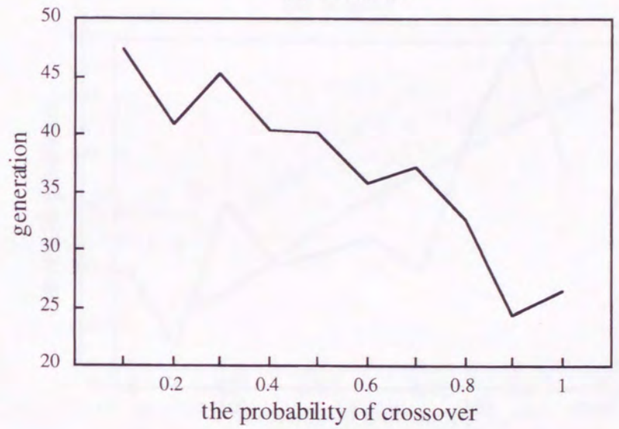

(b) convergent generation

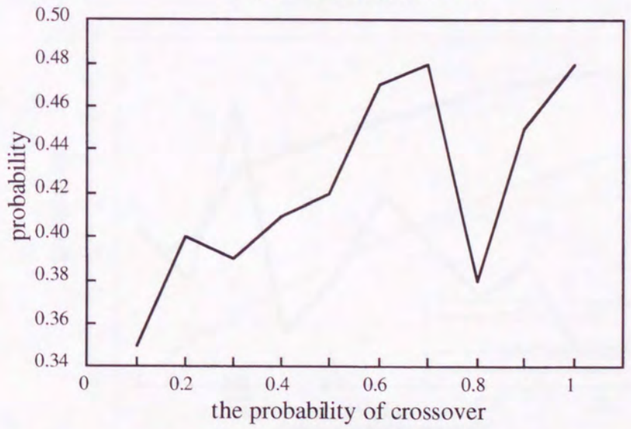

(c) probabilities to reach global minimum

Figure 4. 9 The dependence of stabilities, convergent generations and probabilities of reach the global minima on p_c in 15 sites network is illustrated.

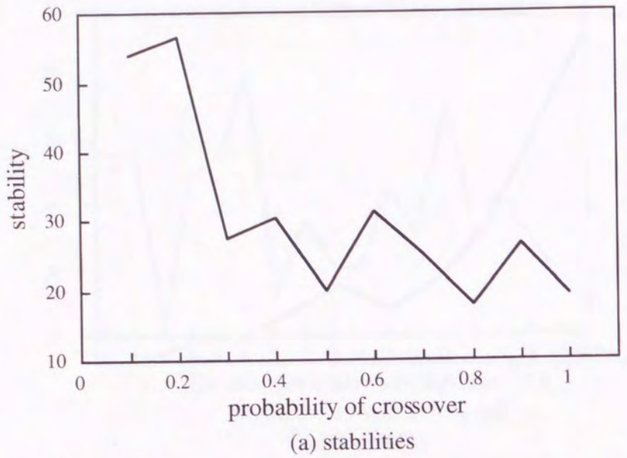

(a) stabilities

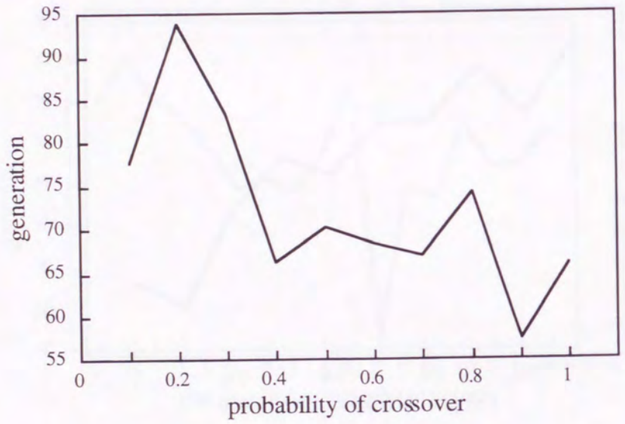

(b) convergent generation

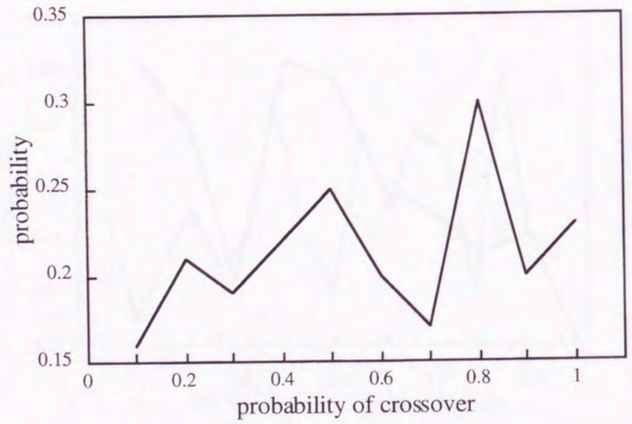

(c) probabilities to reach global minimum

Figure 4. 10 The dependence of stabilities, convergent generations and probabilities of reach the global minima on p_c in 19 sites network is illustrated.

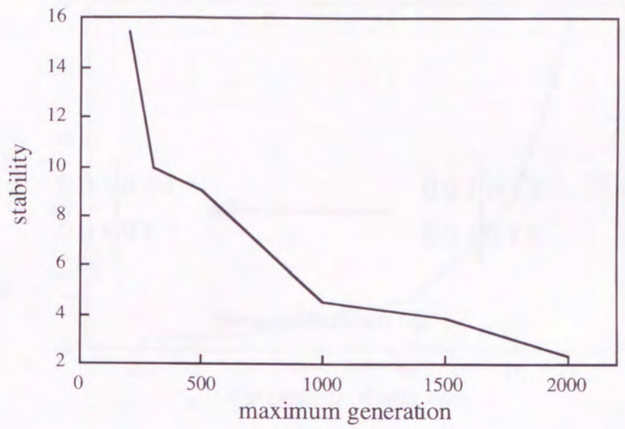

(a) stability

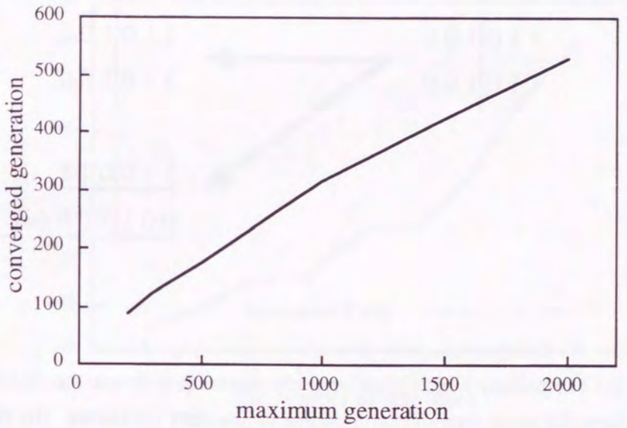

(b) generation

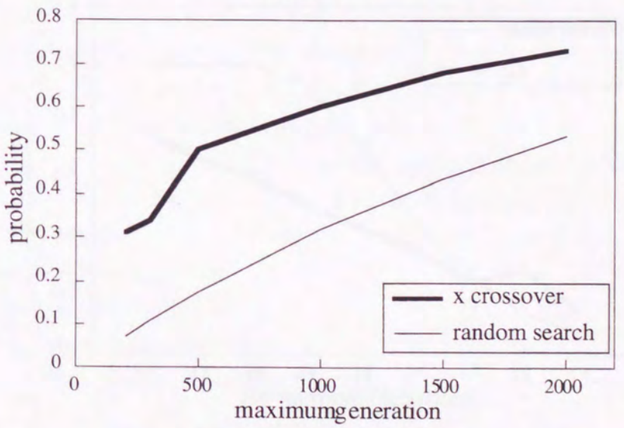

(c) probability

Figure 4. 11 The dependence of stabilities, convergent generations and probabilities of reach the global minima on k_{max} of GA's with $\bar{x}$ crossover for 19 spin sites is illustrated.

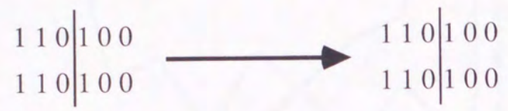

(a) standard crossover

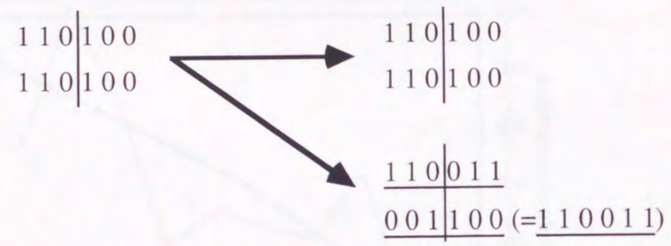

(b) $\overline{x}$ crossover

Figure 4. 12 (a) The parents which have same chromosome generate the children which have the same type of chromosome by standard crossover. (b) The new type of chromosome (underlined) is generated even if two parents have same chromosome.

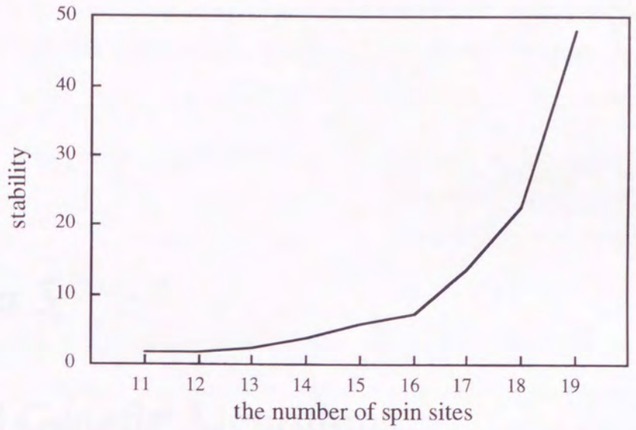

(a) stabilities

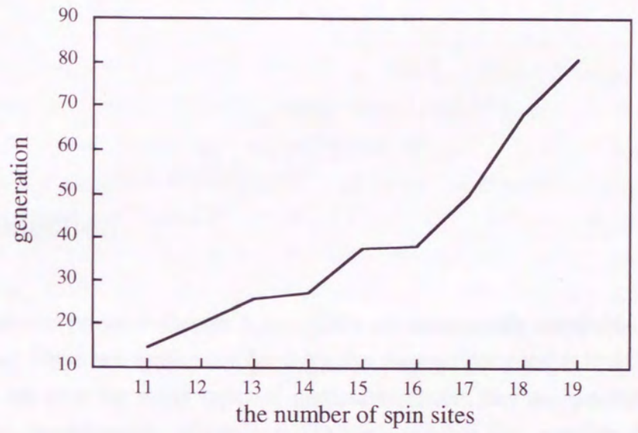

(b) convergent generation

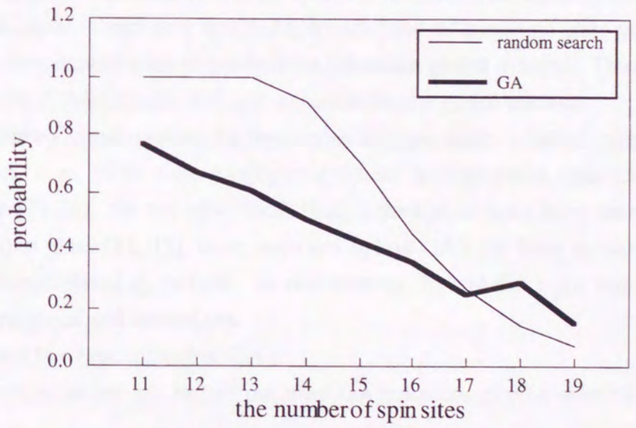

(c) probabilities to reach the global minima

Figure 4. 13 The dependence of stabilities, convergent generations and probabilities of reach the global minima on the number of spin sites is illustrated.

Chapter 5

Hybrid Genetic Algorithms

5. 1 Introduction

As shown in previous chapter 4, pure GA's are occasionally unsuitable for search for global minima. There is a weak point for GA's that they are not good at local search. Thus, though GA's can give the many types of metastable states, they are not able to give just global minima, occasionally. Some pure GA's are suitable for searches for the global minima, i. e. $\overline{x}$ crossover in section 2. 5. 2 and 4. 4, GA's with replacement of randomly generated individuals in section 4. 6. 1 and GA's for fixed $\pm J$ Ising spin glass proposed by Pái [8], however, they require a lot of generations till obtain global minima. Thus, hybrid GA's which include local searches are desirable to search for the global minima.

In geometry optimizations for molecules and polymers, a lot of hybrid GA's have been proposed, i. e., GA's with conjugate-gradient minimization, molecular dynamics quenching, etc [71-76]. On the other hand, though the hybrid GA's have been proposed for fixed $\pm J$ EA spin glass [11, 12], there were not hybrid GA's for Ising model spin network problems with calculated J_{ab} values. In this chapter, hybrid GA's for Ising model spin networks are proposed and carried out.

There are two types of hybrid GA's:

(1) The heuristic searches are carried out after GA calculations (GA solution → heuristic) [87].

(2) The individuals are obtained by heuristic methods before GA trials (heuristic solutions → GA) [88].

In this chapter, type (2) hybrid GA's are carried out.

In following section 5. 2, local search around hamming distance of 1 is used with GA's. Because this is simplest local search procedure, it is good example for investigation of hybrid GA's.

In section 5. 3, hill climbing algorithm is mixed with GA's. In this algorithm, the local search mentioned in section 5. 2 is repeated till fall into local minima. These local minima are adopted as individuals of GA's, and pure GA's are carried out.

Summary of this chapter is described in section 5. 4.

5. 2 1- neighborhood search

5. 2. 1 The neighborhood having hamming distance of 1

In GA's, candidate of solutions which have similar genotypes state to each other are known as the "neighborhood". For GA's for Ising model, similar genotypes decode to similar phenotypes. The degrees of resemblance between two individuals are described by hamming distance mentioned in section 3. 2. The nearer neighborhood have smaller hamming distance.

Though GA's can search through the various possible solutions, they are frequently unsuitable for local search. In GA's discussed previous chapter 4, local search are carried out in only mutation phase. In selection phase, individuals are simply selected and their neighborhood is not considered. In crossover phase, because the phenotypes of generated children are generally different from those of parents, the neighborhood is not searched, as shown in **Fig 5. 1**. Even though a fit individual which are very similar to global minima is obtained, crossover operators frequently break this precious individual.

For Ising model, the neighborhoods which have hamming distance of 1 (abbreviated as 1-neighborhood) are the nearest pair, as shown in **Fig 5. 2** (a). When the length of chromosome is n, there are n 1-neighborhoods around one individual, as illustrated in **Fig 5. 2** (b). These neighborhoods are different from an original individual at only one gene. The fitness of the original and neighborhoods are compared with each other, the fittest one is adopted in next generation. The selected individual is nearer to global or local minima than original one, as shown in **Fig 5. 3**.

5. 2. 2 Methods and procedures

When the generation change, a new population is given. Before all genetic operations, one individual is picked up, and all 1-neighborhoods of it are considered. The difference of fitness between the original and one of the neighborhoods is equal to following eq. (5. 1):

$$\delta E = 2\sum_{j\neq i} J_{ij} s_i s_j \qquad (5.\ 1)$$

where,

$$\delta E = E(neighborhood) - E(original)$$

i:the locus which is occupied by different gene in the original and the neighborhood.

When some of neighborhoods have larger fitness than an original individual, the fittest neighborhood replace the original, as shown in **Fig. 5. 4**. When no neighborhoods has larger fitness than an original individual, the original individual is adopted without change. In this case, this individual is the local or global minimum. This procedure is adopted to all individuals, a new population is given. Genetic operators are used for this new population.

In this method, neighborhoods are different from an original individual at only one gene, therefore, 1-neighborhood search is similar to mutations. This search is able to be regarded as the particular situation of a mutation depending on energies, mentioned as following eq. (5. 2)

mutation depending on energies:

$$\begin{aligned} p_m &= e^{\beta\delta E} && \left(f_{current}(x) > f_{mutate}(x)\right) \\ &= 1 && \left(f_{current}(x) \le f_{mutate}(x)\right) \end{aligned} \qquad (5.\ 2)$$

1-neighborhood search:

$$\begin{aligned} p_m &= 0 && \left(f_{original}(x) > f_{neighbor}(x)\right) \\ &= 0 && \left(f_{original}(x) \le f_{neighbor}(x),\ f_{neighbor}(x) \neq \max(f(x))\right) \\ &= 1 && \left(f_{original}(x) \le f_{neighbor}(x),\ f_{neighbor}(x) = \max(f(x))\right) \end{aligned} \qquad (5.\ 3)$$

As shown in these equations, 1-neighborhood search is similar to very low-T situations of mutation depending on energies.

In order to investigate the validity of this type of GA, 15 and 19 sites network are calculated. For this GA, CP=8 (for 15 sites) and CP=10 (for 19 sites) are adopted, and elitist preserving selection is used. Mutations are not carried out, because 1-neighborhood search plays a role of mutations. Other parameters are same as S-GA.

5. 2. 3 Results and discussions

The stabilities, convergent generations and probabilities to reach the global minima for adding 1-neighborhood search are shown in **Table 5. 1** and **5. 2**. For 15 sites networks, this type of GA gives global minima for all calculations, and for almost all 19-spin clusters, global minima are given. These solutions are given in much earlier generations than pure GA's. Pure GA's frequently are not more suitable than random search for 15 sites networks, however, GA with 1-neighborhood search can give better results than random search. These

results suggests that a local search method can compensate for weak points of GA's even though it is very simple.

5. 3 Hill climbing

5. 3. 1 Hill climbing search

The hill climbing search is one of the search methods to obtain local and global minima. This search is carried out by subsequential local search till it gives the local minima, as illustrated in **Fig. 5. 5** (a). At first, the energy (or fitness, etc.) of an initial point is calculated, and more stable states than initial are found. One of these states is chosen, and more stable neighborhood states than chosen one are found, again. This procedure are repeated till reach local or global minima, it is like a rolling stone on a slope.

Because the hill climbing search is too simple to find global minima, it is not suitable for optimizations. When the local minima are obtained, the hill climbing search is not able to avoid the minima. Thus, it explore only a little pattern of spin states, a lot of spin states remain without search. On the other hand, this search and GA's are used together, they are complemented each other. GA's are not suitable for local search, and hill climbing always can fall into local minima. The hill climbing is unsuitable for wide search, and GA's are able to explore various states. GA's with hill climbing search is illustrated in **Fig. 5. 5** (b).

5. 3. 2 Methods and procedures

In previous section 5. 2, 1-neighborhood search was provided. The hill climbing search is same as sequential trial of 1-neighborhood search. When the original individual is given, neighborhoods around it are considered by same approach of 1-neighborhood search. When the fittest neighborhood is selected, it is regarded as the next original individual in the hill climbing search. The neighborhoods around the new original individual are calculated again, and this approach is continued till fall into the local or global minimum. When the local minimum is obtained, it is adopted as the individual of GA's, and GA's are carried out.

According to the results of a previous section, global minima of 15 and 19 sites spin networks were almost obtained by GA with 1-neighborhood search, and these networks are too small to investigate the validity of GA with hill climbing. Thus, 100 sites clusters are considered for this algorithm. CP=50 are adopted, and elitist preserving selection is used. Other operators and parameters are same as S-GA.

5. 3. 3 Result and discussions

For 100 sites clusters, because all spin states are not able to be obtained, stabilities

and probabilities to reach the global minima are not able to be given. Thus, energies of the fittest individuals given by pure GA, GA with 1-neighborhood search and GA with hill climbing search are compared. The calculated energies given by GA with hill climbing search are shown in **Table 5. 3**.

GA with hill climbing search almost gives the most stable solutions of all. GA with hill climbing search always gives much more stable solutions than pure GA, and more stable than those of GA with 1-neighborhood search without only one cluster. From these results, GA's with more efficiently local search algorithm are expected to be able to give fitter solutions. On the other hand, the solutions are frequently obtained in more early generations by this GA than by pure GA's. It suggests that this type of GA is suitable for big clusters.

5. 4 Conclusion

It is found that more improvements for GA's give more suitable solutions, though some of pure GA's gave reasonable results for search for global minima of randomly generated Ising clusters. These improvements belong to last class of section 4. 7. The calculations of large clusters can be carried out by using of these improvements.

The GA's with local searches are useful for search for the global minima of randomly generated Ising model spin clusters. Even if very simple search was adopted, calculational results were more reasonable than pure GA's. Though pure GA's with $\overline{x}$ crossover or replacement by randomly generated individuals gave more suitable results than random search, GA's with the local search were much more suitable results. If more accurate local search are adopted, more reasonable results are expected to be obtained.

The local searches can not be always used with GA's, and appropriate local searches for given problem are required, however, hybrid GA's are frequently one of the best methods for optimizations.

Table 5. 1 The stabilities, convergent generations and probabilities to reach the global minima calculated by GA's with 1-neighborhood search for 15 sites spin networks.

	pure GA	GA's with 1-neighborhood search
average of stabilities	5.04	1.00
convergent generation	44.49	3.07
probability to reach the global minima	0.50	1.00
(probability in random search)	(0.704988)	(0.704988)

Table 5. 2 The stabilities, convergent generations and probabilities to reach the global minima calculated by GA's with 1-neighborhood search for 19 sites spin networks.

	pure GA	GA's with 1-neighborhood search
average of stabilities	30.19	1.02
convergent generation	77.23	4.98
probability to reach the global minima	0.22	0.98
(probability in random search)	(0.073456)	(0.073456)

Table 5. 3 The energies and convergent generation calculated by several hybrid GA's for 10 types of 100 sites spin clusters.

	energy/cm^{-1} (convergent generation)		
	pure GA	GA with 1-neighborhood search	GA with hill climbing search
cluster 1	-19144.821058 (299)	-19146.338207 (144)	◎- 19146.344495 (292)
cluster 2	-77835.026778 (289)	-77842.153410 (203)	◎- 77842.156823 (13)
cluster 3	-35095.175993 (221)	-35125.835278 (291)	◎- 35126.210076 (215)
cluster 4	-93113.395320 (256)	-93127.607569 (256)	◎-93127.793423 (164)
cluster 5	-53557.570196 (284)	◎- 53571.773003 (187)	-53571.771496 (209)
cluster 6	-109606.919753 (299)	-109616.993566 (204)	◎- 109618.485822 (235)
cluster 7	-84319.688287 (203)	-84325.201073 (240)	◎-84325.208202 (57)
cluster 8	-136162.984815 (296)	-136183.494138 (276)	◎-136183.528589 (231)
cluster 9	-55228.791826 (241)	-55240.873537 (166)	◎-55240.950263 (289)
cluster 10	-63555.887060 (268)	-63560.886179 (294)	◎- 63560.90461 (45)

◎ : The most stable solution.

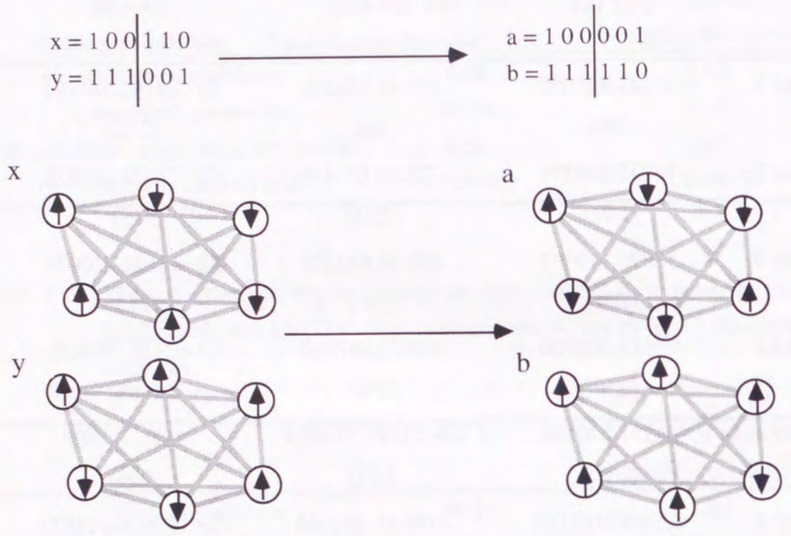

Figure 5. 1 The difference between parents and children. It is mentioned by hamming distance, and it is frequently large. In this figure, about half of all genes are different in parental and child chromosomes.

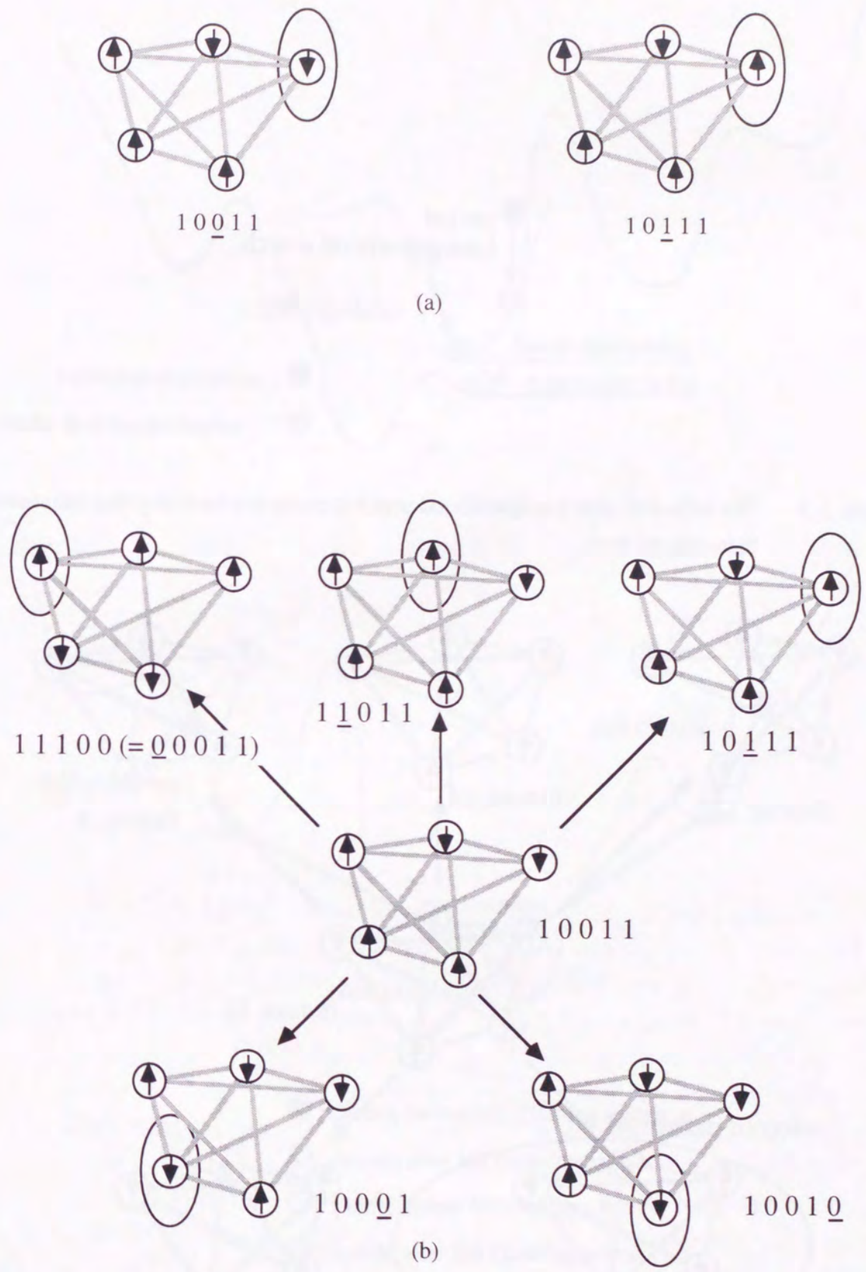

Figure 5. 2 (a) Two individuals whose hamming distance is 1. They are different at only one spin site. (b) n individuals which have 1 hamming distances from an original individual are illustrated.

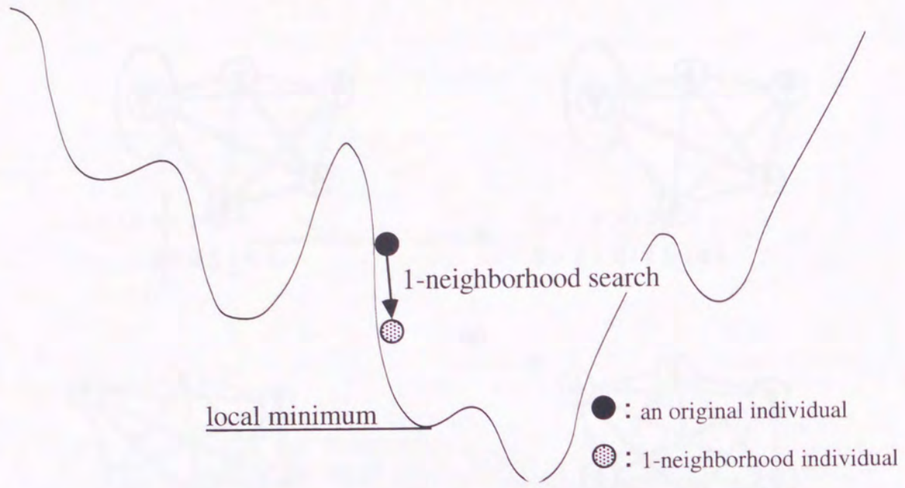

Figure 5. 3 The individual after 1-neighborhood search is nearer to a local or global minimum than original one.

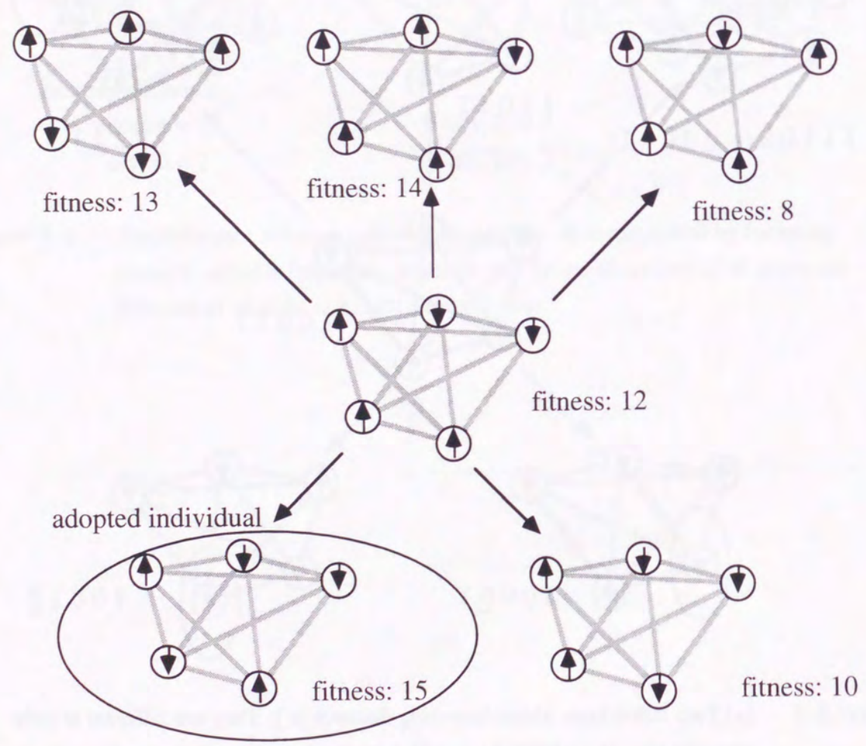

Figure 5. 4 1-neighborhood search is illustrated. The fittest individual of n+1 candidates is adopted to the current generation.

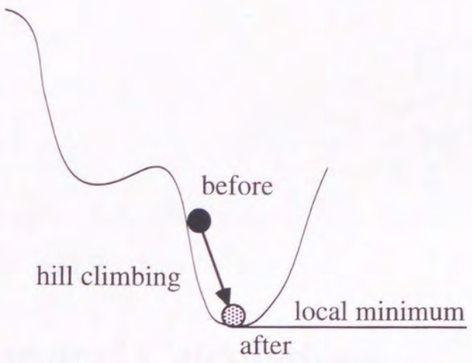

(a)

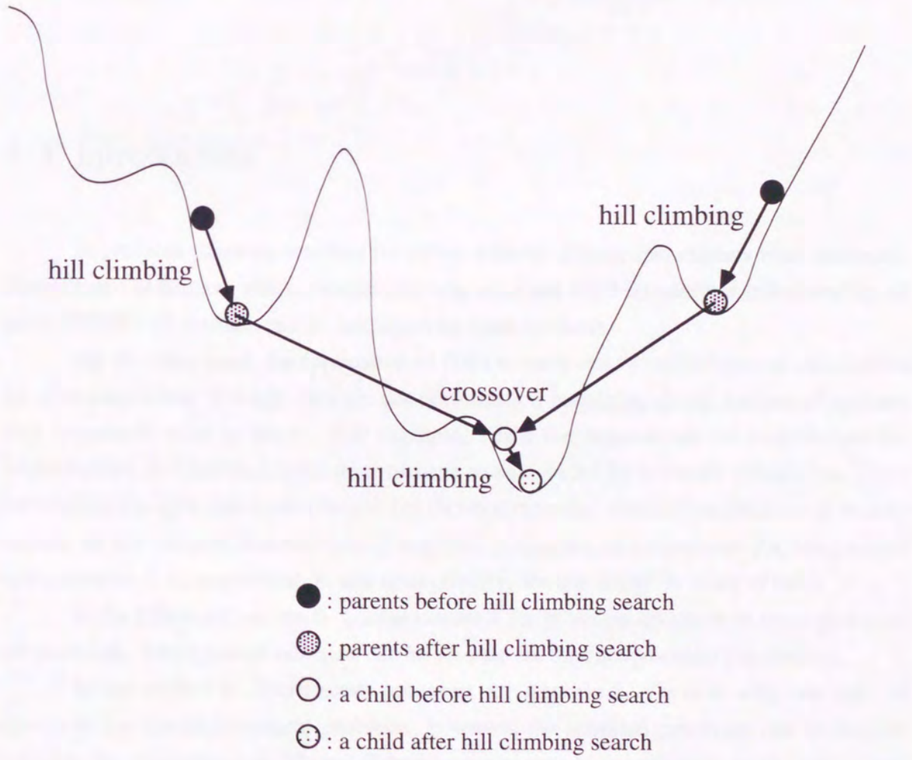

(b)

Figure 5. 5 (a) The hill climbing search and (b) GA's with the hill climbing search are illustrated.

Chapter 6

Thermodynamical Calculations

6. 1 Introduction

In previous chapters, searches for global minima of Ising spin clusters were discussed. Complicated networks, which contain 100 spin sites and 4950 interactions calculated by *ab initio* UHF/4-31G method, can be calculated by these methods.

On the other hand, the application of GA's to carry out thermodynamical calculations are also considered. Though they are not optimization problems, global minima of systems play important roles in them. For example, when the dependence on temperature for magnetization is calculated, local minima have to be avoided for a correct calculation. GA's are expected to give reasonable results for thermodynamical calculations because of widely search. In this chapter, dependences of magnetic properties on temperature for Ising model spin networks, i. e., magnetization and susceptibility, are calculated by using of GA's.

In the following section 6. 2, improvements for selection operators to these problems are provided. Two types of selection can be adopted for thermodynamical calculations.

In the section 6. 3, crossover operators are improved. There is only one type of crossover for thermodynamical problems, however, the standard crossover can be used to calculate the magnetization. Though $\overline{x}$ crossover can not use for this purpose by itself, it can assist the other operator.

In the section 6. 4, improvements for the mutation operators are provided. It is equal to the Metropolis method.

In the section 6. 5, the combinations of these improved operators are carried out, and thermodynamical properties are calculated. GA's are compared with the Metropolis method.

Summary of this chapter is described in section 6. 6.

6. 2 Improvement for selection

6. 2. 1 Selection based on Boltzmann distribution (S_e)

When there are a lot of states for one system, the probabilities of state i are equal to eq. (6. 1).

$$P_i = \frac{e^{\beta E_i}}{\sum e^{\beta E_i}} \tag{6. 1}$$

where, β is related to temperature, $\beta = 1/kT$. Thus, thermodynamical properties are obtained by this distribution. Though the exponential scaling provided in section 2. 3 is similar to this rule, the distribution of individuals in the last generation is not equal to eq. (6. 1) because k_{max} trials of selection operators are carried out. Assuming the random initial population and large enough population size, the distribution of individuals are able to be calculated as follows.

In the first generation, the probability of survival of one individual x_i is defined as eq. (6. 2), because all individuals randomly exist in initial generation.

$$p_{i,1} = \frac{f(x_i)}{\sum_j f(x_j)} \tag{6. 2}$$

where, the individual x_i decode to state i, and $f(x_j)$ is the fitness of x_i. The expectation value of the number of individuals which can decode to state i in first generation (abbreviated as $N_{i,1}$) is equal to eq. (6. 3).

$$N_{i,1} = N \times p_{i,1} = \frac{f(x_i)}{\sum_j f(x_j)} \times N \tag{6. 3}$$

where, N is the population size, which is the number of all individuals in a population.

In second generation, when only selection operators are considered, the individuals of this type survive with the probability $p_{i,2}$ mentioned as follows:

$$p_{i,2} = \frac{f(x_i)}{\sum_j \left(N_{j,1} \times f(x_j)\right)}$$

$$= \frac{f(x_i)}{\sum_j \left(\frac{f(x_j)}{\sum_k f(x_k)} \times N \times f(x_j) \right)}$$

$$= \frac{f(x_i)}{N \times \frac{\sum_j f(x_j)^2}{\sum_k f(x_k)}} \tag{6. 4}$$

Thus, $N_{i,2}$ is equal to eq. (6. 5) because individuals which belong to state i survive with probability $N_{i,1} \times p_{i,2}$ through the twice selection.

$$N_{i,2} = N_{i,1} \times p_{i,2} \times N$$

$$= \frac{f(x_i)}{\sum_j f(x_j)} \times N \times \frac{f(x_i)}{N \times \frac{\sum_j f(x_j)^2}{\sum_k f(x_k)}} \times N$$

$$= \frac{f(x_i)^2}{\sum_j f(x_j)^2} \times N \tag{6. 5}$$

Thus, in the last generation k_{max}, the expectation value of the number of individuals which belong to i $N_{i,k_{max}}$ is equal to eq. (6. 6).

$$N_{i,k_{max}} = \frac{f(x_i)^{k_{max}}}{\sum_j f(x_j)^{k_{max}}} \times N \tag{6. 6}$$

For this reason, Boltzmann distribution is not obtained by using exponential scaling. To the

purpose of Boltzmann distribution, scaling proposed in eq. (6. 7) is adopted.

$$g(x) = \exp\left(\frac{\beta f(x)}{k_{\max}}\right) \tag{6. 7}$$

By using this scaling, Boltzmann distribution is obtained in the last generation $k_{\max}$.

This scaling are expected to be similar to the exponential scaling discussed in section 4. 3. For example, eq. (6. 7) with T=1.0 is equal to the exponential scaling with T=1.0 $\times k_{max}$. Because GA's can search better states with higher T in exponential scaling, the larger k_{max} are desirable in eq. (6. 7). The larger k_{max} needs the larger computational times, and it is one of the weak points of this scaling.

6. 2. 2 Random selection (S_r)

The scaling proposed in eq. (6. 7) gives the Boltzmann distribution, however, this scaling has serious weak points, which is discussed not only in section 6. 2. 1, but also as follows. If the number of individuals (=population size) is infinite, eq. (6. 7) give the reasonable solutions to the purpose of investigations of thermodynamical properties. However, the population size is finite (in fact, only N=100 or 1000 is adopted), this scaling is not suitable for this purpose because the differences of fitness between superior and inferior individuals is overestimated in the low temperature, same as discussed in section 4. 4. To overcome this weak point, population size need to increase, it is frequently difficult because of the bounds of computers.

Without this scaling, any selection rules using fitness function can not give the Boltzmann distribution. Random selection (S_r), which does not use fitness, can be adopted for this purpose. By S_r, a population does not change from the current generation to the next generation. When the improvements of crossover and mutation operators achieve the Boltzmann distribution, this distribution is not broken because selection operators do nothing.

When S_r is adopted, improvements for crossover and mutation are indispensable to investigate thermodynamical properties. They are discussed in the sections 6. 3 and 6. 4.

6. 2. 3 Elitist preserving selection

Though the elitist preserving selection is a useful operator for search global minima, as discussed in section 4. 3, it prevents the Boltzmann distributions. When it is adopted in GA's, N-1 individuals are selected by the roulette rules, and operated by the crossovers and mutations. On the other hand, one individual, which is "elitist", does not obey these rules. Thus, the distribution of individuals is not equal to Boltzmann distribution because of the elitist individual. For this reason, the elitist preserving selection are not adopted for the studies of thermodynamical properties.

6. 3 Improvement for crossover

Crossover operators play important roles in GA's, because the wide searches are given by them. It is the one of advantages of GA's for thermodynamical problems that they can frequently avoid local minima, and this merit is obtained by crossover operations. When GA's are adopted for thermodynamical calculations, the improvements of crossover operators are indispensable.

6. 3. 1 Standard crossover (C_s)

In general, magnetic properties are broken by standard crossover operators because spin states are frequently different between parents and children, as mentioned in section 5. 2 and **Fig 5. 1**. When a pair of parents and children is picked up, not only spin states but also magnetizations are different between them. Naturally, susceptibilities and other magnetic properties can not be calculated. On the other hand, when all individuals in a population are considered, only magnetization can be calculated.

In crossover phase, the exchange of genes between two parents are done, however, no gene loses, no gene adds and no gene mutate. The genes in divided parts of parents never change, though the spin states change by crossover operators. Because the numbers of "1" and "0" of all individuals does not change by crossover, the sum of magnetizations of all children is same as that of parents. Only magnetization can be calculated by standard crossover (C_s).

6. 3. 2 Crossover with Metropolis method (C_M)

For the calculations of not only magnetizations but also other magnetic properties, C_s is not suitable because the Boltzmann distribution can not be obtained by C_s. The improvement for crossover is indispensable, and the procedures of improved crossover (C_M) are as follows.

After standard crossover, one of children and one of parents are randomly selected, the energies of them are calculated. The differences of energies between them are obtained, as eq. (6. 12).

$$\Delta E = E_{child} - E_{parent} \tag{6. 12}$$

where, E_{child} and E_{parent} are the energies of the child and their parent, respectively. By using ΔE, Metropolis method is carried out [85]. The crossover is adopted with the probability p_c' defined as follows:

$$\begin{aligned} p_c' &= e^{-\beta\Delta E} \quad (\Delta E > 0) \\ &= 1 \quad (\Delta E \le 0) \end{aligned} \tag{6. 13}$$

where, $\beta = 1/kT$, and k is equal to Boltzmann constant. When the crossover is not adopted, the parental individual remains in next generation.

6. 3. 3 $\bar{x}$ crossover ($C_{\bar{x}}$)

Because $\bar{x}$ crossover ($C_{\bar{x}}$) proposed in section 2. 5. 2 changes the number of "1" and "0", it can not be used together with C_s for the purpose of studies of magnetizations. On the other hand, it can be used with C_M provided in section 6. 3. 2. Though C_M is suitable for thermodynamical calculations, it frequently falls into the local minima in very low temperature. On the other hand, though individuals can escape from local minima by $C_{\bar{x}}$, it is unsuitable for thermodynamical calculations. Thus, the method C_M used with $C_{\bar{x}}$ is expected to give suitable solutions for Ising model spin networks.

In $C_{\bar{x}}$, four children are obtained by two parents, as mentioned in section 2. 5. 2. For the thermodynamical studies, only two children have to remain. Thus, either x_1-y_2 or x_1-$\bar{y}_2$, and either y_1-x_2 or y_1-$\bar{x}_2$ are randomly selected, two individuals are adopted. After this step, survivals are determined by C_M.

6. 3. 4 Results for the investigations of improvements of crossover

In order to investigate the behavior of improvements of crossover, searches for global minima are carried out. At first, only crossover operator is improved. The dependence of stabilities, convergent generations and probabilities to reach the global minima on temperature of C_M and C_M+$C_{\bar{x}}$ are shown in **Table 6. 1** and **Table 6. 2**, respectively. For these calculations, selection and mutation are same as pure GA's. Next, S_r provided in section 6. 2. 2 are adopted. In **Table 6. 3**, the results of GA's with S_r, $C_{\bar{x}}$ and C_M are shown. These results are compared and illustrated in **Fig. 6. 1** and **Fig 6. 2**.

For these calculations, parameters are adopted as follows: n=15 and 19, N=100, CP=1, p_m=0.01 in standard mutation. k_{max}=200 (for 15 sites) and 300 (for 19 sites) are adopted for GA without $C_{\bar{x}}$, k_{max}=200 (for 15 sites) and 1000 (for 19 sites) are used for GA's with $C_{\bar{x}}$. $T = 1 \times 10^{-5}$ to 1×10^{5} are adopted

The results of $C_M + C_{\bar{x}}$ are better than those of only C_M, and the results of $S_r + C_M + C_{\bar{x}}$ are the best of all. C_M can not avoid local minima, similar as C_s. $C_M + C_{\bar{x}}$ can make up for this disadvantage, however, C_M occasionally does not work well in low temperature even though $C_{\bar{x}}$ is used with. As shown in **Table 6. 1** and **6. 2**, the convergence is much faster in lower temperature by these algorithms. In lower temperature, the crossover is carried out in less probability than in higher temperature. Because the crossover is the key of GA's, better solutions can not be obtained when crossover are less adopted. Adopting S_r, this problem is overcome. The generation gap by S_r is much smaller than that of standard roulette rule, because S_r does nothing for a population. Because the population changes more slowly in GA's with S_r than any other selection operators, the bottleneck problem come more slowly.

6. 4 Improvement for mutation

In standard mutation, the mutational loci are randomly selected, and the properties of individuals are not considered. It can not be used for thermodynamical calculations. Only the mutation discussed in section 2. 6. 2 and 4. 5, which is similar to Metropolis method, can be adopted for this purpose.

6. 5 GA's for thermodynamical calculations

6. 5. 1 Methods and procedures

For thermodynamical calculations, improvements proposed in previous sections 6. 2, 6. 3 and 6. 4 are adopted. There are 6 types of combinations of them.

for all properties	only for the magnetization
I : $S_e + C_M + M_e$	I' : $S_e + C_s + M_e$
II : $S_r + C_M + M_e$	II' : $S_r + C_s + M_e$
III : $S_e + C_M + C_{\bar{x}} + M_e$	
IV : $S_r + C_M + C_{\bar{x}} + M_e$	

(S_e: exponential scaling, S_r: random selection, C_M: crossover with Metropolis methods, $C_{\bar{x}}$: $\bar{x}$ crossover, C_s: standard crossover, M_e: mutation depending on energies)

At first, these algorithms are used for search for global minima, and the validities of them are investigated.

Not only search for global minima, but also temperature dependences of magnetic behaviors of spin clusters are calculated. For 15 sites spin networks, thermodynamical calculations are carried out. For these calculations, $T = 1 \times 10^{-5}$ to 1×10^{5} are adopted. In order to search for global minima and thermodynamical calculations, k_{max} = 1000 and k_{max} = 3000 are adopted, respectively. The calculations of magnetization and susceptibility are started at 2000th generation because the no influence of initial individuals are required.

6. 5. 2 Results and discussions

search for global minima

The results of search for the global minima by 6 types of GA's are illustrated in **Fig. 6. 3**. These results suggest that selection operator is the most important operator for the search for the global minima. S_r gives more suitable solutions than S_e. Local minima are

occasionally obtained by GA's with S_e in very low and high temperature, because GA's with S_e occasionally can not avoid local minima in low temperature, and they possibly avoid global minima because of too many crossovers and mutations in high temperature. S_r is not influenced by temperature, therefore, GA's with S_r gives better solutions than GA's with S_e.

On the other hand, GA's with C_x^- are able to escape local minima, especially, $S_r + C_M + C_x + M_e$ perfectly gives global minima. Though C_x assists in searching for the global minima, $S_e + C_M + C_x + M_e$ occasionally falls into local minima similar to other algorithms including S_e.

thermodynamical calculations

The results of thermodynamical calculations for 15-spin clusters shown in **Fig. 6. 4** (A) and (B) are illustrated in **Fig. 6. 5** and **6. 6**, respectively. These results are compared with Metropolis Monte Carlo simulations (MC). Though initial individuals are randomly generated for GA's, ground states of spin clusters are adopted for MC calculations. For simpler network (A), the magnetizations calculated by all algorithms without $S_r + C_s + M_e$ are similar to results of MC. Though S_r was more suitable for searches for global minima than S_e as discussed in section 6. 3. 4, $S_r + C_s + M_e$ gave the most unsuitable solutions for thermodynamical calculations. Though S_r is one of the selection operators, it does not "select" the individuals but it rearrange the individuals. Thus, "survival of the fittest" is carried out very slowly and various individuals remain even though many generations change. Though the wide variety is desirable for the search for global minima, it is undesirable for the thermodynamical calculations. Because the average of all individuals is used for thermodynamical calculations, the wide variety frequently makes an error. It is desirable that all individuals become global minima for thermodynamical calculations.

On the other hand, C_M operates like as selections. Though the selection operator S_r does not "select", the crossover operator C_M "select" the individuals. The probability of crossover defined in eq. (6. 13) depends on energies of clusters, and it is substituted for the roulette rule. M_e is contained in all GA's for thermodynamical calculations, and it also operate similar to selection operator. In this operator, the probability of mutations defined in eq. (2. 8) is substituted for the roulette rule. Though only one operator M_e selects the individuals in $S_r + C_s + M_e$, two operators C_M and M_e are substituted for selection operator in $S_r + C_M + M_e$ and $S_r + C_M + C_x + M_e$. S_r is useful for the search for the global minima, and $C_M + M_e$ makes up for the weak points of S_r. Thus, $S_r + C_M + M_e$ and $S_r + C_M + C_x + M_e$ were able to give much more suitable solutions than not only $S_r + C_s + M_e$, but also $S_e + C_s + M_e$ and $S_e + C_M + M_e$.

The peaks of susceptibility curve by 3 types of GA's are equal to each other (5.0×10^{-5} K), and the peak of $S_e + C_M + M_e$ is 1.0×10^{-5} K higher than other GA's. The peak of susceptibility curve of MC is only 1.0×10^{-5} K lower than that of 3 types of GA's. For more complex network (B), $S_r + C_M + M_e$, $S_e + C_M + C_x + M_e$ and $S_r + C_M + C_x + M_e$ gives suitable results even though randomly generated initial states are used. The peaks of the susceptibility curve by these 3 algorithms and MC are almost equal to each other, similar to cluster (A).

It is interesting that $S_e + C_M + C_x + M_e$ worked better than $S_r + C_s + M_e$ for thermodynamical

calculations, though $S_r + C_s + M_e$ was more suitable for the search for global minima. Because C_x are expected to be able to avoid the local minima, $S_e + C_M + C_x + M_e$ gives much better solutions than other algorithms with S_e. It suggests that C_x^- plays an important role of thermodynamical calculations.

6. 6 Conclusion

Thermodynamical calculations requires different procedures from the search for the global minima. Two types of selections, three types of crossovers and one types of mutation were used for this purpose.

For selection operators, two types of operators were used. S_e is the one of the exponential scaling, which gives Boltzmann distribution. Though S_r is the selection operator, it does not "select" the individuals. It does nothing, and it can preserve the variety of individuals. GA's with S_r almost gave more suitable results for calculations of magnetic properties than those with S_e, except for $S_r + C_s + M_e$ which can not sufficiently select the fittest individuals.

There are three types of crossovers, which is C_s, C_M and $C_M + C_x^-$. For searches for global minima of spin clusters, GA's with $C_M + C_x^-$ can not always give reasonable results, however, they gave much better results than others for thermodynamical calculations. Because $C_M + C_x$ can overcome the weak points of S_r, $S_r + C_M + C_x^- + M_e$ is expected to be one of the most suitable algorithms for thermodynamical calculations of Ising spin clusters.

M_e is the only one type of mutation, and only one type of local search method which can use for thermodynamical calculations. Though the GA with $C_M + C_x^-$ occasionally gave unsuitable results for searches for global minima (**Table 6. 2**, **Fig. 6. 1** and **Fig. 6. 2**), GA's with $C_M + C_x^- + M_e$ almost gave global minima (**Fig. 6. 3**). Thus, it is expected to work well for local search.

Table 6. 1 The dependence of stabilities, convergent generations and probabilities to reach the global minima on the temperature of GA with C_M.

15 spin sites (100 trials)

temperature/K	stabilities	generation	probability
1.0×10^{-5}	9.01	22.67	0.33
1.0×10^{-4}	10.55	25.70	0.34
1.0×10^{-3}	11.27	23.44	0.31
1.0×10^{-2}	7.01	26.62	0.36
1.0×10^{-1}	6.78	22.57	0.37
1.0	8.66	24.46	0.44
1.0×10^{1}	6.77	21.50	0.38
1.0×10^{2}	7.49	25.60	0.34
1.0×10^{3}	6.85	31.56	0.41
1.0×10^{4}	5.86	43.08	0.44
1.0×10^{5}	6.52	49.41	0.40

19 spin sites (100 trials)

temperature/K	stabilities	generation	probability
1.0×10^{-5}	96.56	44.16	0.15
1.0×10^{-4}	66.87	36.59	0.20
1.0×10^{-3}	39.39	39.71	0.19
1.0×10^{-2}	111.63	40.50	0.10
1.0×10^{-1}	69.89	36.78	0.15
1.0	65.09	36.33	0.16
1.0×10^{1}	61.35	36.42	0.11
1.0×10^{2}	66.24	39.01	0.11
1.0×10^{3}	45.85	50.63	0.22
1.0×10^{4}	45.92	64.54	0.15
1.0×10^{5}	64.11	77.48	0.19

Table 6. 2 The dependence of stabilities, convergent generations and probabilities to reach the global minima on the temperature of GA with $C_M + C_x$.

15 spin sites (100 trials)

temperature/K	stabilities	generation	probability
1.0×10^{-5}	4.95	22.97	0.44
1.0×10^{-4}	5.67	26.22	0.47
1.0×10^{-3}	6.89	28.01	0.43
1.0×10^{-2}	5.05	21.90	0.49
1.0×10^{-1}	5.17	25.92	0.46
1.0	8.29	21.73	0.47
1.0×10^{1}	7.03	20.36	0.40
1.0×10^{2}	4.80	34.62	0.48
1.0×10^{3}	5.04	36.16	0.51
1.0×10^{4}	4.60	46.37	0.54
1.0×10^{5}	2.02	65.95	0.72

19 spin sites (100 trials)

temperature/K	stabilities	generation	probability
1.0×10^{-5}	30.61	87.85	0.29
1.0×10^{-4}	35.11	59.58	0.20
1.0×10^{-3}	30.29	59.04	0.20
1.0×10^{-2}	54.05	67.82	0.22
1.0×10^{-1}	37.49	76.44	0.17
1.0	29.00	99.85	0.23
1.0×10^{1}	35.86	79.51	0.14
1.0×10^{2}	65.45	55.90	0.33
1.0×10^{3}	27.60	102.12	0.23
1.0×10^{4}	31.95	186.18	0.29
1.0×10^{5}	8.28	228.03	0.56

Table 6. 3 The dependence of stabilities, convergent generations and probabilities to reach the global minima on the temperature of GA with $S_r + C_M + C_x$.

15 spin sites (100 trials)

temperature/K	stabilities	generation	probability
1.0×10^{-5}	1.43	27.43	0.85
1.0×10^{-4}	1.62	28.25	0.83
1.0×10^{-3}	1.36	28.51	0.82
1.0×10^{-2}	1.38	28.44	0.89
1.0×10^{-1}	1.66	26.39	0.84
1.0	1.43	29.64	0.89
1.0×10^{1}	1.57	30.11	0.84
1.0×10^{2}	1.49	30.48	0.81
1.0×10^{3}	1.80	42.12	0.77
1.0×10^{4}	1.44	59.25	0.81
1.0×10^{5}	1.41	75.51	0.70

19 spin sites (100 trials)

temperature/K	stabilities	generation	probability
1.0×10^{-5}	5.25	70.86	0.57
1.0×10^{-4}	3.88	59.93	0.55
1.0×10^{-3}	6.74	93.05	0.58
1.0×10^{-2}	4.84	69.25	0.59
1.0×10^{-1}	5.35	86.42	0.60
1.0	5.06	67.32	0.60
1.0×10^{1}	4.07	64.19	0.52
1.0×10^{2}	7.11	101.58	0.51
1.0×10^{3}	3.53	112.75	0.48
1.0×10^{4}	6.65	213.60	0.52
1.0×10^{5}	2.32	386.54	0.55

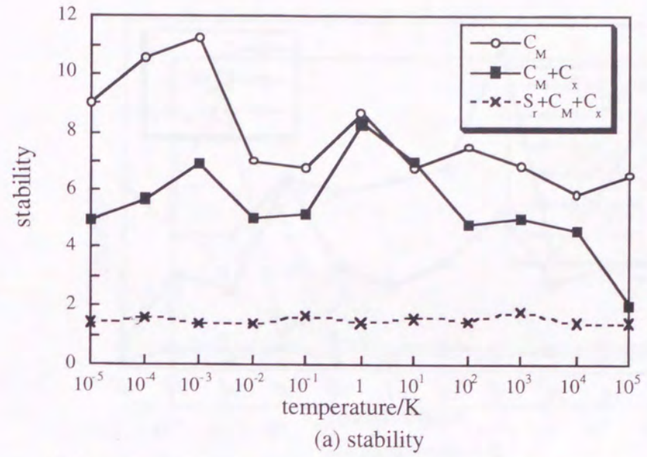

(a) stability

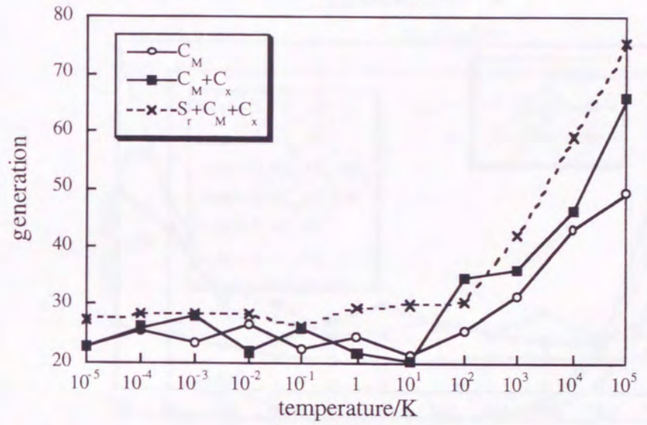

(b) convergent generation

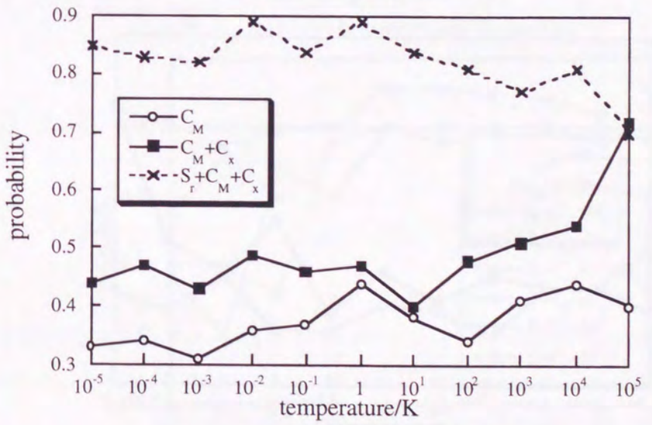

(c) probability to reach the global minima

Figure 6. 1 The dependence of stabilities, convergent generations and probabilities to reach the global minima on the temperature of GA's with C_M for 15 sites networks.

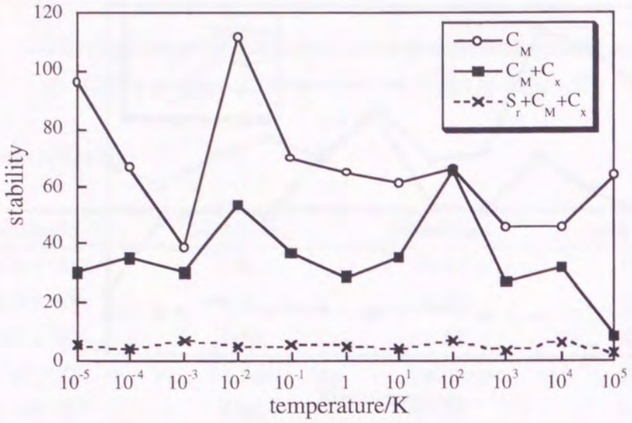

(a) stability

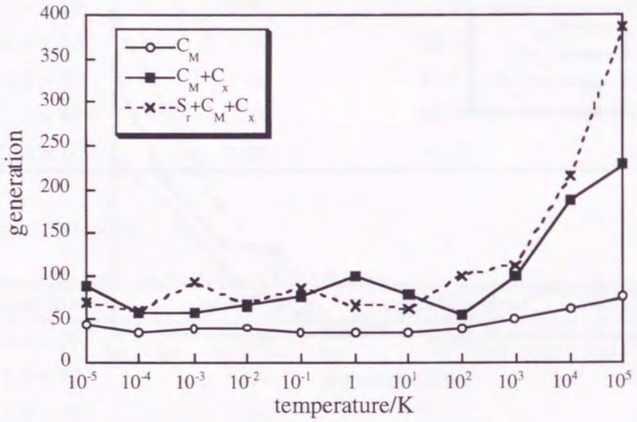

(b) convergent generation

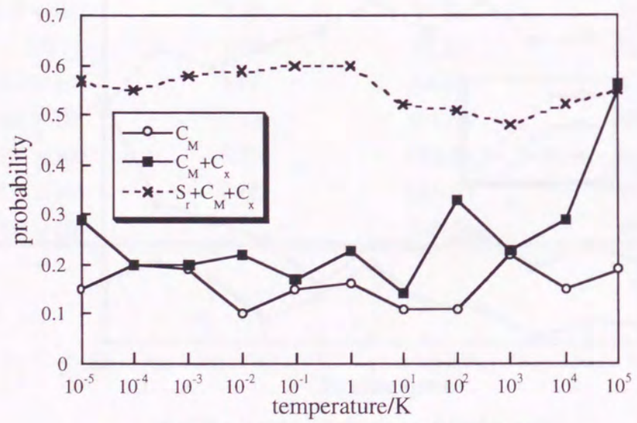

(c) probability to reach the global minima

Figure 6. 2 The dependence of stabilities, convergent generations and probabilities to reach the global minima on the temperature of GA's with C_M for 19 sites networks.

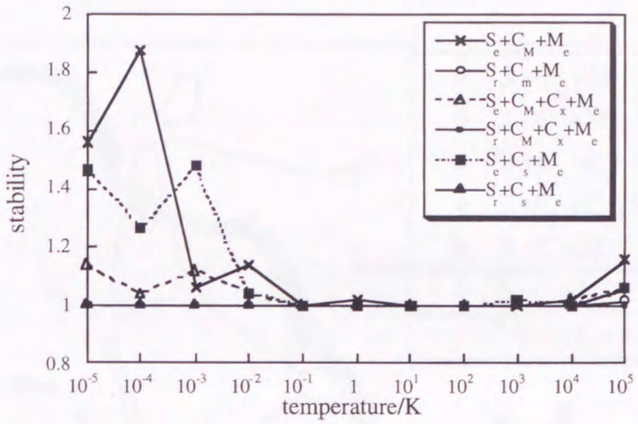

(a) stability

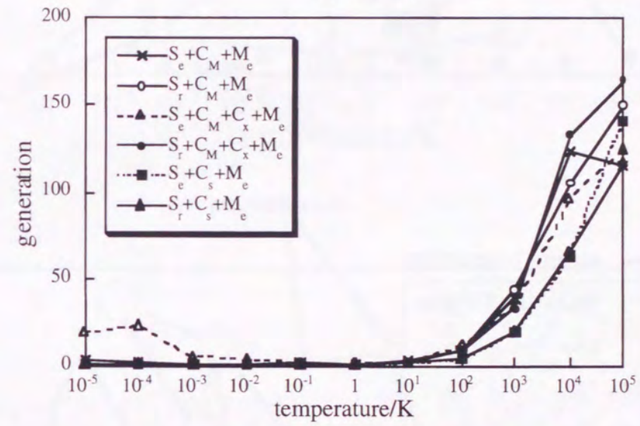

(b) convergent generation

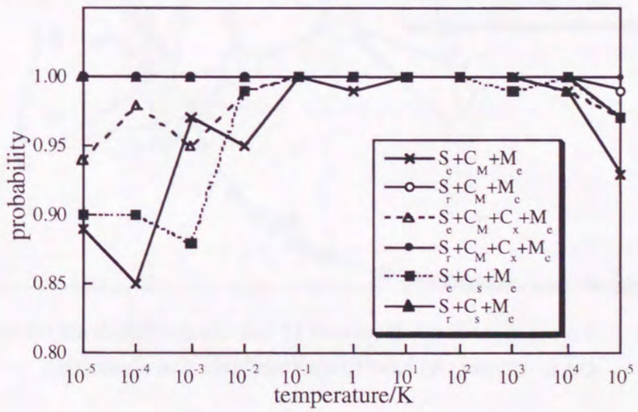

(c) probability to reach the global minima

Figure 6. 3 The results of search for the global minima by several improved GA's.

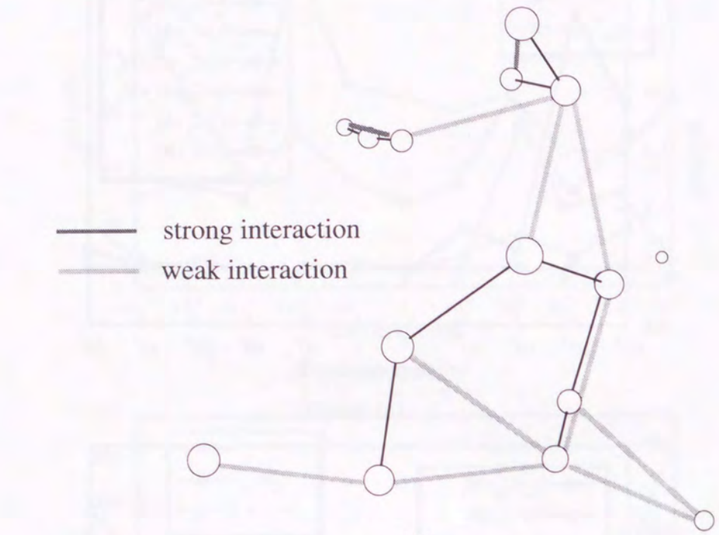

(A)

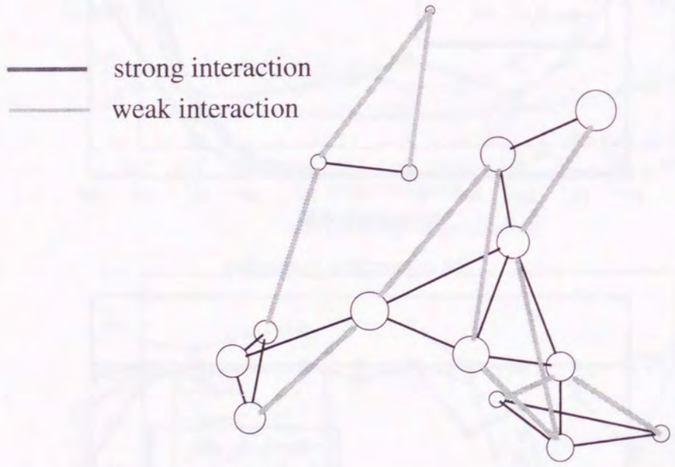

(B)

Figure 6. 4 2 types of randomly generated 15-spin clusters which are calculated by improved GA's. Cluster (A) have simpler network than cluster (B).

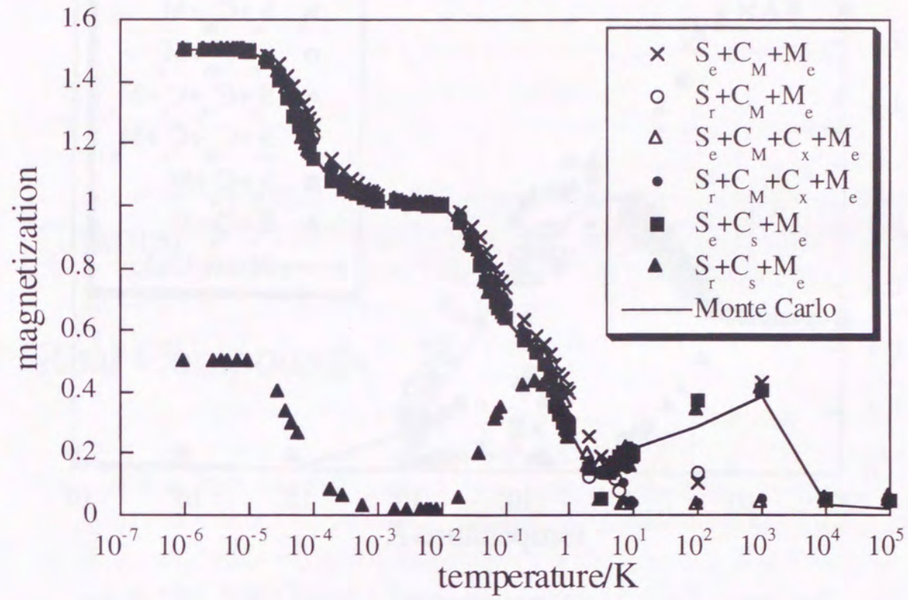

(A) magnetization

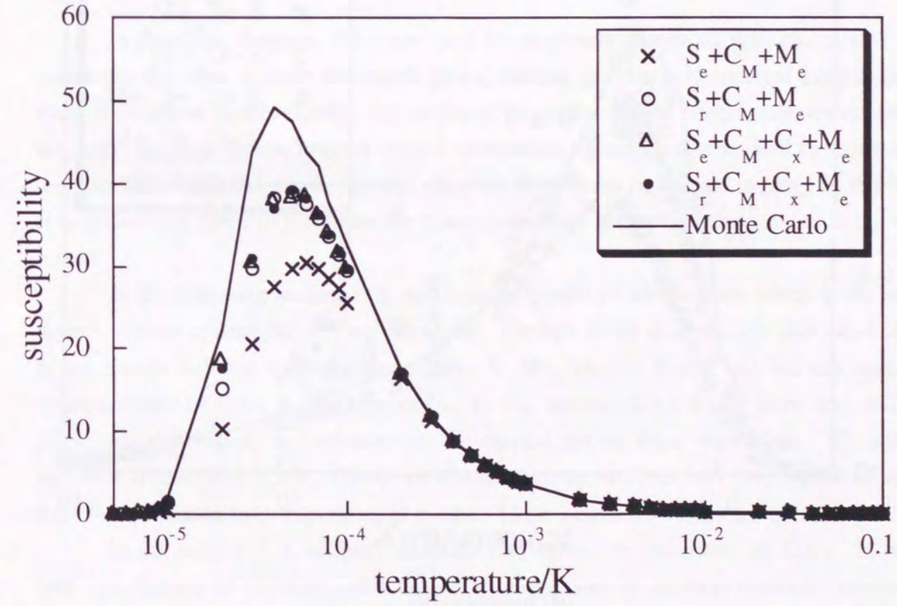

(B) susceptibility

Figure 6. 5 The dependence of magnetic properties on temperature in 15-spin cluster shown in **Fig. 6. 4** (A).

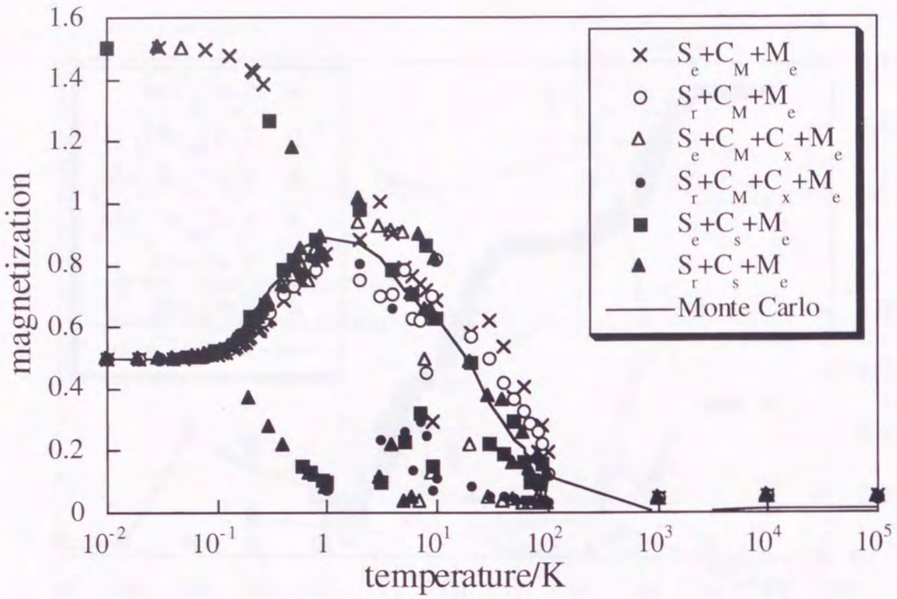

(A) magnetization

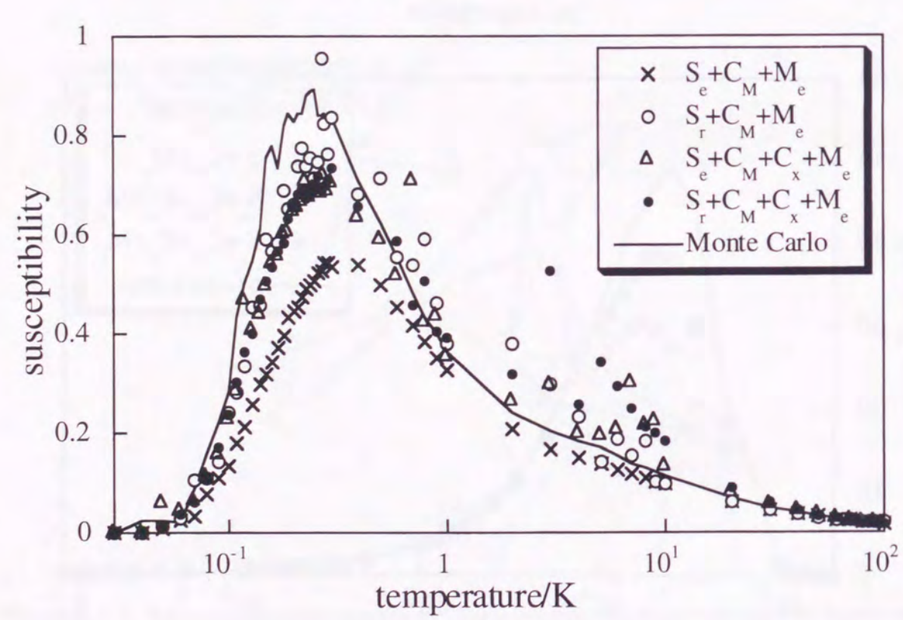

(B) susceptibility

Figure 6. 6 The dependence of magnetic properties on temperature in 15-spin cluster shown in **Fig. 6. 4** (B)

Chapter 7

Real Compounds

7. 1 Introduction

In previous chapters, GA's are used for randomly generated spin clusters. It was found that GA's are suitable for search global minima and thermodynamical calculations of various clusters. In this chapter, the magnetic properties of real compounds are calculated. Recently, magnetic interactions of several compounds have been investigated by calculations and experiments, for example, nitronyl nitroxide derivatives mentioned in part I of this these. It is interesting that GA's operate for investigations of magnetic behaviors by using these results.

In the following section 7. 2, magnetic properties of Mn_{12} cluster which is the metal-organic radical system [89, 90] are calculated. Though S=1/2 is adopted in previous GA's, it is not always suitable for real compounds. In Mn_{12} cluster, S=3/2 and 4/2 are used, and improvements of GA's are indispensable. In this section, GA's which have four and five alleles are developed, and calculations are carried out by these algorithms. Though the magnetic interactions of Mn_{12} cluster are not obtained by MO methods, four types of J values have been assumed from experimental results. These assumed J values are used for GA's.

In the section 7. 3, nitronyl nitroxide derivatives are calculated by GA's. In part I, MO calculations of intermolecular magnetic interactions of nitronyl nitroxide derivatives crystals were carried out. It was found that DFT methods reproduced the experimental results, qualitatively. According to these results, thermodynamical calculations of nitronyl nitroxide derivatives are carried out by using calculated J_{ab} values in this section.

7. 2 Mn_{12} cluster

7. 2. 1 Cluster structure and magnetic behavior of Mn_{12}

Considerable effort has been directed at understanding magnetic exchange interactions occurring in polynuclear transition-metal complexes. Recently, Sessoli and his co-worker reported the syntheses and electrochemical and magnetochemical properties of $[Mn_{12}O_{12}(O_2CPh)_{16}(H_2O)_4]$ (**3**), its solvate **3**·PhCOOH·CH_2Cl_2, and $[Mn_{12}O_{12}(O_2CMe)_{16}(H_2O)_4]$·MeCOOH·$3H_2O$ (**4**) [89]. These compounds have four Mn^{IV} and eight Mn^{III}. **3** consists of a central $[Mn^{IV}_4O_4]^{8+}$ cubane held within a nonplanar ring of eight Mn^{III} atoms by eight μ_3-O_2^- ions. Peripheral ligation is provided by 16 μ_2-O_2CPh^- and four terminal H_2O groups, where the four H_2O ligands are located on two Mn atoms.

Magnetization measurements are used to determine that in these fields complex **3** and **3**·PhCOOH·CH_2Cl_2 have S=10 and S=9 ground states, respectively. AC susceptibility data in zero applied field are given for complexes **3** and **4**, and it is concluded that **3** has S=9 ground state and **4** has S=10 ground state at zero field.

In $Mn_4^{IV}Mn_8^{III}$ complex, there are at least four different types of pairwise exchange interaction illustrated as **Fig. 7. 1**. The parameter J_1 refers to Mn^{IV}... Mn^{III} pairs bridged by two μ-oxo ions; J_2 to Mn^{IV}... Mn^{III} pairs bridged by one μ_{oxo} ion; J_3 to Mn^{IV}... Mn^{IV} pairs; and J_4 to Mn^{III}... Mn^{III} pairs. Theoretical calculations of spin-state orderings assuming $J_1 > J_2$, $J_3 \gg J_4$ are presented to rationalize the S=8-10 ground states.

7. 2. 2 GA's for S≠1/2

Though S=1/2 is adopted for all GA calculations in previous chapters, s_i is not always equal to ±1/2 for real compounds, for example, S=3/2 and 4/2 in Mn_{12} cluster. The bitstring coding can not be used for these systems, and the improvements of three principal operators for GA's, which are selection, crossover and mutation, are indispensable.

coding

When S=1/2, spin states are described by binary bitstrings. s_i=1/2 and s_i=-1/2 code to "1" and "0", respectively. When S≠1/2, spin states can not be expressed only two alleles "1" and "0". For the purpose of GA calculations, it is necessary that all different spin states are given different alleles. Calculations for Mn_{12} cluster, alleles are defined as follows:

for spin sites i=1 to 8 of **Fig. 7. 1**:

s_i	-4/2	-2/2	0	+2/2	+4/2
allele	0	1	2	3	4

for spin sites i=9 to 12 of **Fig. 7. 1**:

s_i	-3/2	-1/2	+1/2	+3/2
allele	0	1	2	3

This type of coding can be used for other S≠1/2 spin clusters.

selection

Ising Hamiltonian is also used for fitness function same as GA's for S=1/2. All selection operators mentioned in previous chapters, which are the roulette rule selection and the random selection, can be adopted for S≠1/2 clusters without improvements. Coding procedure does not have an influence for selection operators.

crossover

Standard crossover (C_s) and Metropolis crossover (C_M) can be used same as S=1/2 clusters because the genes are not rewritten by these operators. On the other hand, improvement of $\bar{x}$ crossover ($C_{\bar{x}}$) are indispensable. In S=1/2 clusters, "1" are replaced "0" and "0" are replaced "1" by $C_{\bar{x}}$. For S=3/2 clusters, "0" ↔ "3" and "1" ↔ "2" are adopted, and for S=4/2 clusters, "0" ↔ "4", "1" ↔ "3" and "2" ↔ "2" are adopted by improved $C_{\bar{x}}$.

mutation

The improvements of mutation operators are indispensable to S≠1/2 clusters. In GA's for S=1/2 spin cluster, the mutation operator is the alternation of "1" ↔ "0". For S≠1/2 clusters, genes in selected loci change in mutation phase, randomly. For example, "0" mutate to "1" or "2" or "3" in S=3/2 spin site.

7. 2. 3 Results and discussions

The dependence of magnetizations and susceptibilities on temperature for Mn_{12} cluster is shown in **Fig. 7. 2** and **7. 3**. For these calculations, k_{max}=5000 and CP=6 are used, and other parameters are defined same as section 6. 5. Initial individuals are randomly generated. The calculations of magnetization and susceptibility are started at 4000th generation because the no influence of initial individuals are required.

S=10 ground states in low temperature are reproduced by two types of GA's with $C_{\bar{x}}$, especially $S_r + C_M + C_{\bar{x}} + M_e$. $S_r + C_M + M_e$, which is the GA with S_r without $C_{\bar{x}}$, can not give reasonable results, though it is able to give suitable spin states for randomly generated 15-spin clusters. According to these calculations, it was found that $C_{\bar{x}}$ play an important role for GA's. GA's without $C_{\bar{x}}$ are frequently not able to avoid the local minima because J_2 and J_3 have similar values to each other. Though the results of $S_e + C_M + C_x + M_e$ are reasonable in low and high temperature, it occasionally fell into the local minima around 30-40K. It suggests that $S_r + C_M + C_{\bar{x}} + M_e$ is the most suitable for thermodynamical calculations of 6 types of GA's.

7. 3 α-HQNN crystal

7. 3. 1 Intermolecular interactions in α-HQNN crystal

Crystal structure and intermolecular interactions of α-HQNN were discussed in chapter 4 in part I. This crystal exhibits a ferromagnetic phase transition at 0.5 K and it is a first organic ferromagnet which is constructed by hydrogen bonds [37-39]. In this crystal, the pair which has bifurcated hydrogen bonds (pair **B**) plays an important role for magnetic behavior of this crystal. This pair forms one hydrogen-bonded chain along c-axis. The interpair interaction along c-axis (pair **A**) is smaller than intrapair interaction. Interchain interactions (pair **C**, **D** and **E**) are smaller than those of pair **A** and **B** [91]. These interactions are illustrated in **Fig. 7. 4**.

In chapter 4 of part I, J_{ab} values have been obtained by several methods, and it was found that DFT methods give reasonable values. In this section, J_{ab} values calculated by UBLYP/4-31G, UB2LYP/4-31G and UB3LYP/4-31G methods are used, and magnetic behavior of α-HQNN is investigated. The $S_r + C_M + C_{\bar{x}} + M_e$ algorithm for $10 \times 10 \times 10$ cells (4000 molecules) and $15 \times 15 \times 15$ cells (13500 molecules) of α-HQNN is carried out. All genes of initial individuals are "1" because α-HQNN crystal has a ferromagnetic phase transition.

7. 3. 2 Results and discussions

The dependence of magnetizations and susceptibilities on temperature for α-HQNN is illustrated in **Fig. 7. 5**, **7. 6** and **7. 7**. According to **Fig. 7. 5**, $k_{max} = 700$ is expected to be enough large for these calculations. The results of calculations shown in **Fig. 7. 6** and **7. 7** are given by the GA's with $k_{max} = 700$. From these results, it was found that GA's can reproduce the ferromagnetic phase transition. The transition temperature is 0.24 K, 0.30 K and 0.31 K by using of the J_{ab} values calculated by UBLYP/4-31G, UB2LYP/4-31G and UB3LYP/4-31G methods, respectively, as shown in **Fig. 7. 6**. GA reproduces the experimental results of dependence of susceptibility on T/T_c in higher temperature than T_c, as shown in **Fig. 7. 7**. In lower temperature than T_c, because the magnetization was not dependent linearly on the external magnetic field, the susceptibility changed irregularly with lowering the temperature.

7. 4 Conclusions

In chapter 6, it was found that S_r is useful for thermodynamical calculations. And in this chapter, it was found that GA's with $C_{\bar{x}}$ are able to give the suitable spin states even if the spin clusters have many local minima. According to these results, $S_r + C_M + C_{\bar{x}} + M_e$ is

expected to be most useful for Ising model spin cluster of 6 types of GA's.

Though C_M is the important operator to thermodynamical calculations, the population tend to be "bottleneck" situation and escape from the "bottleneck" are difficult by C_M especially in low temperature. On the other hand, though $C_{\bar{x}}$ is not indispensable to thermodynamical calculations, it is expected to avoid the bottleneck problem. It is considered that the advantages of C_M and C_x make up for disadvantages of each other, and GA's with $C_M + C_x$ give reasonable results for Ising spin clusters.

For α-HQNN crystal, $S_r + C_M + C_x + M_e$ with J_{ab} values calculated by DFT methods give ferromagnetic phase transition and they reproduced the qualitatively experimental results. It suggests that both GA's and DFT methods are strong methods to study the magnetic behavior of organic radical crystals.

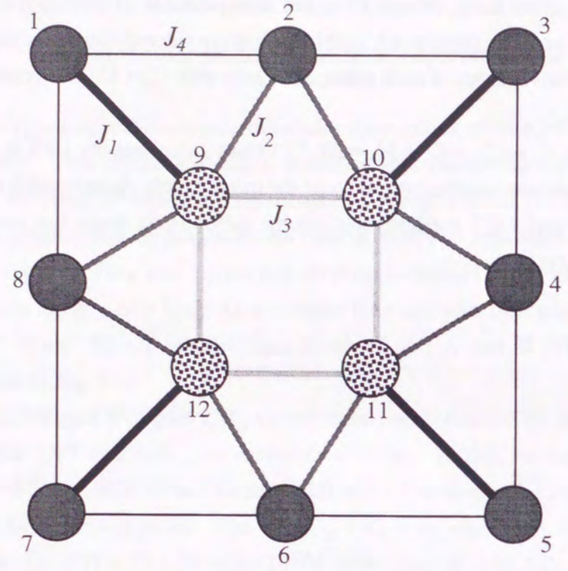

Figure 7. 1 Magnetic interactions in Mn_{12}.

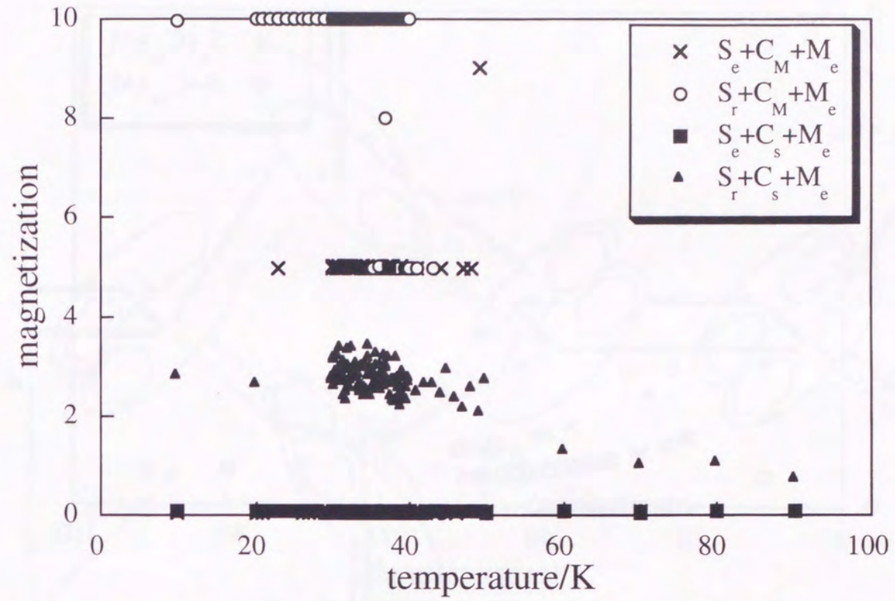

(a) GA's without C_x^-

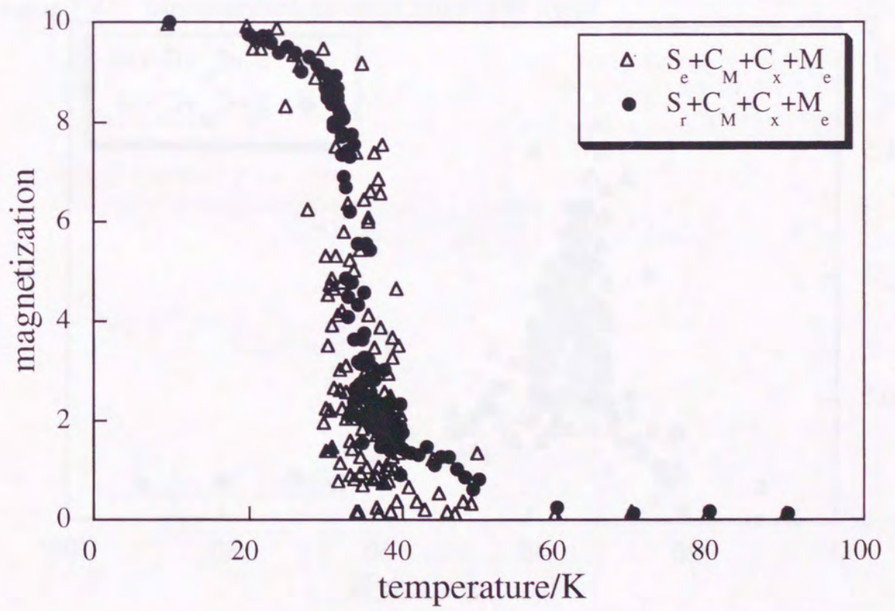

(b) GA's with C_x^-

Figure 7. 2 The dependence of magnetizations of Mn_{12} on the temperature calculated by several GA's.

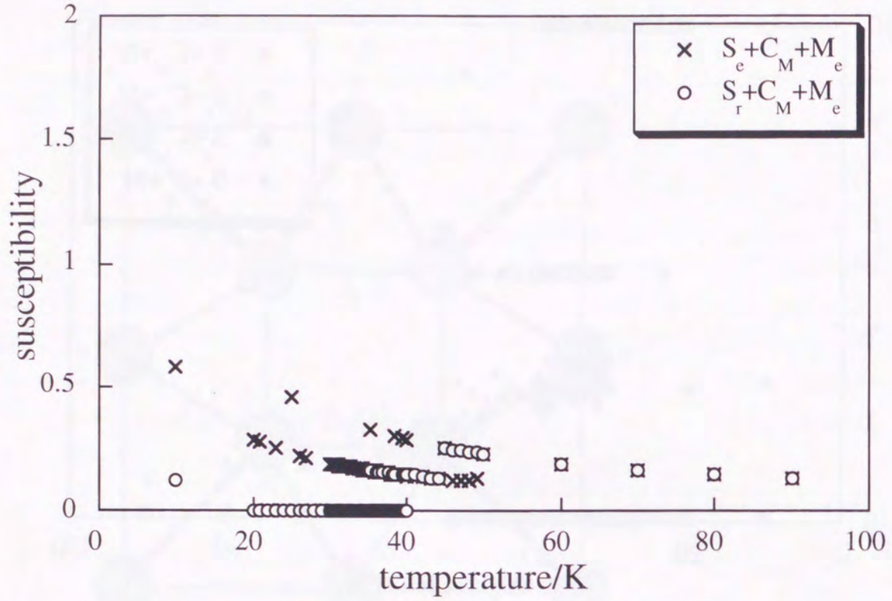

(a) GA's without C_x

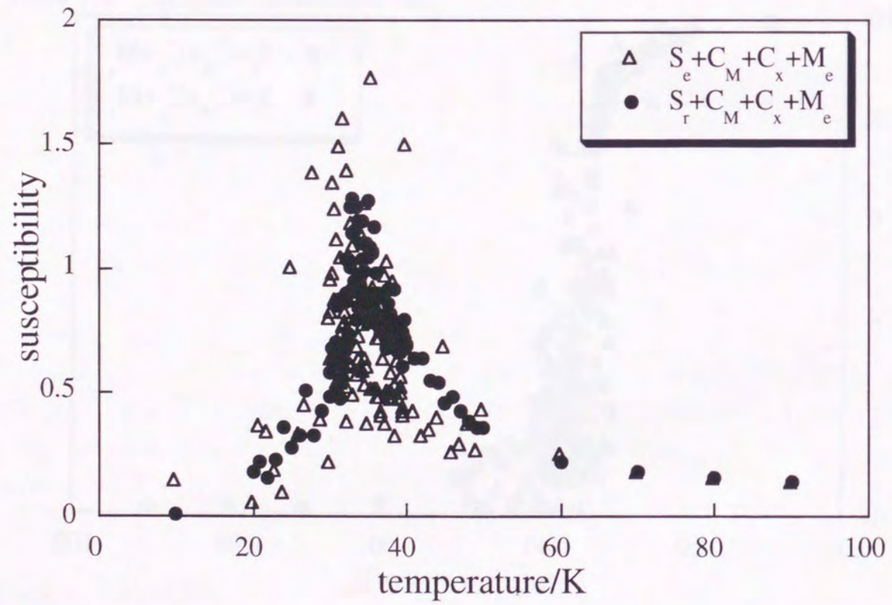

(b) GA's with C_x

Figure 7. 3 The dependence of susceptibilities of Mn_{12} on the temperature calculated by several GA's.

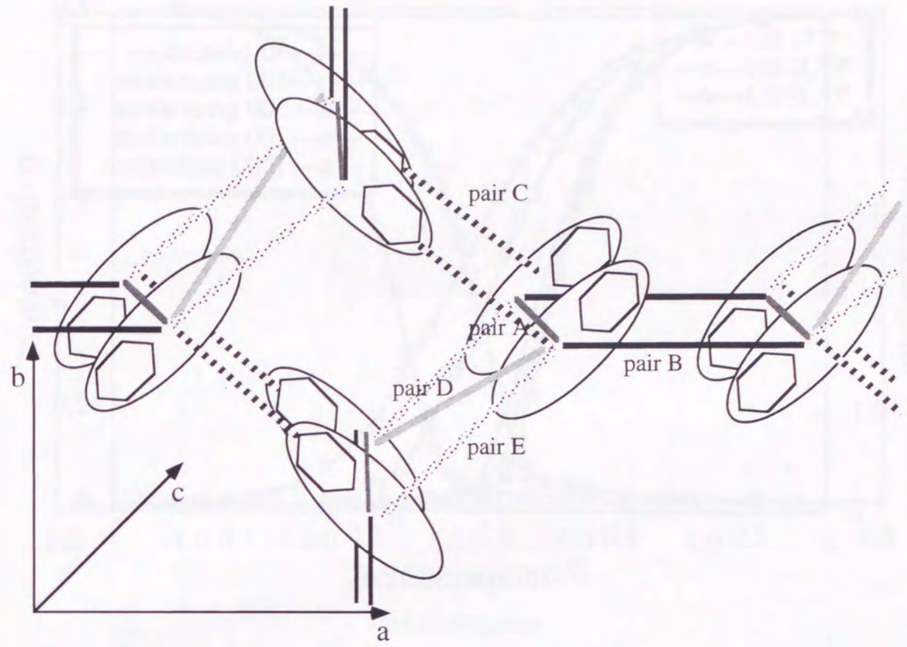

Figure 7. 4 Intermolecular interactions in α-HQNN crystal.

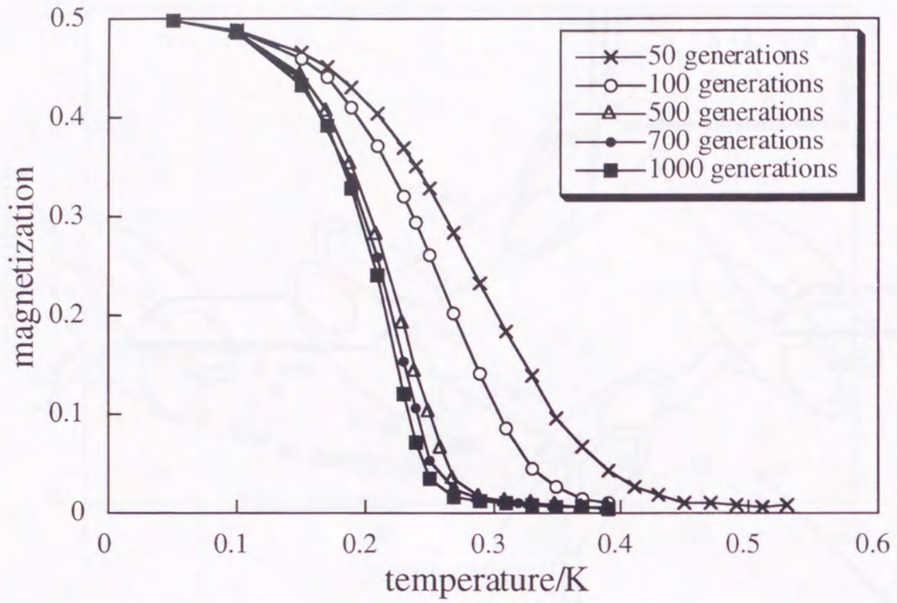

(a) magnetization

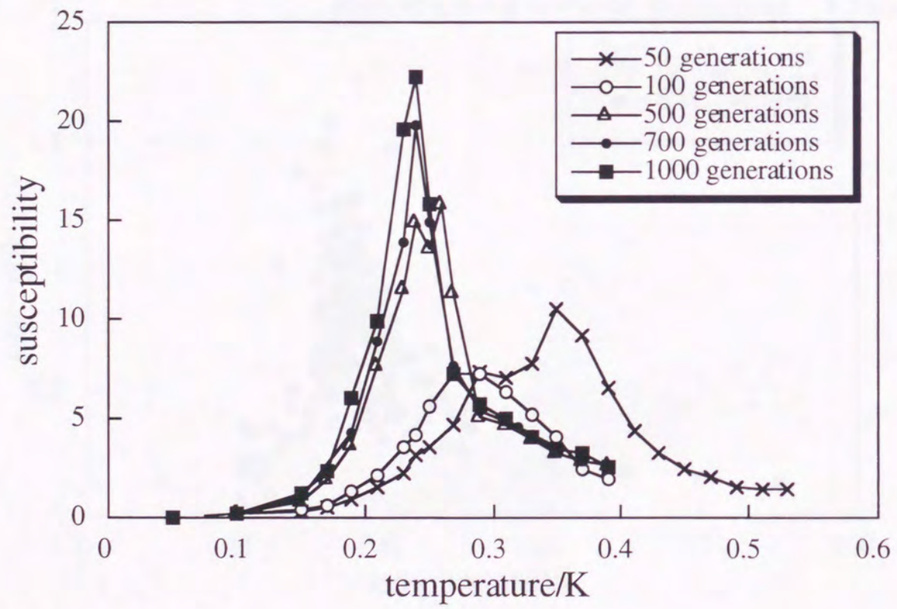

(b) susceptibility

Figure 7. 5 The dependence of the magnetizations and the susceptibilities on temperature for α-HQNN crystal.

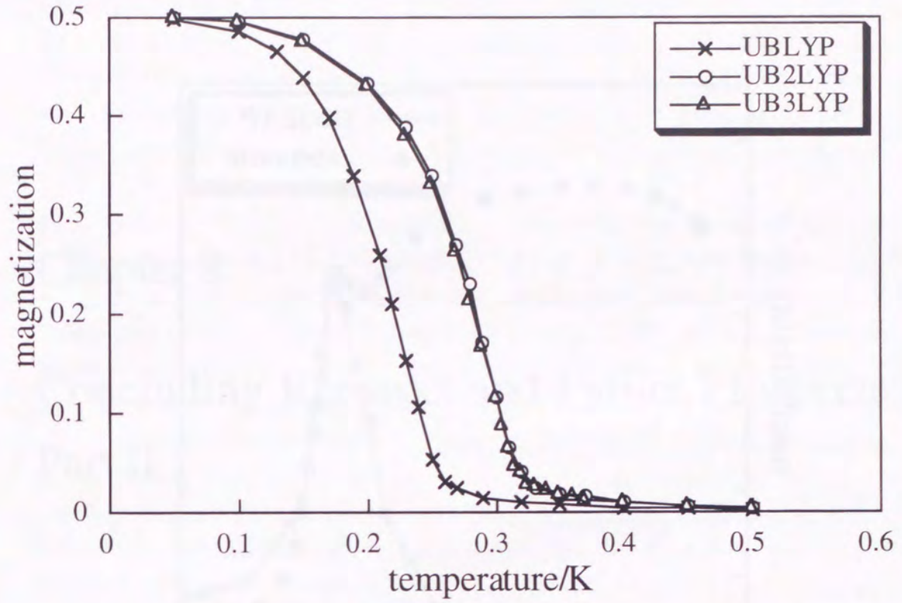

(a) magnetization

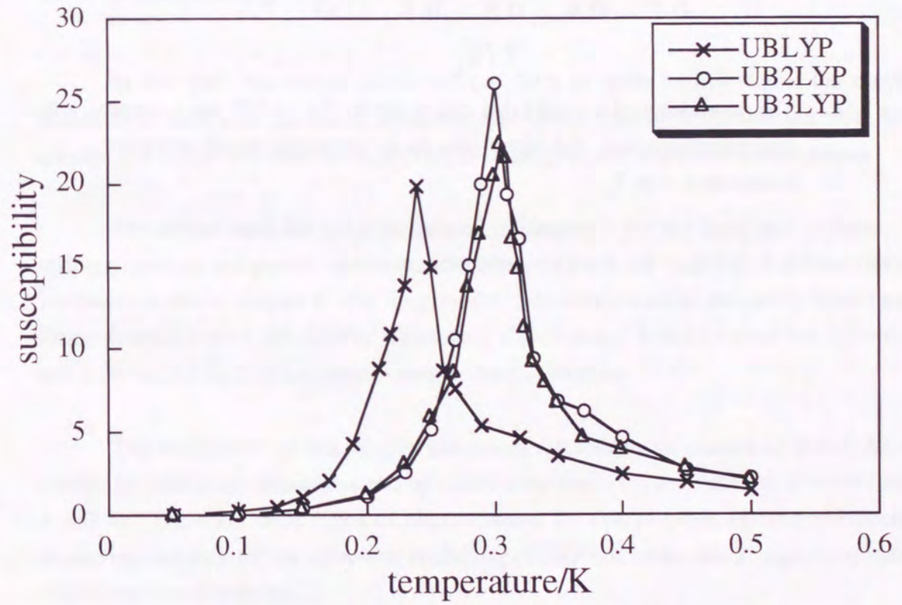

(b) susceptibility

Figure 7. 6 The dependence of the magnetization and the susceptibility on temperature for α-HQNN crystal by using intermolecular interactions calculated by three types of DFT methods.

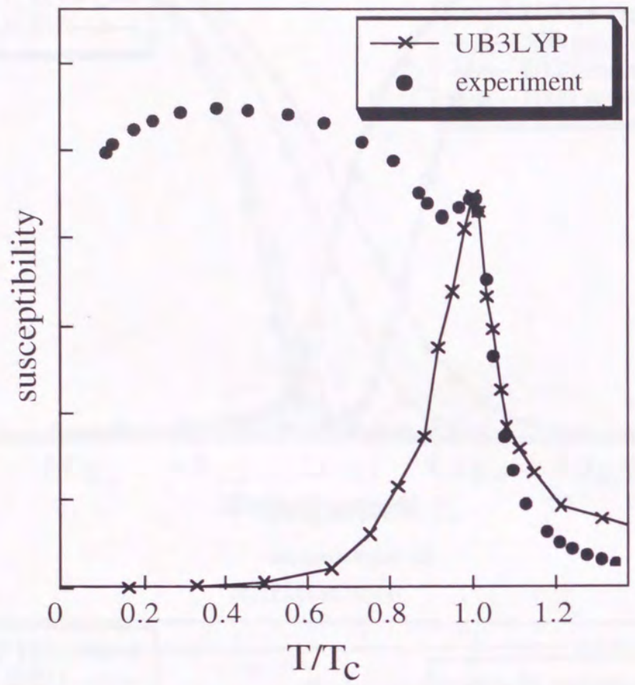

Figure 7. 7 The dependence of susceptibility calculated by GA on T/T_c are compared with experimental values. GA reproduces the experimental results in higher temperature than T_c.

Chapter 8

Concluding Remarks and Future Prospects in Part II

8. 1 Concluding remarks

In this part, the author developed the GA's in order to investigate the magnetic behaviors of Ising spin clusters by using magnetic interactions between two spin sites. In this chapter, the author will summarize the results of this part and make future discussions.

The author used the GA's mentioned in chapter 1 for the Ising spin clusters. The coding procedure and genetic operators, selection, crossover and mutation, had been improved for these clusters in chapter 2. For Ising model, individuals were expressed by bitstrings and fitness functions were obtained by Heisenberg Hamiltonian. It is important that individual x and $\overline{x}$ shown in **Fig. 2. 4** have same energies for this clusters.

The searches for global minima and thermodynamical calculations by pure GA's were carried out, and some parameters and operators were improved for these calculations (chapter 4 and 6). There are three types of improvements for this purpose; (1) improvements for preserving varieties, (2) the tightening up the rule of "survival of the fittest" and (3) hybridizing of GA's and local searches.

Improvements of type (1) are most useful and they are important not only for search for global minima but also for thermodynamical calculations. The exponential scaling in high temperature, an increase in the number of crossover points, an increase in the probability of crossover, $\overline{x}$ crossover and the replacement by the randomly generated individuals (described in chapter 4) and S_r and $C_{\overline{x}}$ (described in chapter 6) are classed in category (1).

Type (2) improvements have both strong and weak points. Fitter individuals are difficult to die, and the varieties of individuals become narrow by using improvements of this type. The exponential scaling in low temperature and elitist preserving selection (described in chapter 4) and S_e (described in chapter 6) belong to category (2). Because improvements of this type are frequently not able to avoid the local minima, they are not suitable for thermodynamical calculations.

GA's improved by type (3) procedures are equal to hybrid GA's discussed in chapter 5. Though GA's are good at widely search, they are not suitable for local searches. On the other hand, heuristic methods can give the local minima, though they can not give the global minima, frequently. Thus, when GA's were used together with the local search, reasonable solutions were frequently obtained. Though improvements of this type are most suitable for the searches for the global minima, they frequently can not be used for thermodynamical calculations, and only M_e (described in chapter 4 and 6) can be adopted for this purpose.

Thermodynamical calculations are carried out for randomly generated spin clusters (described in chapter 6) and real compounds (described in chapter 7). Because GA's could avoid local minima, they gave reasonable results even if initial individuals were randomly generated. $S_r + C_M + C_x + M_e$ is the most suitable methods for thermodynamical calculations. In this algorithm, S_r and C_x avoid the local minima, and C_M and M_e are carried out the rule of "survival of the fittest". It can calculated the magnetic behaviors of real compounds, which have many sites and many local minima. For α-HQNN crystal, $S_r + C_M + C_x + M_e$ gives the ferromagnetic phase transition, and it reproduces qualitatively experimental results. It suggests that it can calculate the magnetic behaviors for organic radical clusters.

8. 2 Future prospects

In this theses, though GA's for Ising model spin clusters were developed, Heisenberg model are frequently required for investigations of the magnetic behavior of organic ferromagnets. Heisenberg Hamiltonian is described as

$$\hat{H} = -2\sum J_{ab}\hat{S}_a \cdot \hat{S}_b \qquad (8.\ 1)$$

where J_{ab} is magnetic interactions.

Because $\hat{S}_a$ and $\hat{S}_b$ are vectors, two or more variables are required for one spin site, and these variables are not integral but real numbers. There are two types of GA's for optimizations of real variables.

(1) Real number is expressed by binary bitstrings, and they are regarded as chromosomes. All genes are expressed by "1" and "0", and GA's are used for bitstrings same as integral variables.

(2) One gene expresses one real number, and genetic operators need to be improved in order to treat the real genes.

They are illustrated in **Fig. 8. 1**.

By (1) type GA's, one GA trial is required for optimization of one real variable. For n sites spin clusters, 2n or more GA trials are necessary. And furthermore, GA's for real numbers expressed by binary bitstrings occasionally do not satisfy the building block hypothesis. For example, chromosomes "1 0 0 0", "0 1 1 1" and "0 0 0 0" express "8", "7" and "0", respectively. On the other hand, hamming distance between "8" and "7" is larger than between "8" and "0". Similar phenotypes do not always mean similar genotypes.

By (2) type GA's, optimization for one spin cluster can be carried out by one GA trial. Spin states code to chromosomes by same procedures as GA's for Ising model, and they satisfy building block hypothesis. For Heisenberg models, (2) type GA's are expected to be reasonable.

In this thesis, though classical Monte Carlo calculations were carried out, quantum Monte Carlo methods are desirable for more accurate calculations. The treatment of real variables are indispensable for the development of GA's using with quantum Monte Carlo methods, same as GA's for the Heisenberg model.

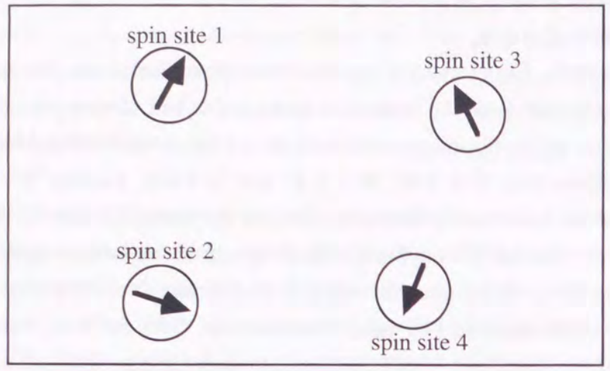

	θ	φ
site 1	0.03	1.01
site 2	0.80	0.00
site 3	3.02	0.62
site 4	1.71	0.88

(a) Heisenberg model spin cluster

	θ	φ
site 1	000000011	1100101
site 2	001010000	0000000
site 3	100101100	0111110
site 4	010101011	1011000

(b) type (1) coding

chromosome = (0.03, 1.01, 0.80, 0.00, 3.02, 0.62, 1.71, 0.88)

(c) type (2) coding

Figure 8. 1 Two types of GA's are illustrated. The phenotype of spin state (a) which have 8 variables code to two genotypes. (b) There are 8 chromosomes, and 8 GA's are required for calculations of this cluster. GA(θ_1), GA(φ_1), GA(θ_2), ..., GA(θ_4) and GA(φ_4) are carried out separately. (c) There is only 1 chromosome for one spin state. One GA's are required for the optimization of this cluster.

Reference

PART I

[1] M. Kinoshita, P. Turek, M. Tamura, K. Nozawa, D. Shiomi, Y. Nakazawa, M. Ishikawa, M. Takahashi, K. Awaga, T. Inabe and Y. Maruyama, Chem. Lett., 1225 (1991).

[2] M. Takahashi, P. Turek, Y. Nakazawa, M. Tamura, K. Nozawa, D. Shiomi, M. Ishikawa and M. Kinoshita, Phys. Rev. Lett., 67, 746 (1991).

[3] Y. Nakazawa, M. Tamura, N. Shirakawa, D. Shiomi, M. Takahashi, M. Kinoshita and M. Ishikawa, Phys. Rev. B, 46, 8906 (1992).

[4] K. Yamaguchi, M. Okumura and M. Nakano, Chem. Phys. Lett., 191, 237 (1992).

[5] M. Okumura, K. Yamaguchi, M. Nakano and W. Mori, Chem. Phys. Lett., 207, 1 (1993).

[6] M. Okumura, W. Mori and K. Yamaguchi, Chem. Phys. Lett., 219, 36 (1994).

[7] J. J. Hopfield, Proceedings of the National Academy of Science of USA, 79, 2554 (1982).

[8] F. Baharona, J. Phys., A15, 3241 (1982).

[9] K. F. Pál, Proceedings of the third Conference on Parallel Problem Solving from Nature, Lecture Notes in Computer Science, Vol. 866, 170 (1994).

[10] K. F. Pál, Biol. Cybern., 73, 335 (1995).

[11] K. F. Pál, Physica A, 223, 283 (1996).

[12] A. K. Hartmann, Europhys. Lett., 40, 429 (1997).

[13] K. Awaga, T. Inabe, U. Nagashima and Y. Maruyama, J. Chem. Soc., Chem. Commun., 1617 (1989); 520 (1990).

[14] Y. Hosokoshi, a doctoral thesis (1995).

[15] K. Inoue and H. Iwamura, Chem. Phys. Lett., 207, 551 (1993).

[16] Y. Hosokoshi, M. Tamura, M. Kinoshita, H. Sawa, R. Kato Y. Fujiwara and Y. Ueda, J. Mater. Chem., 4, 1219 (1994).

[17] K. Yamaguchi, M. Okumura, J. Maki, T. Noro, H. Namimoto, M. Nakano, T. Fueno and K. Nakasuji, Chem. Phys. Lett., 190, 353 (1992).

[18] M. Okumura, W. Mori and K. Yamaguchi, Mol. Cryst. Liq. Cryst., 232, 35 (1993).

[19] T. Kawakami, S. Yamanaka, W. Mori, K. Yamaguchi, A. Kajiwara and M. Kamachi, Chem. Phys. Lett., 235, 414 (1995).

[20] T. Kawakami, S. Yamanaka, H. Nagao, W. Mori, M. Kamachi and K. Yamaguchi, Mol. Cryst. Liq. Cryst., 272, 117 (1995).

[21] T. Nogami, T. Ishida, M. Yasui, F. Iwasaki, N. Takeda, M. Ishikawa, T. Kawakami and K. Yamaguchi, Bull. Chem. Soc. Jpn., 69, 1841 (1996).

[22] K. Yamaguchi, H. Fukui and T. Fueno, Chem. Lett., 625 (1986).

[23] M. Dupuis, A. Marquez and E. R. Davidson, HONDO 95. 3 from CHEM-Station, (1995) IBM Corporation, Neighborhood Road, Kingston, NY. 12401

[24] M. J. Frisch, G. W. Trucks, H. B. Schlegel, P. M. W. Gill, B. G. Johnson, M. A. Robb, J. R. Cheeseman, T. A. Keith, G. A. Petersson, J. A. Montgomery, K. Raghavachari, M. A. Al-Laham, V. G. Zakrzewski, J. V. Ortiz, J. B. Foresman, J. Cioslowski, B. B. Stefanov, A. Nanayakkara, M. Challacombe, C. Y. Peng, P. Y. Ayala, W. Chen, M. W. Wong, J. L. Andres, E. S. Replogle, R. Gomperts, R. L. Martin, D. J. Fox, J. S. Binkley, D. J. Defress, J. Baker, J. P. Stewart, M. Head-Gordon, C. Gonzalez and J. A. Pople, *Gaussian 94* (Revision A.1) (1995) Gaussian, Inc., Pittsburgh PA.

[25] R. G. Parr and W. Yang, Density functional theory of atoms and molecules (Oxford Univ. Press, Oxford, 1989).

[26] D. M. Dreizler and E. K. U. Gross, Density functional theory. An approach to the quantum many body problem (Springer, Berlin, 1990).

[27] S. H. Vosko, L. Wilk and M. Nusair, Can. J. Phys., 58, 1200 (1980),

[28] J. P. Perdew and A. Zunger, Phys. Rev., B23, 5048 (1981).

[29] J. P. Perdew, Phys. Rev., B33, 8822 (1986).

[30] C. Lee, W. Yang and R. G. Parr, Phys. Rev., B37, 785 (1988).

[31] T. Kawakami, A, Oda, W. Mori, K. Yamaguchi, K. Inoue and H. Iwamura, Mol. Cryst. Liq. Cryst., 279, 29 (1996).

[32] Y. Hosokoshi, M. Tamura, K. Nozawa, S. Suzuki, M. Kinoshita, H. Sawa and R. Kato, Synth. Met., 71 1795 (1995).

[33] Y. Hosokoshi, M. Tamura, K. Nozawa, S. Suzuki, H. Sawa, R. Kato and M. Kinoshita, Mol. Cryst. Liq. Cryst., 271 115 (1995).

[34] T. Nogami, K. Tomioka, T. Ishida, H. Yoshikawa, M. Yasui, F. Iwasaki, H. Iwamura, N. Takeda and M. Ishikawa, Chem. Lett., 29 (1994).

[35] T. Sugimoto, M. Tsuji, T. Suga, N. Hosoito, M. Ishikawa, N. Takeda and M. Shiro, Mol. Cryst. Liq. Cryst., 272, 183 (1995).

[36] Y. Hosokoshi, M. Tamura, H. Sawa, R. Kato and M. Kinoshita, J. Mater. Chem., 5, 41 (1995)

[37] T. Sugawara, M. M. Matsushita, A. Izuoka, N. Wada, N. Takeda and M. Ishikawa, J. Chem. Soc., Chem. Commun., 1723 (1994).

[38] M. M. Matsushita, A. Izuoka and T. Sugawara, Mol. Cryst. Liq. Cryst., 279, 139 (1996).

[39] M. M. Matsushita, A. Izuoka, T. Sugawara, T. Kobayashi, N. Wada, N. Takeda and M. Ishikawa, J. Am. Chem. Soc., 119, 4369 (1997).

PART II

[40] J. H. Holland, *Adaptation in Natural and Artificial Systems* (Univ. Michigan Press, Ann Arbor, 1975).

[41] J. H. Holland and J. S. Reitman, Cognitive systems based on adaptive algorithms, in D. A. Waterman and F. Hayes-Roth (eds.), *Pattern-Directed Inference Systems* (Academic Press, New York, 1978).

[42] D. E. Goldberg, *Genetic Algorithms in Search, Optimization, and Machine Learning* (Addison Wesley 1989).

[43] L. Davis, Proc. 1st. ICGA, 136 (1985).

[44] D. E. Goldberg and Ligle, R. Jr., Proc. 1st. ICGA, 154 (1985).

[45] J. J. Grefenstette and R. Gopal, B. Rosmaita and D. Van Gucht, Proc. 1st. ICGA, 160 (1985).

[46] L. D. Whitley, T. Starkweather and D'A Fuquay, Proc. 3rd. ICGA, 133 (1989).

[47] T. Starkweather, S. McDaniel, K. Mathias, C. Whitley and L. D. Whitley, Proc. 4th. ICGA, 69 (1991)

[48] B. R. Fox and M. B. McMahon, Foundations of Genetic Algorithms, 284 (Morgan Kaufmann Publishers, 1991)

[49] Z. Michalewicz, *Genetic Algorithms + Data Structures = Evolution Programs* (Springer-Verlag, 1992)

[50] 西川, 玉置, 計測自動制御学会論文集, Vol. 27, No. 5, 593 (1991).

[51] S. Bagchi, S. Uckun, Y. Miyabe and K. Kawamura, Proc. 4th. ICGA, 10 (1991).

[52] R. Nakano, Proc. 4th. ICGA, 474 (1991).

[53] H. Tamaki and Y. Nishikawa, *Parallel Problem Solving from Nature* 2, 573 (Elsevier Science Publishers, 1992).

[54] T. Yamada and R. Nakano, *Parallel Problem Solving from Nature* 2, 281 (Elsevier Science Publishers, 1992).

[55] 坂和, 加藤, 砂田, 澤田, 日本ファジィ学会誌, Vol. 6, No. 1, 177 (1994).

[56] 坂和, 加藤, 砂田, 園田, 日本ファジィ学会誌, Vol. 7, No. 2, 361 (1995).

[57] P. Tuffery, C. Etchebest, S. Hazout and R. Lavery, J. Biomol. Struct. Dynam., 8, 1267 (1991).

[58] R. S. Judson, M. E. Colvin, J. C. Meza, A. Huffer and D. Gutierrez, Int. J. Quantum Chem., 44, 277 (1992).

[59] R. S. Judson, E. P. Jaeger, A. M. Treasurywala and M. L. Peterson, J. Comp. Chem., 14, 1407 (1993).

[60] D. B. McCarrah and R. S. Judson, J. Comp. Chem., 14, 1385 (1993).

[61] R. Smith, Comp. Phys.: Comm., 71, 134 (1992).

[62] R. S. Judson, J. Phys. Chem., 96, 10102 (1992).

[63] T. Dandekar and P. Argos, Protein Eng., 5, 637 (1992).

[64] R. Unger and J. Mount, J. Mol. Biol., 231, 75 (1993).

[65] S. Sun, Protein Sci., 2, 762 (1993).

[66] T. Dandekar and P. Argos, J. Mol. Biol., 236, 844 (1994).

[67] S. Sun, P. D. Thomas and K. A. Dill, Protein Eng., 8, 769 (1995).

[68] J. T. Pedersen and J. Mount, J. Mol. Biol., 269, 240 (1997).

[69] D. M. Standley, J. R. Gunn, R. A. Friesner and A. E. McDermott, Proteins: Struct. Funct. Genet., 33, 240 (1998).

[70] Y. Zeiri, Phys. Rev., E51, 2769 (1995).

[71] D. M. Deaven and K. M. Ho, Phys. Rev. Lett., 75, 288 (1995).
[72] J. R. Morris, D. M. Deaven and K. M. Ho, Phys. Rev., B53, 1740 (1996).
[73] S. K. Gregurick and M. H. Alexander, J. Chem. Phys., 104, 2684 (1996).
[74] J. A. Niesse and H. R. Mayne, J. Chem. Phys., 105, 4700 (1996).
[75] D. M. Deaven, N. Tit, J. R. Morris, K. M. Ho, Chem. Phys. Lett., 256, 195 (1996).
[76] Y. H. Luo, J. Zhao, S. Qiu and G. Wang, Phys. Rev., B59, 903 (1999).
[77] V. Venkatasubramanian, K. Chan and J. M. Caruthers, Computers chem. Engng., 18, 833 (1994).
[78] A. Z. Maksymowicz, J. E. Galletly, M. S. Magdoń and I. L. Maksymowicz, J. Magn. Magn. Mater., 133, 40 (1994).
[79] K. S. Kirkpatrick, C. D. Gelatt and M. Vecchi, Science, 220, 671 (1983).
[80] K. S. Kirkpatrick, J. Stat. Phys., 34, 975 (1984).
[81] W. H. Press, B. P. Flannery, S. A. Teukolsky and W. T. Vetterling, *Numerical Recipes: The Art of Scientific Computing (FORTRAN Version)*, 2nd. Ed. (Cambridge University Press, Cambridge 1990).
[82] P. J. M. van Laarhoven and E. H. L. Aarts, *Simulated Annealing: Theory and Applications* (Reidel, Dordrecht 1987).
[83] K. A. De Jong, Doctoral dissertation, (University of Michigan 1975).
[84] G. Syswerda, Proc. 3rd. ICGA, 2 (1989).
[85] N. Metropolis, A. Rosenbluth, M. Rosenbluth, A. Teller and E. Teller, J. Chem. Phys., 21, 1087 (1953).
[86] T. N. Bui and B. R. Moon, Proc. 5th. ICGA, 102 (1993).
[87] H. Kitano, Proc. AAAI-90, 7 (1990).
[88] D. Powell, S. Tong and M. Skolnick, Proc. 3rd. ICGA, (1989)
[89] R. Sessoli, H. L. Tsai, A. R. Schake, S. Wang, J. B. Vincent, K. Folting, D. Gatteschi, G. Christou and D. N. Hendrickson, J. Am. Chem. Soc., 115, 1804 (1993).
[90] I. Mirebeau, M. Hennion, H. Casalta, H. Andres, H. U. Güdel, A. V. Irodova and A. Caneschi, Phys. Rev. Lett., 83, 628 (1999).
[91] A. Oda, T. Kawakami, S. Takeda, W. Mori, M. M. Matsushita, A. Izuoka, T. Sugawara, K. Yamaguchi, Mol. Cryst. Liq. Cryst., 306, 151(1997).

List of publications

Papers

[1] Theoretical studies of the ferromagnetic intermolecular interaction of *p*-carboxylate phenyl nitronyl nitroxide
T. Kawakami, A, Oda, W. Mori, K. Yamaguchi, K. Inoue, H. Iwamura
Mol. Cryst. Liq. Cryst. 279 (1996) 29-38.

[2] Magnetic interaction via β-hydrogen atoms in TEMPO derivatives
T. Kawakami, A. Oda, S. Takeda, W. Mori, T. Ishida, M. Yasui, F. Iwasaki, T. Nogami and K. Yamaguchi
Mol. Cryst. Liq. Cryst. 306 (1997) 141-150.

[3] Theoretical studies of magnetic interactions in 2', 5'- dihydroxyphenyl nitronyl nitroxide crystal
A. Oda, T. Kawakami, S. Takeda, W. Mori, M. M. Matsushita, A. Izuoka, T. Sugawara, K. Yamaguchi
Mol. Cryst. Liq. Cryst. 306 (1997) 151-160.

[4] Theoretical studies of magnetic interactions in *p*-cyanophenyl nitronyl nitroxide crystal
A. Oda, T. Kawakami, S. Takeda, W. Mori, Y. Hosokoshi, M. Tamura, M. Kinoshita, K. Yamaguchi
Mol. Cryst. Liq. Cryst. 306 (1997) 331-338.

[5] Theoretical Studies of the Pressure Effects for β-Phase of *p*-NPNN
M. Okumura, T. Kawakami, A. Oda, K. Yamaguchi, M. Mito and K. Takeda
Mol. Cryst. Liq. Cryst. 335 (1999) 623-632.

[6] Theoretical Studies of Magnetic Interactions in 3', 5'-Dihydroxyphenyl Nitronyl Nitroxide Crystal
A. Oda, T. Kawakami, G. Maruta, S. Takeda, W. Mori, K. Yamaguchi, M. M. Matsushita, A. Izuoka and T. Sugawara
Mol. Cryst. Liq. Cryst. 335 (1999) 633-642.

[7] Theoreticaal Studies of Intra- and Inter- magnetic Interactions in TMAO (1, 3, 5, 7 - tetramethyl - 2, 6 - diazaadamantane N, N' - dioxyl)
T. Kawakami, A. Oda, S. Takeda, W. Mori and K. Yamaguchi
Mol. Cryst. Liq. Cryst. 335 (1999) 697-706.

[8] Theoretical studies on network systems with interspin interactions by using the genetic algorithm
A. Oda, H. Nagao and K. Yamaguchi
Prog. theor. phys., Suppl. in press.

Books

[1] MO-Theoretical Elucidation of Spin Alignments in Organic Magnetic Crystals
K. Yamaguchi, T. Kawakami, A. Oda and Y. Yoshioka
(P. M. Lahti Ed., Marcell Declcer, 1999) chapter 4.